TEST OF TIME REVERSAL INVARIANCE IN INELASTIC ELECTRON SCATTERING FROM A POLARIZED PROTON TARGET

A CEA

A thesis presented

by

Jeffrey A. Appel

to

the Department of Physics

in partial fulfillment of the requirements

for the degree of

Doctor of Philosophy

in the subject of

Physics

Harvard University

Cambridge, Massachusetts

December, 1968

ABSTRACT

Electrons have been scattered inelastically from a hydrocarbon target containing protons polarized normal to the scattering plane. Scattered electrons with energies corresponding to the production of the $\Delta(1236)$, N(1512) and N(1688) pion-nucleon resonances were observed. A search was made for changes in the cross-section as the target polarization was reversed. Any changes would have been evidence of a violation of time reversal invariance in the electromagnetic interactions of the hadrons. No such changes were observed.

Early attempts at a coincidence polarization experiment are described in the Appendix.

ACKNOWLEDGMENTS

To Professor Richard Wilson, my thesis advisor, whose incisive criticism and breadth of understanding have been an inspiration to me,

To James Chen, my fellow thesis student, for his early and continued interest in this experiment,

To Dr. Jack Sanderson, Professor R. V. Pound, and Dr. C. Zajde who, with James Chen, implemented the polarized target,

To Drs. Michael Goitein, Robert Budnitz, and Charles Mistretta, whose thesis experiments, performed in part with the same detection apparatus, made our efforts so much easier,

To Drs. Derek C. Imrie, Michael Goitein, Thomas Kirk and John R. Dunning, Jr., and to K. Hanson, G. Gladding, R. Madaras, and L. Price, members of the Electron Scattering Group active at the time of this experiment, whose miriad efforts defy enumeration,

To the staffs of the Harvard Cyclotron Laboratory and Cambridge Electron Accelerator with their great variety of skills and willingness to react quickly to changing experimental needs,

To Miss Anne Hudson and her careful typing of this thesis,

To the Danforth Foundation Graduate Fellowship Program which has been my primary financial support throughout my graduate career and to its directors whose encouragement has gone beyond financing,

To my parents and their unquestioned love and encouragement,

To my ever wonderful wife and daughter, my refuge and delight throughout this work,

To all these I acknowledge my profound debt of gratitude and write these few words of sincere thanks.

TABLE OF CONTENTS

LIST OF FIGURES

LIST OF FIGURES (Cont.)

LIST OF TABLES

CHAPTER 1 BACKGROUND AND THEORY

1.1 HISTORICAL BACKGROUND

Since the discovery of the violation of CP invariance in the decay of the long-lived neutral K-meson,[1] interest has been revived in the search for violations of time reversal (T) invariance which must occur if the CPT symmetry is to hold. Previous work[2] had placed a limit of a few percent on possible T violating amplitudes in several strong and weak interactions. Furthermore, Quantum Electrodynamics, which has been so successful in explaining the electromagnetic interactions of photons and leptons, is a T invariant theory. Until recently, however, there has been no effective test of T invariance in the electromagnetic interactions of the strongly interacting particles.

In 1965, Bernstein, Feinberg, and Lee[2] pointed out that just such a violation of T invariance in the electromagnetic interaction could be responsible for the observed violation of CP invariance. For one thing, the magnitude of the CP violating effect is given by[3]

$$|\eta_{+-}| = \frac{\Gamma(K_L \to \pi^+\pi^-)}{\Gamma(K_S \to \pi^+\pi^-)} \sim 2.0 \times 10^{-3} \sim \frac{\alpha}{\pi} \qquad (1.1)$$

This order-of-magnitude suggests that a CP violating virtual electromagnetic effect might be responsible for the observed violation.

More recent work has uncovered the corresponding neutral CP violating decay mode with

$$|\eta_{00}| = \frac{\Gamma(K_L \to \pi^0\pi^0)}{\Gamma(K_S \to \pi^0\pi^0)} \qquad (1.2)$$

Although the experimental situation regarding the value of $|\eta_{00}|$ remains chaotic, it is possible that, although of the same order of magnitude

$$|\eta_{00}| \neq |\eta_{+-}|$$

The "Superweak" Theory,[4] one of the leading possibilities for explaining the K-decay CP violation, predicts $|\eta_{00}| = |\eta_{+-}|$. A failure of this equality would immediately disqualify the Superweak Theory and leave the field open to the standard strong, electromagnetic, and weak interactions.

If an electromagnetic amplitude is to account for the CP violation, it would be of comparable size to the usual electromagnetic amplitudes. This fact led Bernstein, Feinberg, and Lee to suggest a new hadronic electromagnetic current K_μ which is even under the operation of the Time Reversal Operator, T. This new current could combine with the usual current J_μ (odd under time reversal) to make up the total hadronic electromagnetic current $\mathcal{J}_\mu$.

$$\mathcal{J}_\mu = J_\mu + K_\mu .$$

In 1966, Christ and Lee[5] refined the idea of the new current K_μ. A mismatch between the time reversal operator appropriate to the electromagnetic interaction T_γ and the time reversal operator appropriate to the strong interaction T_{st} was necessary in order to retain the "minimal electromagnetic interaction" principle for strongly interacting particles.

Independent of these theoretical considerations relating to the observed CP violation, the question of T invariance in the electromagnetic interactions of non-leptons is fundamental. In their paper, Christ and Lee suggested lepton-nucleus scattering tests of T invariance. The only straightforward experimental test is the scattering of unpolarized leptons from a polarized nucleon target. As is well known,[2] <u>elastic</u> lepton-nucleon scattering is not an appropriate reaction for testing T invariance. For elastic scattering, an apparent violation of T invariance would also be a violation of conservation of the electromagnetic current $\mathcal{J}_\mu$. There is no evidence for non-conservation of $\mathcal{J}_\mu$. Thus, Christ and Lee suggested <u>inelastic</u> scattering of leptons from a polarized nucleon target. The work reported here is just such an experiment, the scattering of unpolarized electrons from a target containing polarized protons.

1.2 THEORETICAL FRAMEWORK

Using the helicity amplitude formalism, Christ and Lee[5] defined the three amplitudes (form factors):

$$F_{\pm} = \mp \tfrac{1}{2} \langle \lambda_\Gamma = \tfrac{1}{2} \pm 1 \,|\, \mathcal{J}_x(0) \pm i\, \mathcal{J}_y(0) \,|\, \lambda_N = \tfrac{1}{2} \rangle$$

$$F_Z = \langle \lambda_\Gamma = \tfrac{1}{2} \,|\, \mathcal{J}_z(0) \,|\, \lambda_N = \tfrac{1}{2} \rangle \tag{1.4}$$

where λ_i is the helicity of the state i = N (nucleon) or Γ (some state excited from the nucleon). Then, assuming Lorentz invariance, conservation of the electromagnetic current, single photon exchange, Quantum Electrodynamics for the leptonic part of the interaction, and a vanishing electron mass, one can express the cross section for inelastic electron-nucleon scattering as[5a]

$$\frac{d\sigma}{d\Omega_e dE'} = \Gamma_T \left\{ \sigma_T + \epsilon \sigma_0 + P\sqrt{2\epsilon(\epsilon+1)}\, \sigma_{0T} \right\} \tag{1.5}$$

where

$$\Gamma_T = \frac{\alpha}{4\pi^2} \frac{K}{q^2} \frac{E'}{E} \left[2 + \frac{\cot^2 \frac{\theta}{2}}{1+\tau} \right]$$

$$\sigma_T = \frac{4\pi^2\alpha}{K} \sum_{\Gamma} \left[|F_+|^2 + |F_-|^2 \right] \delta(E + M - E' - E'_{hadrons})$$

$$\sigma_0 = \frac{4\pi^2\alpha}{K} \frac{1}{\tau} \sum_{\Gamma} |F_Z|^2 \, \delta(E + M - E' - E'_{hadrons}) \tag{1.6a}$$

$$\sigma_{OT} = \frac{4\pi^2\alpha}{K} \frac{1}{\sqrt{\tau}} \eta \sum_{\Gamma} \mathrm{Im}\; F_-^* F_z \;\delta(E+M-E'-E'_{hadrons}) \qquad \text{(1.6a, con't.)}$$

with
$$\eta = \pi_N \pi_\Gamma^{-1} e^{i\pi(J_N - J_\Gamma)} \qquad \text{(1.6b)}$$

and $J_N = \frac{1}{2}$ is the spin of the nucleon, J_Γ is the spin or total angular momentum of the state Γ, π_N is the parity of the nucleon and π_Γ is the parity of the state Γ, and P is the polarization of the initial nucleon normal to the scattering plane.

The statement of T invariance is that $\sigma_{OT} = 0$ since the F_- and F_z are relatively real. The relative reality of the F's requires that the current operators $\mathcal{J}_\mu$ be evaluated between particular helicity states $|\lambda_i\rangle$. In particular, the states must be eigenstates of the strong interaction Hamiltonian H_{st} and an operator $T_{st}\, e^{-i\pi J_y}$; i.e.,

$$\mathcal{O}|\lambda_i\rangle = T_{st}\, e^{-i\pi J_y} |\lambda_i\rangle = \eta_i^* \langle\lambda_i| \qquad (1.7)$$

where J_y is the y component of the total angular momentum operator and η_i is a phase factor independent of the helicity of the state i. Then, for

$$T_{st}\, \mathcal{J}_\mu(0)\, T_{st}^{-1} = -\mathcal{J}_\mu(0) \qquad (1.8)$$

i.e., $K_\mu = 0$,

$$\begin{aligned} F_z &= \langle \lambda_\Gamma = \tfrac{1}{2} | \Theta^{-1}\Theta\, \mathcal{J}_z(0)\, \Theta^{-1}\Theta | \lambda_N = \tfrac{1}{2} \rangle \\ &= \langle \lambda_\Gamma = \tfrac{1}{2} | \Theta^{-1}\, \mathcal{J}_z(0)\, \Theta | \lambda_N = \tfrac{1}{2} \rangle \\ &= \eta_\Gamma \eta_N^* \langle \lambda_N = \tfrac{1}{2} | \mathcal{J}_z(0) | \lambda_\Gamma = \tfrac{1}{2} \rangle \\ &= \eta_\Gamma \eta_N^* F_z^* \end{aligned}$$

so that the phase of F_z is given by the phase factors η_Γ and η_N.

$$\frac{F_z}{F_z^*} = \eta_\Gamma \eta_N^* \qquad (1.9)$$

Similarly,

$$\begin{aligned} F_\pm &= \mp \tfrac{1}{2} \langle \lambda_\Gamma = \tfrac{1}{2} \pm 1 | \Theta^{-1}\Theta\, (\mathcal{J}_x(0) \pm i\, \mathcal{J}_y(0))\, \Theta^{-1}\Theta | \lambda_N = \tfrac{1}{2} \rangle \\ &= \mp \tfrac{1}{2} \langle \lambda_\Gamma = \tfrac{1}{2} \pm 1 | \Theta^{-1}\, (\mathcal{J}_x(0) \pm i\, \mathcal{J}_y(0))\, \Theta | \lambda_N = \tfrac{1}{2} \rangle \end{aligned}$$

and

$$\frac{F_1}{F_1^*} = \eta_r \eta_N^* = \frac{F_2}{F_2^*} \tag{1.10}$$

The requirement that the form factors F be evaluated with eigenstates of the strong Hamiltonian corresponds to the experimental requirement of detecting incident and final hadron states which are also eigenstates of the strong Hamiltonian. The initial polarized proton, which is the nucleus of a hydrogen atom in the target, is, of course, an eigenstate of H_{st}. If, on the other hand, a particular charge mode of the excited state were detected, say $p + \pi^0$, then the final state would <u>not</u> be an eigenstate of H_{st}. The detection of all contributions to a resonance at a given energy or of the continum states at a given energy would be eigenstates of H_{st}. Similarly, if one could isolate all contributions to a given total angular momentum or a given isospin at some energy, then one would have an eigenstate of H_{st}.

The problem of isolating the contributions of a particular resonance or a particular total angular momentum state would require great experimental and analytic capability. However, if one agrees to sum over all outgoing hadron states (the sums over Γ in Eq. 1.6), then one will have an eigenstate of H_{st} without the complications just described. Thus, the experimental test of time reversal discussed here was a single arm measurement. Only the scattered electrons of a given energy, E', corresponding to a given energy of the hadron state Γ, were detected. Attempts at a coincidence experiment (which would not have been a test of T invariance) are discussed in the Appendix.

A note is in order about the Fermi-Watson Final State Theorem.[6] This theorem relates the phases of single pion electroproduction and photoproduction multipole amplitudes to the pion-nucleon phase shifts. In so doing, specific basis states of isospin, I, orbital angular momentum, ℓ, and total angular momentum, J, are selected. Since these states are eigenstates of orbital angular momentum, they are not relevant to the proof in this Section. That is, it is not "by" the Fermi-Watson Theorem that one shows the relative reality of amplitudes and the consequent lack of an asymmetry. In fact, the Fermi-Watson Theorem only applies in purely elastic (single pion production) regions. Rather, a failure of time reversal invariance would invalidate the proof of the Fermi-Watson Theorem.

1.3 THE THEORETICAL ASYMMETRY AND "MAXIMAL EFFECT"

a) Introduction.

Given the cross section in Equation 1.5, one can define an asymmetry α as

$$\alpha = \frac{1}{P} \frac{\sigma_+ - \sigma_-}{\sigma_+ + \sigma_-} \tag{1.11}$$

where σ_+ (σ_-) represents the doubly differential cross section $d\sigma/dE'd\Omega_e$ with the spin of the target nucleon parallel (antiparallel) to the normal to the scattering plane, $\hat{n}$. Then

$$\alpha = \sqrt{2\epsilon(\epsilon+1)} \; \frac{\sigma_{0T}}{\sigma_T + \epsilon\sigma_0} \tag{1.12}$$

$$\alpha = \sqrt{2\epsilon(\epsilon+1)} \; \frac{\eta}{\tau} \; \frac{\sum_\Gamma |F_-|\,|F_z| \sin\delta_\Gamma}{\sum_\Gamma \left[|F_+|^2 + |F_-|^2 + \frac{\epsilon}{\tau}|F_z|^2 \right]} \tag{1.13}$$

where the sum is understood to apply only to states which conserve energy and δ_Γ is the relative phase between F_-^* and F_z.

b) "Maximal Effect" Model.

In order to obtain an estimate of a "maximal effect", we make the following assumptions and definition:

1) A single phase angle δ is appropriate to all terms in the sum over Γ.

2) The hadronic helicity amplitudes F_- and F_+ are related by a constant A; i.e.,

$$A = \frac{\eta\,|F_-|}{\left[\sum_{\Gamma}\left(|F_+|^2 + |F_-|^2\right)\right]^{1/2}} \tag{1.14}$$

3) The ratio of the scaler to the transverse amplitude is defined to be R so that

$$R^2 = \frac{\sigma_0}{\sigma_T} = \frac{\sum_{\Gamma} \frac{1}{2}|F_z|^2}{\sum_{\Gamma}\left(|F_+|^2 + |F_-|^2\right)} \tag{1.15}$$

The asymmetry can then be expressed as

$$\alpha = \sqrt{2\epsilon(\epsilon+1)}\; A\left(\frac{R}{1+\epsilon R^2}\right)\sin\delta \tag{1.16}$$

For forward angle scattering, ϵ is very near to 1. For the angles in this experiment, $\epsilon \gtrsim 0.95$ and we can consider

$$\alpha \sim 2A\left(\frac{R}{1+R^2}\right)\sin\delta \tag{1.16a}$$

As can be seen from the symmetry of this expression in terms of R and 1/R, there is little sensitivity to R for R near 1. Furthermore, for R, A, and $\sin\delta \sim 1$, the asymmetry is also $\sim$ 1.

c) Other Models for a T Violation Effect.

There is interest in possible T violation effects for more restricted models than those in the class just discussed. For example, the time reversal violation may be restricted to (1) resonant single pion production or (2) an interference between the resonant and background amplitudes. In these cases, σ_{OT} contains only those amplitudes which interfere to give a T violation effect. The resultant predicted asymmetry α is, therefore, smaller than it was for the class of models discussed in the previous section.

One can still use Equation 1.16 to estimate the T violating phase angle δ. However, one must make the substitution

$$A \rightarrow A' = A\, f_1\, f_2 \qquad (1.17)$$

where

$$f_1 = \frac{(F_-)_{restricted}}{(F_-)_{total}} \quad \text{and} \quad f_2 = \frac{(F_2)_{restricted}}{(F_2)_{total}}$$

In these models, we again make the assumptions of the appropriateness of a single phase angle δ and a constant A'.

1.4 PROBLEMS OF INTERPRETATION

Had a large asymmetry been found, it would be difficult to interpret it except as an evident violation of time reversal invariance in the electromagnetic interaction. No such large asymmetry was found. The interpretation of a small asymmetry is impeded by two effects; (1) possible non-T violation effects due to two photon exchange and (2) lack of a compelling model for time reversal non-invariance itself.

a) Two Photon Exchange Effects.

In the derivation of the asymmetry formulae, the single photon exchange approximation (Figure A.1, except that the final hadron state may contain any number of pions) was made. The amplitude for two photon exchange, M_4, is represented in Figure 1.1b. Effects due to this amplitude would first appear as an interference with the larger single photon exchange amplitude, M_2. The basic reason for the surpression of the two photon exchange amplitude is an additional factor of (1/137) due to the extra electromagnetic vertices. This implies that two photon exchange effects are totally negligible at the level of accuracy obtained in this experiment. However, an enhancement might occur in the integration over q_1 implied for a

TWO PHOTON EXCHANGE AMPLITUDES

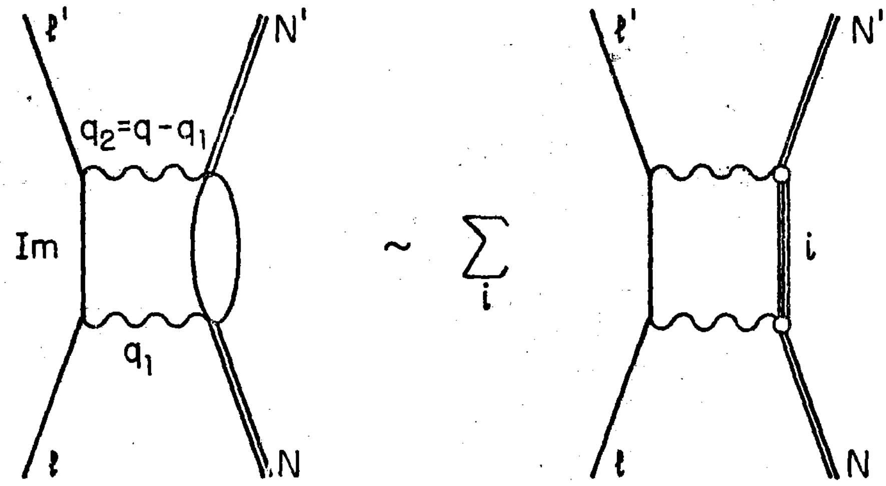

a) ELASTIC SCATTERING

$$\mathrm{Im}\left\langle \ell' N' \middle| M_4 \middle| \ell N \right\rangle = \sum_i \left\langle \ell' N' \middle| M_2 \middle| i \right\rangle \left\langle i \middle| M_2 \middle| \ell N \right\rangle \quad (1.18a)$$

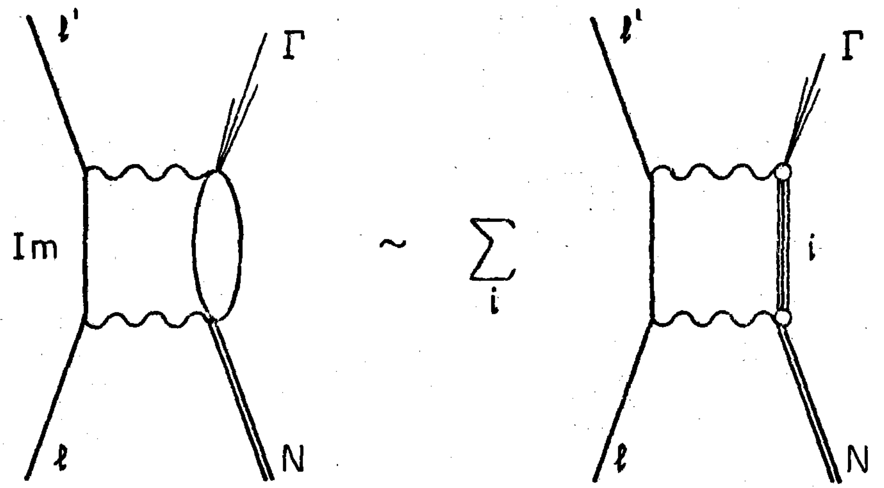

b) INELASTIC SCATTERING

$$\mathrm{Im}\left\langle \ell' \Gamma \middle| M_4 \middle| \ell N \right\rangle = \sum_i \left\langle \ell' \Gamma \middle| M_2 \middle| i \right\rangle \left\langle i \middle| M_2 \middle| \ell N \right\rangle \quad (1.18b)$$

FIGURES 1.1

measurement at a given net momentum transfer, q. Then one might expect to see a two photon exchange effect. Any two photon effects visible in this experiment would be proportional to the imaginary part of the interference between the one and two photon exchange amplitudes. <u>No experiment has yet reported results on this interference for inelastic scattering</u>.

However, one can make some extrapolations from other, not unrelated experiments and calculations to see what would be required for a sizable two photon exchange contribution.

If one accepts the real part of the interference as a guide, one may be consoled in that no effects have been found[7] on the two percent level in the ratio of positron to electron inelastic scattering at the first resonance at $q^2 = 0.2$ and $0.7\ (\mathrm{GeV}/c)^2$. If one further allows elastic scattering as an indication of inelastic effects, then it is worth noting that no real part of the interference has been observed in $e^-p - e^+p$ scattering up to $q^2 = 5(\mathrm{GeV}/c)^2$ on the same level of precision.[8]

Using the elastic scattering as an indication of inelastic effects is not as unjustifiable as it may seem, especially if one is comparing effects due to the imaginary parts of the interferences. One may use the unitarity condition to calculate the imaginary part of the two photon exchange amplitudes for both elastic and inelastic lepton scattering. One may approximate the intermediate hadron states by a small number of physical intermediate states, i; namely, the resonances. See Figures 1.1a and b and Eq. 1.18. Thus, half of the factors in the amplitudes are identical and the only difference is in the addition of one or more pions to the outgoing state Γ. In a calculation of this type, Guérin and Piketty[9] get a maximum elastic scattering effect of about -0.3% for 1 GeV incident electrons and large q^2. The exact dependence of the photon-hadron vertex functions (form factors) appeared to be unimportant in their calculation. Even with constant form factors, the contributions of the first and second resonances were -5% and -0.33% respectively. These values are expected to be upper limits on the elastic scattering asymmetry when it is calculated using the isobaric model we have just discussed. Experiments on recoil proton polarization give a measure of the imaginary part of the interference for elastic electron-proton scattering. Results[10] show no effect on the few percent level up to $q^2 = 0.8$ (GeV/c)^2.

Again, it must be noted that there is no experimental data on the imaginary part of two photon exchange effects in inelastic scattering. Extrapolations from the above data are not conclusive, but do give some indication that no anomolously large effect occurs. On that basis, we expect any two photon exchange asymmetry to be less than a few percent, i.e., at or below the uncertainty of the final result, $\delta\alpha$. Therefore, we neglect such possible effects in the interpretation of this time reversal experiment.

b) Lack of a Compelling Model.

A more serious problem of interpretation arises from the lack of a specific model to be tested. The addition of the current K_μ is a framework within which it may be convenient to define a model. Lee has suggested two such models,[11] but has not calculated the expected effect of either on inelastic lepton scattering.

In suggesting a "maximal effect" (Section 3 of this chapter), we have essentially defined a class of crude models. This class includes models in which J_μ contains the purely transverse interaction and K_μ contains the non-transverse interactions.

In essence, we must think of the time reversal experiment as a search for T violations in the electromagnetic interaction more than as a test of T invariance in electromagnetic interactions. The same is true, of course, for all the so-called tests of invariances which produce null results.

1.5 SELECTION OF KINEMATIC REGIONS FOR STUDY

In any experiment which is a search for an unknown there is a certain amount of chance involved. The exact nature of the unknown phenomenon, if it exists at all, may not be visible where one decides to look. However, one can ordinarily make a best choice of running conditions based on what knowledge does exist. Thus, it is evident from the preceeding theoretical framework that any effect due to time reversal violation may manifest itself in an interference between scalar and transverse production amplitudes. It is necessary, then, to select kinematic regions in which both scalar and transverse production amplitudes exist and are of comparable magnitude.

There is direct experimental evidence that there are large scalar production amplitudes in the first resonance region for momentum transfers of 3 and 6 F^{-2} (0.12 and 0.24 $(GeV/c)^2$).[12,13] These scalar amplitudes are thought to be associated primarily with non-resonant backgrounds due to such Born amplitudes as those used by Mistretta, et al.[13] in attempting to isolate the pion form factor. The relevant diagram is

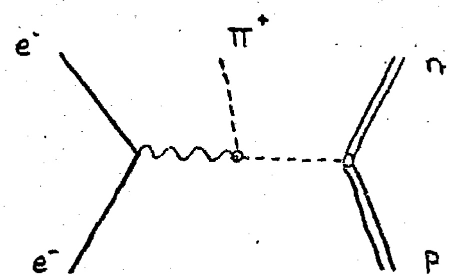

Figure 1.2

PION FORM FACTOR BORN DIAGRAM

The resonance itself is dominantly transversely produced, as is well known.[13] It is possible to imagine, therefore, a time reversal noninvariance manifested through an interference between the resonant and background amplitudes. Such an effect would be largest between the threshold and peak of the resonance since it is in these regions that the scalar and transverse amplitudes, respectively, are largest. We can search for structure in the asymmetry as a function of energy E' to look for such behavior.

Similarly, both longitudinal and transverse contributions are known to exist in the production of the higher resonances.[14] However, the analysis of these deeper inelastic regions is not as complete as it is for the first resonance region.

The kinematic regions studied, which were chosen with the aim of maximizing the longitudinal contribution to the cross section,[15] are listed in Table 1.1 .

TABLE 1.1

KINEMATIC REGIONS STUDIED

RESONANCE REGION	W_c MeV	ΔW MeV	ELECTRON SCATTERING ANGLE	INCIDENT ELECTRON ENERGY	E'_W GeV	q_W^2 $(GeV/c)^2$
First	1229	189	7.34	3.98	3.52	.23
Second	1529	154	7.59	5.98	4.93	.52
Second	1507	174	9.05	5.97	4.85	.72
Third	1690	167	7.59	5.98	4.66	.49
Third	1686	183	9.05	5.97	4.56	.68

W_c is the central value of the pion-nucleon center-of-mass energy in the bin width, ΔW

E'_W and q_W^2 are the scattered electron energy and four-momentum transfer for the central energy value, W_c.

1.6 OTHER DIRECT TESTS OF THE T INVARIANCE OF H_γ.

a) Introduction.

Four other types of experiment have been performed relating directly to the T invariance of the electromagnetic interactions: (1) measurements of the angular and polarization dependence of γ-ray absorption and emission using Mössbauer nuclei,[16,17] (2) searches for the electric dipole moment interaction of the neutron,[19,20] (3) measurement of the recoil deuteron vector polarization in elastic electron-deuteron scattering,[22] and (4) a reciprocity test in the angular distributions of the reactions $\gamma + d \rightleftharpoons n + p$.[23,24] Results from the first three experiments have been published and reveal no violations of time reversal invariance. Preliminary analysis of the fourth experiment are consistent with a nearly maximal violation for part of the data.

b) Nuclear Matrix Elements.

Bernstein, Feinberg, and Lee[2] noted that nuclear matrix elements might contain a small T noninvariant admixture which is $\sim(10^{-2} - 10^{-3})$ times the T invariant amplitude. Two experiments using the Mössbauer effect were subsequently reported at this level of accuracy. If one expresses the lack of T invariance in terms of the relative phase η of interfering amplitudes, then Kistner[16] obtained

$$\eta = \pi - (1.0 \pm 1.7) \times 10^{-3}$$

for the 90-keV Mössbauer γ-ray in Ru^{99} and Atac, Chrisman, Debrunner, and Frauenfelder[17] obtained

$$\eta = (+\ 1.1 \pm 3.8) \times 10^{-3}$$

for the 73 keV γ-ray in Ir^{193}. The difference in these angles from 0 or π represents a deviation from T invariance in the single photon exchange approximation. More recent investigation however, has disclosed that the single photon approximation is insufficient to describe the process on the above level of accuracy. Hannon and Trammell[18] noted that effects related to internal conversion cause an additional phase shift ξ which is totally unrelated to time reversal noninvariance. They calculated ξ for the Ru and Ir Mössbauer transitions and obtained

$$\xi(Ru) = -6.5 \times 10^{-3},$$

$$\xi(Ir) = 0.9 \times 10^{-3}.$$

Using the Kistner data and assuming T invariance, Hannon and Trammell obtained

$$\xi(Ru) = (-8.6 \pm 10.2) \times 10^{-3},$$

still in agreement with T invariance, but rather insensitive. It is clear that further work will require higher accuracy and that both η and ξ will have to be measured before any interpretable results can be obtained. Fortunately, Hannon and Trammell have pointed out an experimental means of separating the effects of η and ξ. At this point, the results from the Mössbauer effect experiments give only rather poor sensitivity to T noninvariant effects.

c) Neutron Electric Dipole Moment.

The electric dipole moment interaction with an external electric field can be represented by a Hamiltonian H_d of the form

$$H_d = -d \cdot E$$

where d is the electric dipole moment and E is the external electric field. The Hamiltonian is odd under both the parity and time reversal operations. Thus, a violation of T invariance can only be observed when in conjunction with the weak interaction which violates P invariance. This provides an upper limit on the order of magnitude of an observable dipole moment, d_{max}, for an electromagnetic violation of T invariance.

$$d_{max} = e\, G_F\, M \simeq 10^{-19} \text{ e-cm.}$$

Various predictions for a neutron electric dipole moment have appeared in the literature and range from 10^{-19} to 10^{-22} e-cm. Two of these predictions are specifically meant to apply to a possible electromagnetic breakdown of time reversal invariance. Feinberg[21a] discussed the order of magnetic argument given above and Salzman and Salzmann[21b] worked with a model in which the hypothesized intermediate vector bosons, $W^{\pm}$, have electric dipole moments. They obtained a prediction of 10^{-20} e-cm for the neutron electric dipole moment. Two preliminary experimental results on a neutron electric dipole have been reported. The latest result[21] from the experiment of Miller, Dress, Baird, and Ramsey[19] is

$$d = (1.6 \pm 1.4) \times 10^{-23} \text{ e-cm}$$

and Shull and Nathans[20] reported

$$d = (2.4 \pm 3.9) \times 10^{-22} \text{ e-cm.}$$

These results appear to rule out maximal type violations in all of the models which have appeared in the literature, including the electromagnetic breakdown predictions.

d) Elastic Electron Deuteron Scattering.

In elastic electron scattering from unpolarized deuterium, one must invoke time reversal invariance to reduce the number of independent deuteron form factors to three. Prepost, Simonds and Wiik[22] have reported results from an experiment which searched for the effect of a fourth form factor in the form of outgoing deuteron vector polarization. The resulting polarization due to possible time reversal non-invariance for incident electrons of 1 GeV and momentum transfers of 0.52 $(\mathrm{GeV}/c)^2$ was

$$P = 0.075 \pm 0.088$$

A maximal effect consistent with what is presently known about elastic deuteron scattering is $P_{max} = 0.34$. Violations of time reversal would appear to be much less than maximal in this electromagnetic interaction, too.

e) Reciprocity in the Reactions $\gamma + d \rightleftharpoons n + p$.

The application of time reversal invariance to reciprocal interactions implies the equality of differential cross sections in equivalent coordinate systems. This equality, in turn, implies the equality of total cross sections. Naturally, differential cross sections in appropriate regions may be much more sensitive to violations of time reversal than the total cross sections. Noting this, Barshay[23] suggested a comparison of the angular distributions in the reactions $\gamma + d \rightarrow n + p$ and $n + p \rightarrow \gamma + d$. The data on photodisintegration of the deuteron already existed at the time of Barshay's suggestion. However, only recently have data become available on the reciprocal reaction.

Longo and co-workers[24] have scattered neutrons from protons at energies from 470 to 720 MeV. They have made a comparison of the differential cross section shapes from their data and earlier $\gamma + d \rightarrow n + p$ data. This method of analysis reduces the effect of systematic normalization differences in the two different types of experiment. Preliminary analysis indicates agreement for the lowest energies, but potentially maximal violation of time reversal invariance at the highest energies. Why a maximal violation of time reversal invariance would occur for only part of the data is not known. The analysis is continuing.

f) Relationships Among the Various Tests.

The so-called maximal effects for each experiment have typically been made in advance of experimental results and are usually rather less than conservative. Nevertheless, such maximal estimates do give some gauge of the relative sensitivity of the various experiments. On this basis, the limit on time reversal violations from the neutron electric dipole moment experiment is clearly the most useful. However, both the neutron electric dipole moment experiment and the experiments on the nuclear matrix elements are essentially low energy tests and there is no a priori reason why any time reversal violation should be independent of energy. One must have a very specific model for any violation before extrapolating from one energy region or, indeed, from one type of experiment to another. Such detailed models await positive evidence of a violation.

Thus, we must view the high energy tests separately from those at lower energy. However, all three high energy tests are closely related. The experiment reported here is a direct test of T invariance in the γNN^* vertex. Barshay invokes a maximal violation of time reversal invariance in just this vertex in calculating the size of any expected effect for the $\gamma + d \rightleftharpoons n + p$ comparison. And the electron deuteron elastic scattering contains the same vertex, at least, in higher order diagrams. There are, however, relevant differences. The photon in the $\gamma + d \rightleftharpoons n + p$ comparison is real while we look for an effect which requires that the relevant photon be virtual. Real photons are purely transverse fields, while we measure possible interference between transverse and scalar components of the fields.

What can already be said is that the time reversal is not violated in a universally maximal fashion, even in the restricted area of the electromagnetic interactions of the hadrons. More subtle models of T violation will undoubtedly await more exact experimental evidence and, for that matter, positive evidence of a violation of time reversal.

CHAPTER 2 EXPERIMENTAL PARAMETERS, APPARATUS AND PROCEDURES

CHAPTER 2 EXPERIMENTAL PARAMETERS, APPARATUS AND PROCEDURES

2.1 INTRODUCTION

In this experiment, we measure the doubly differential cross section $d\sigma/(d\Omega_e dE')$ (Eq. 1.5) for inelastic electron scattering from polarized protons with both signs of polarization. Thus, the electrons scattered into our angular acceptance are detected and momentum analysed. The cross sections obtained are then used to compute the asymmetry due to any changes in cross section correlated with the proton polarization.

Since we are making an asymmetry measurement, stability is the all important feature in this experiment. Furthermore, not very great precision is required of the absolute numbers which are to be determined. The discussion in this chapter will reflect these two characteristics of asymmetry measurements.

For example, the solid angle, energy bite, and detection efficiencies need not be determined if they do not change. Since both cross sections in the asymmetry are measured with the same spectrometer and without changes in magnetic fields or typical scattering trajectories, the above factors cancel out of the asymmetry.

In this experiment, the final asymmetries are near zero relative to the statistical uncertainty. Thus, the normalization of the asymmetry is relevant to the uncertainty only. Since it is unrealistic to ask better than a 20% estimate of the uncertainty, the absolute normalization of the asymmetry need be no better.

To put it another way, one must first determine the existence or nonexistence of an asymmetry. Making the effort to get the normalization well known before its importance has been demonstrated may be a waste of time. In this experimental effort, the goal has been to search for a time reversal effect as soon as possible. Had such an effect been found, a large experimental program would have been called for to determine the nature of the effect. Among other things, a more exact normalization would be necessary. However, since the normalization is of limited value, we will concentrate on the stability of the apparatus in this discussion. The normalization will be discussed in Section 3.6.

The parameters we have mentioned so far are those which enter explicitly into the asymmetry calculation. Most of these explicit parameters cancel out of the asymmetry calculation if their value is stable. Another important group of variables are those which enter the asymmetry calculation only through the measured cross section, the implicit parameters. The unpolarized doubly differential cross section is a function of three independent variables. We monitored the physically measurable incident and scattered electron energies, E and E', and the electron scattering angle, $\bar{\theta}$. Since the cross section is a rapidly varying function of these implicit parameters, the stability of the implicit parameters must be even greater than that demanded of the cancelling explicit parameters.

The discussion in this chapter will deal first with the apparatus and explicit parameters, then with the implicit parameters, and finally with the method of data acquisition.

2.2 APPARATUS AND EXPLICIT PARAMETERS

a) Introduction.

Schematic views of the apparatus are shown in Figures 2.1 and 2.2.

An external electron beam (#8) of the Cambridge Electron Accelerator was directed at a target containing polarized protons. Charged particles scattered at forward angles to the incident electron beam were momentum analysed in a spectrometer consisting of a half-quadrupole magnet and 25 scintillation counters. Separation of electrons from other scattering products was accomplished with the combined use of a threshold gas Cerenkov counter and a lead-lucite shower counter. Only the scattered electrons were detected in this experiment. A discussion of the attempts at coincidence measurements can be found in the Appendix.

Data were stored, event-by-event, on magnetic tape using a PDP-1 on-line computer, which permitted experimental checks during data acquisition and detailed post-run analysis.

A complete description of the various elements of the electron detection apparatus, electronic circuitry and computer system may be found in the thesis of M. Goitein.[25] Those elements which changed from that earlier experiment will be discussed here.

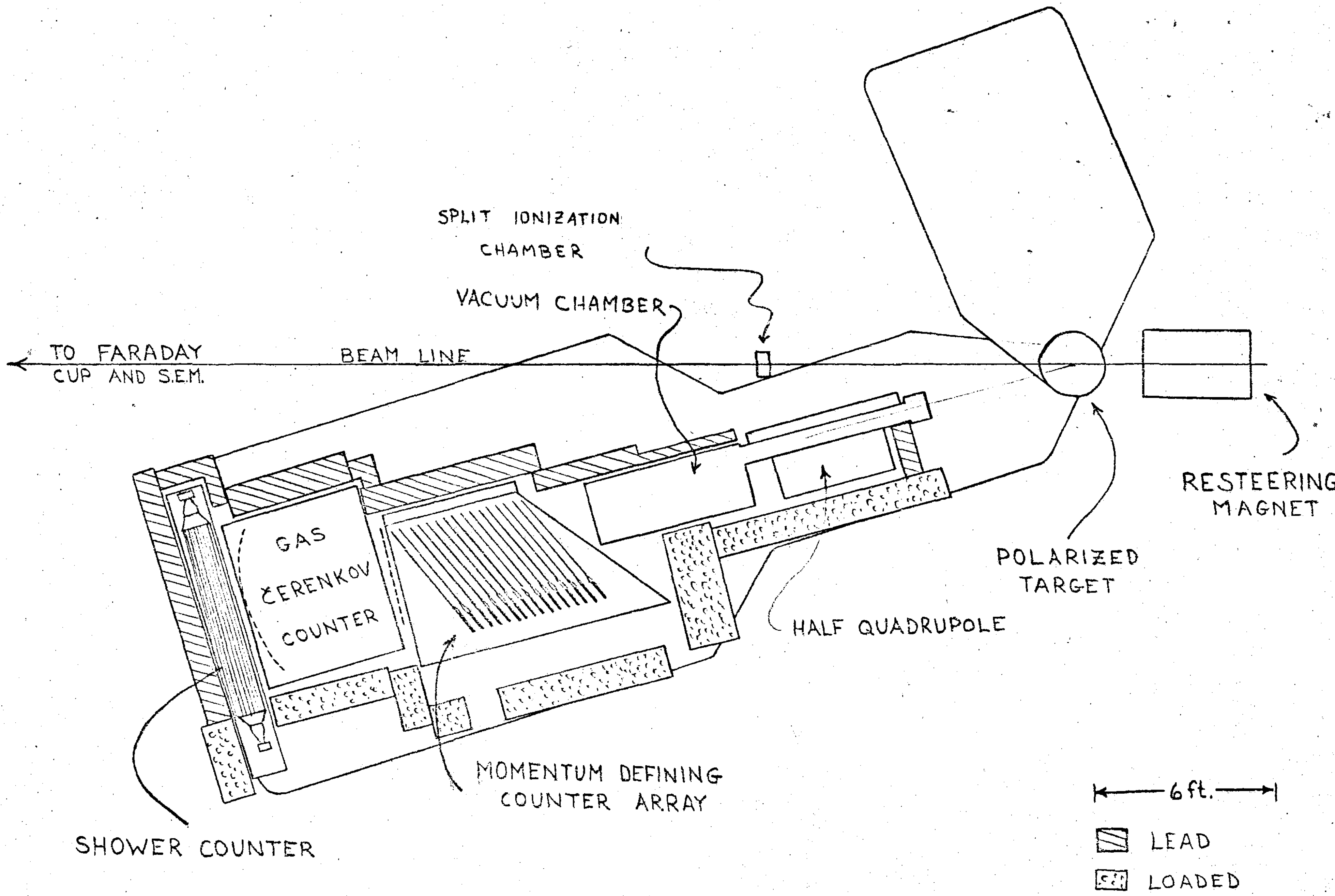

Figure 2.1

PLAN VIEW OF THE APPARATUS

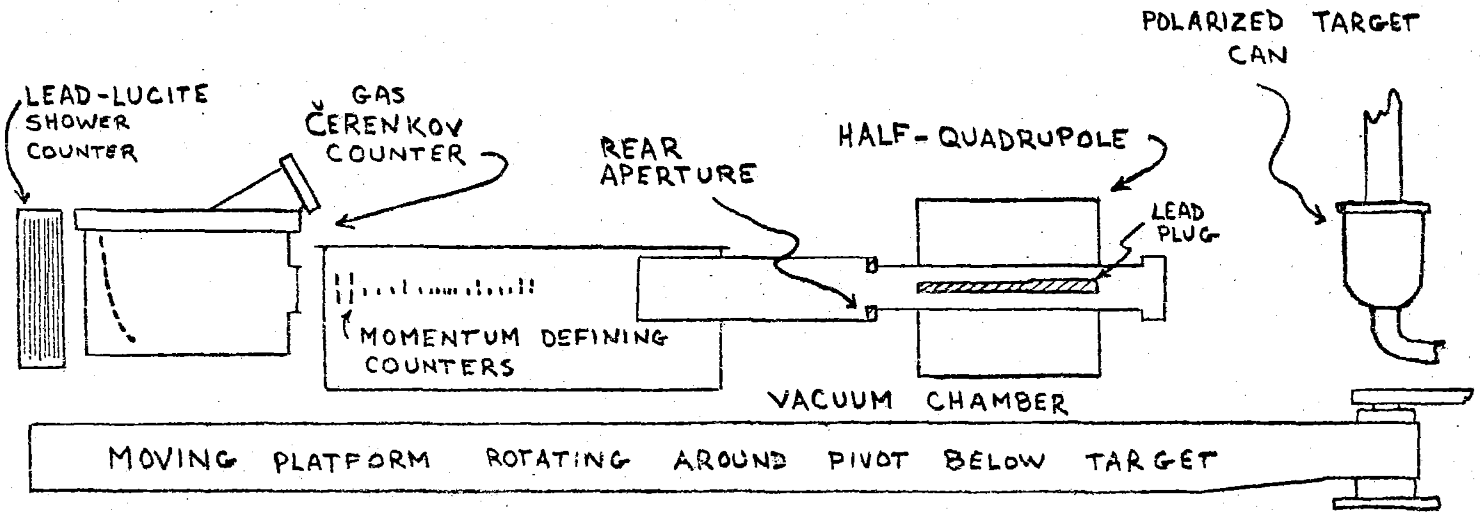

FIG. 2.2 SIDE VIEW OF THE APPARATUS

b) The Incident Electron Beam

1) The New Beam Line. The physical situation in this experiment differed from that of others performed with the same detection apparatus due to the high magnetic field associated with the polarized target. This magnetic field necessitated a resteering magnet in order to maintain the previous beam dump downstream of the target. See Figure 2.3.

In order to steer the beam into the Faraday cup (beam dump), a bending magnet was placed upstream of the target. Since the strength of the target field was fixed by the requirements of the polarization process, the beam line varied with the incident electron energy. The target was movable so that it could be positioned in the final adjusted beam line.

When the external beam was first brought out of the machine after a long period without beam, a standard procedure was followed. The procedure began with a request to the machine operations crew for a beam at the appropriate energy and corresponding to an extracted intensity of about 15 nanoamperes (which allowed for efficient use of the beam position monitors in the extracted beam transport system). The operations crew were instructed that the exact value of the energy was not important compared with the requirement of finding a stable setting of the machine

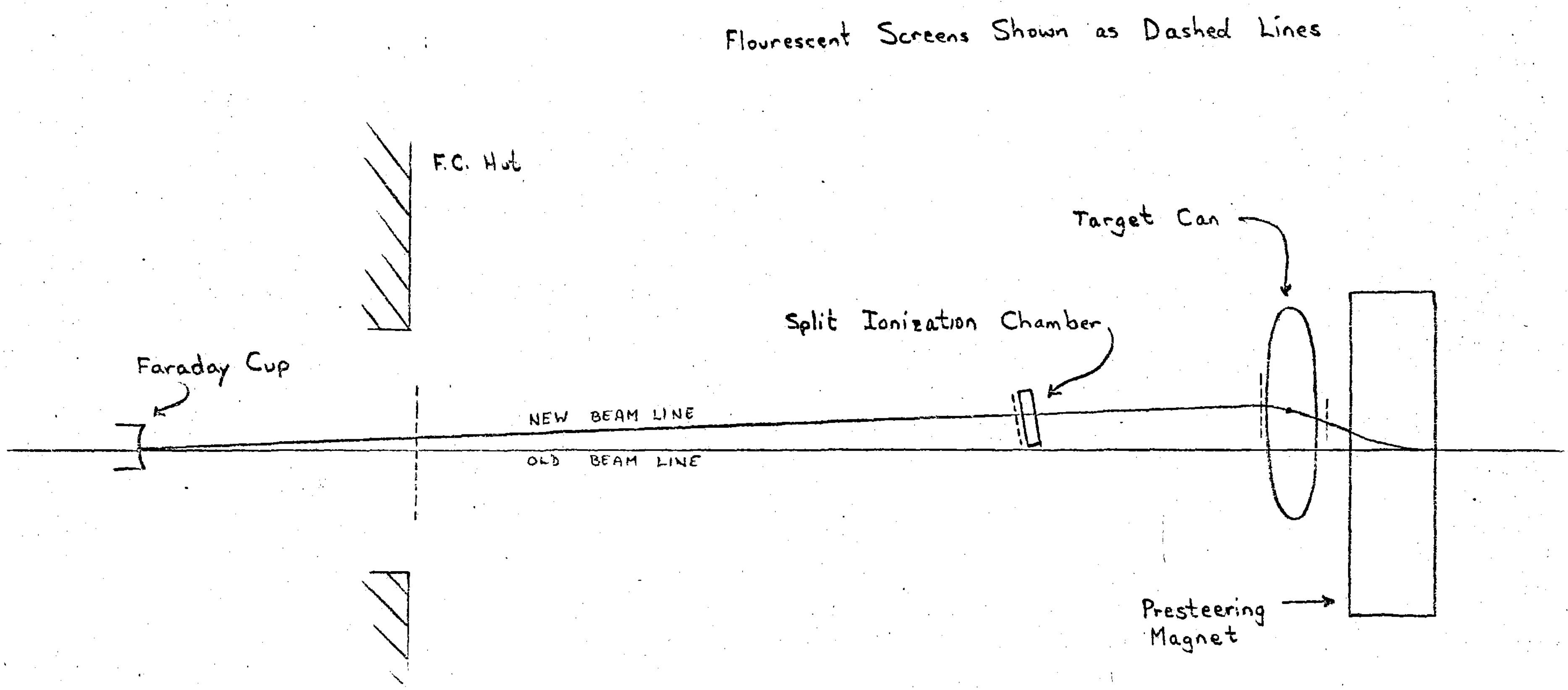

Figure 2.3

Schematic Lay Out of New Beam Line

parameters. When the machine was operating reliably, however, there was no inconsistency between obtaining a given energy and maintaining stability.

Once the stable internal beam was obtained, the beam was brought onto the floor through a transport system (#8) consisting of bending and quadrupole magnets. The beam was centered in the transport system by nulling a series of beam position monitors. This nulling procedure was designed to bring the beam onto the floor in the same way for every series of runs. When the beam was clean (without halo or tails), the monitors worked without ambiguity. At other times locating a null in several of the monitors was a problem. Eventual installation and use of beam clippers early in the transport system aided in cleaning up the beam sufficiently to center it without ambiguity.

It required about one hour to power the cryogenic magnet of the polarized target from zero to full field. In order to save machine time, the cryomagnet and presteering magnet were powered before the start of the run. Thus, the location of the beam line had to be known in advance. The target can was positioned so that the beam would go through the center of the can when the beam was first allowed into the experimental area. At first, improper account was taken of the difference between our "nominal beam line" marked on the floor of the area and the beam line as it actually would have been without the cryomagnet and presteering magnet. We were aided in understanding our error by the liberal use of scintillation screens in the beam line (Figure 2.3). These screens were viewed via closed circuit TV in both the counting room and machine control room.

We finally redeemed the situation by observing the shadow of a movable portion of the target on the target flourescent screen. A recognizable, irregular part of the central portion of the target was raised and lowered through the beam while sweeping the beam with the magnetic field of the presteering magnet. An iterative procedure of target can moves and electron shadowing brought us to an acceptable situation. The situation was less than perfect, however, due to slight differences in the emergent beam angle from one running period to another (probably due to differences in the central orbit in the machine).

After one series of runs, the mylar envelope holding the target material was displayed with a blur of radiation damage running along its center. Radiation damage to the target material was also visible as a blackening of the still frozen sample.

In the earliest runs, when confidence was lowest, the beam was allowed into the experimental area at a reduced pulsing rate to avoid producing large radiation levels on the floor. When we were satisfied that the target can was where it should be, the full sixty pulses per second (or whatever fraction of 60 we were allotted; never less than 7/8 of the full 60 for data runs) were used for final tuning of the beam position. Slight differences in beam position were noted as a function of pulsing rate when we were receiving less than half the total rate. Once the beam was set up, the intensity was lowered at the linear preaccelerator. No changes were made to the other machine transport or control systems.

2) Beam Focusing. The quadrupole magnets in the beam transport system allowed a choice of focusing properties for the extracted beam. When the beam was first set up, it was focused horizontally at the split ionization chamber and vertically just downstream of the target.

The choice of horizontal focusing was aimed at (1) keeping the current density low at the target in order to reduce depolarization effects and (2) minimizing the variations in scattering angle due to horizontal spread in the beam and fluctuations in the beam position at the target. See Sections 2.3c and 2.2c, respectively, for discussion of these points.

The choice of vertical focusing was designed to aid the resolution of the spectrometer system. The vertical dimension of the beam (beam height) contributes 2.3% FWHM to the resolution function per mm of beam height. Our beam height contributed about 3.5% in the middle of the momentum acceptance.

3) Beam Stability. Nowhere in the experiment does it appear that beam stability was a problem. Figures 2.4 to 2.7 show the machine parameters as recorded during the runs. See Section 3.4c for a discussion of the corrections due to the drifts in these parameters.

The position of the beam at the split ionization chamber is the best overall indication of the stability of both the dc and ac components of the accelerator system (Section 2.3c). Changes in ejection, for example, cause a change in the location and direction of the emergent beam. The beam is also sensitive to the central orbit in the machine. Since the beam position directly affects the scattering angle, to which the counting rate is very sensitive, it is necessary to monitor the beam position and correct for the effect of changes in the electron scattering angle. See Section 3.4b for the corrections and Figures 2.15 for the run to run stability of the scattering angle.

When short losses of beam (trip outs) occurred, the policy was to restart the machine as quickly as possible. The hope was to minimize the drifts associated with the trip out. Figures 2.4 to 2.7 show an apparent correlation between rf trip outs and changes in the frequency

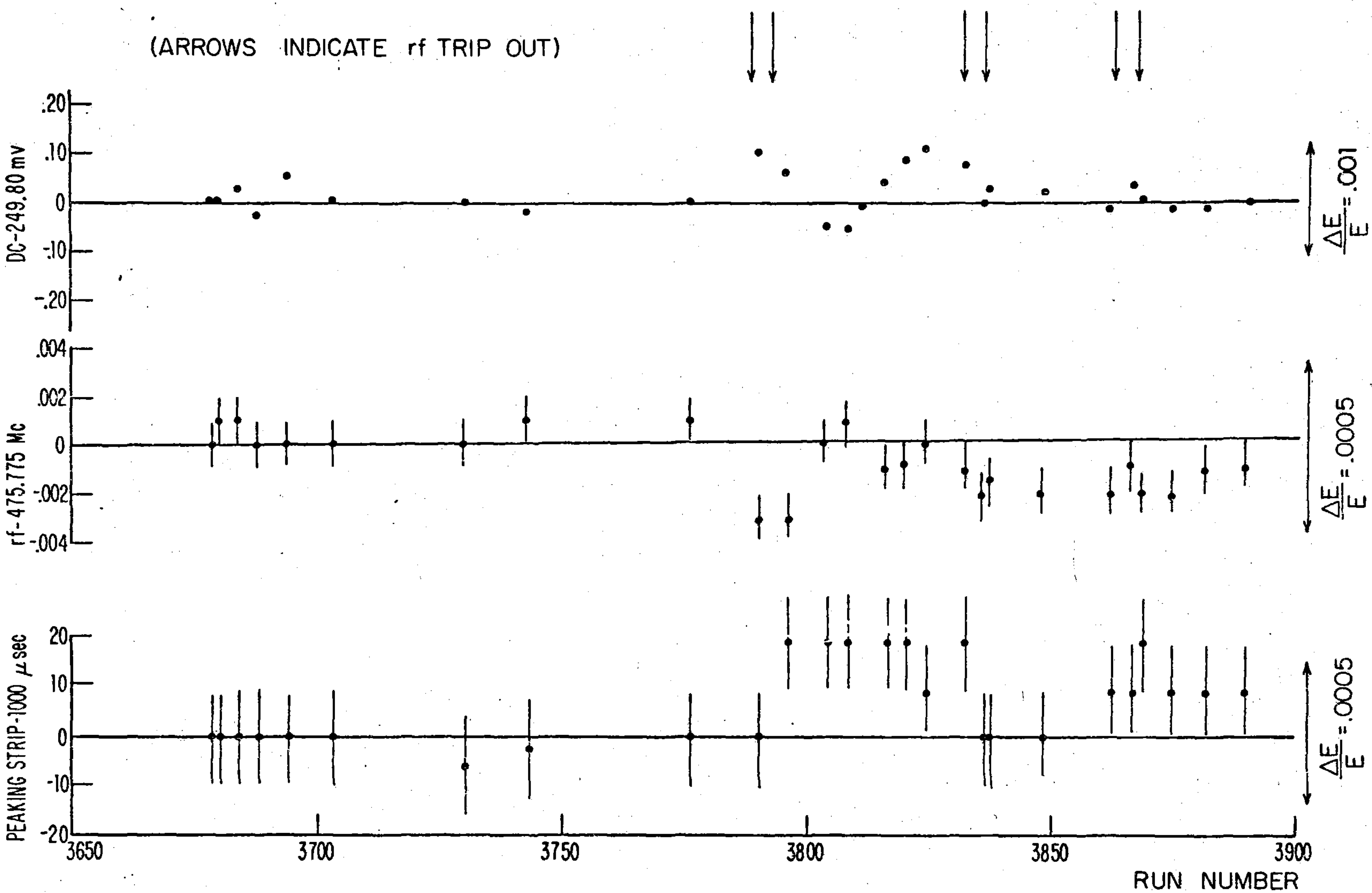

FIG. 2.4 LONG TERM DRIFTS IN MACHINE PARAMETERS, E = 4 GeV, $\overline{\theta}$ = 7.34°

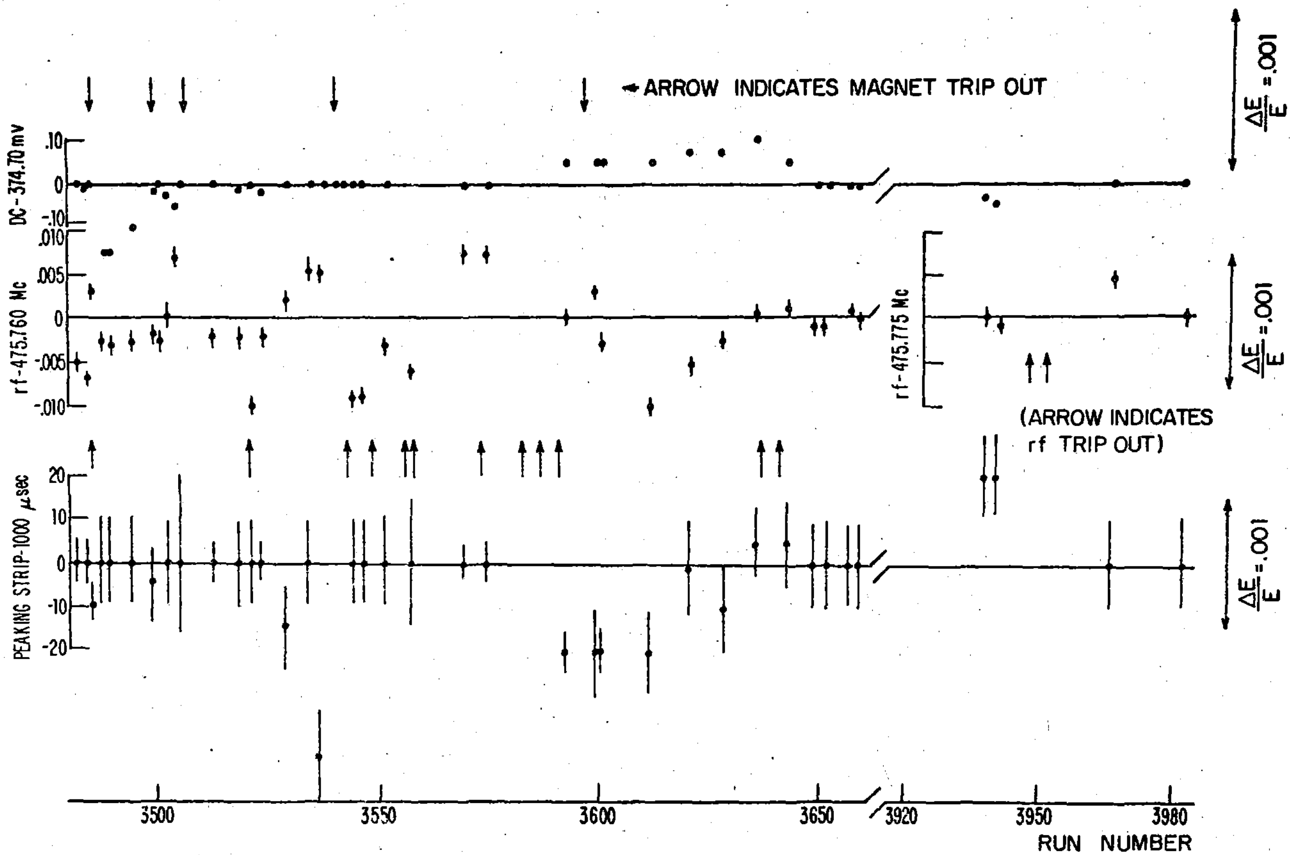

FIG. 2.5. LONG TERM DRIFTS IN MACHINE PARAMETERS, E = 6 GeV, $\bar{\theta}$ = 7.59°

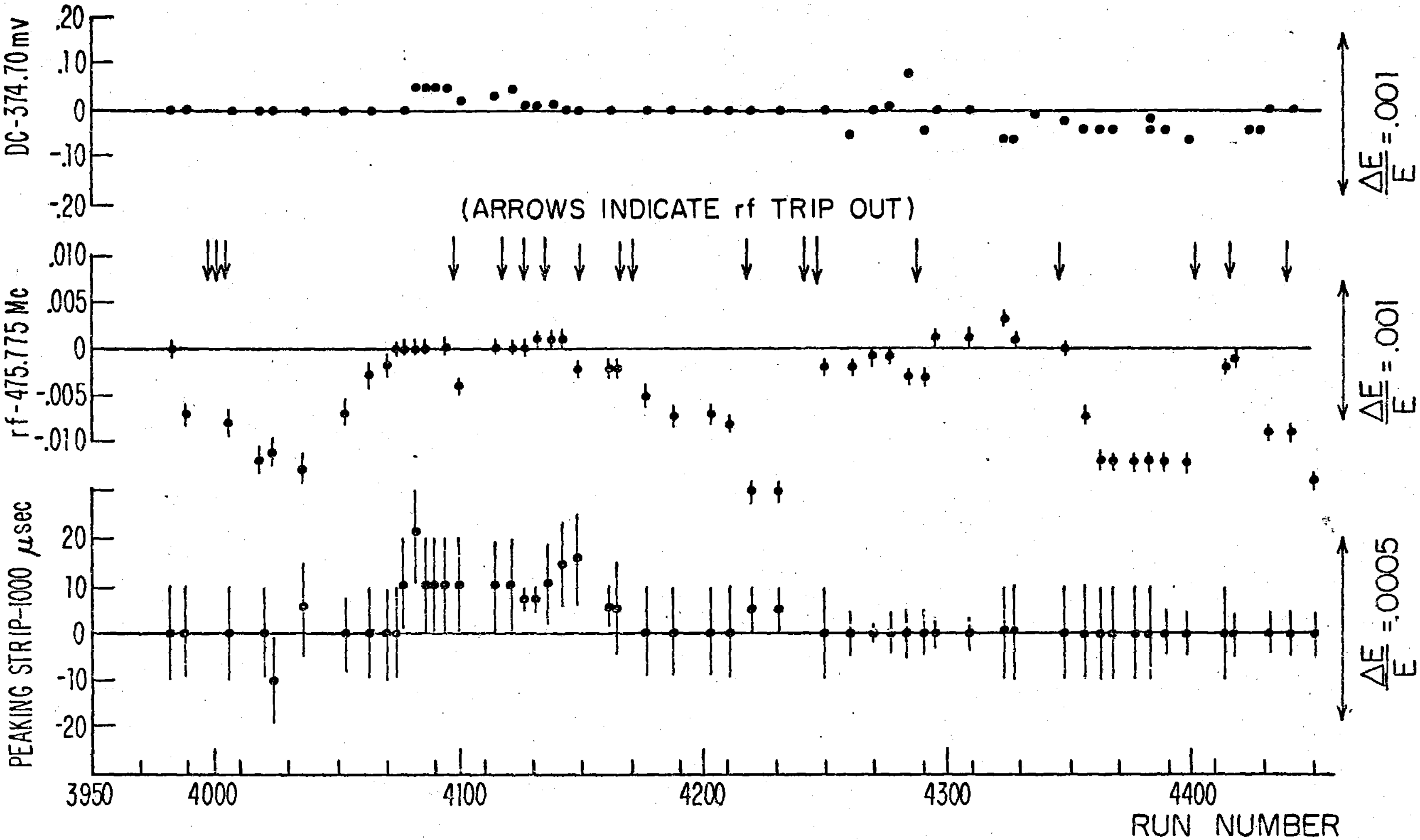

FIG. 2.6 LONG TERM DRIFTS IN MACHINE PARAMETERS, E = 6 GeV, $\overline{\theta}$ = 9.05°
PART 1

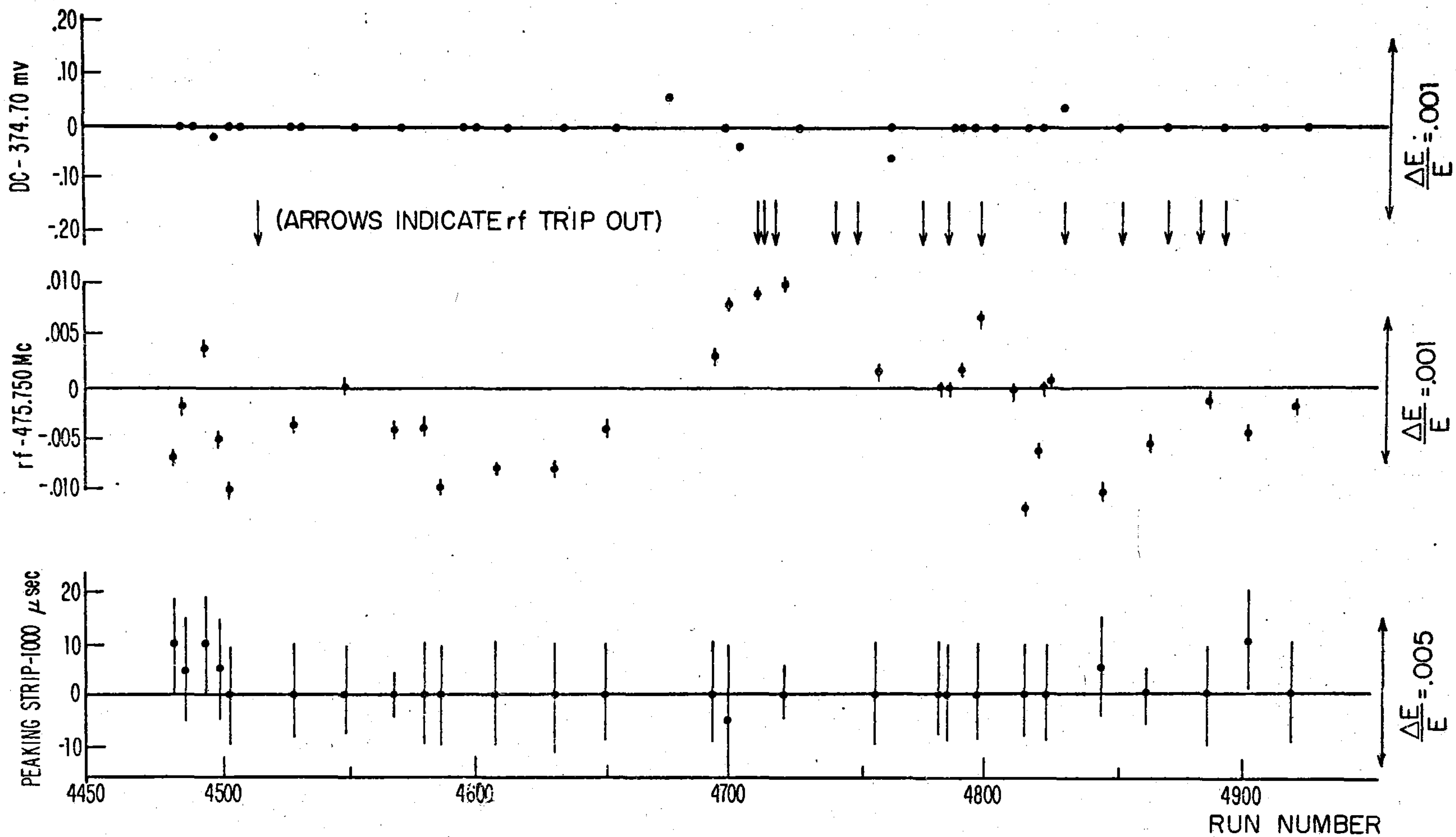

FIG. 2.7 LONG TERM DRIFTS IN MACHINE PARAMETERS, E = 6 GeV, $\bar{\theta}$ = 9.05°, PART 2

of the accelerator rf. This rf change leads directly to a change in the incident energy. Fortunately, even at the 6 GeV energy where rf drifts were at their worst, the drifts were too small to have an effect at our level of accuracy. In addition, we did not record the rf parameter often enough to allow corrections to be made to all the data. Very often the values were only recorded once between rf trip outs.

During rf trip outs, the temperature of the accelerator cavities was maintained artificially in order to maintain the cavity quality as it was before the trip out.

While at the high energy, the rf was the dominant instability in the machine. During the low energy runs, the dc magnet offset was not as stable as it should have been. But again, the instability was negligible at the level of accuracy of the experiment.

c) The Target

The major new feature of the apparatus for this experiment was the polarized target built by J. Chen, J. Sanderson, and R. V. Pound.[26] The operation of the target is described in the thesis of J. Chen.[27] Only a very brief description will be given here.

The target material was a mixture of ethanol and water doped with the paramagnetic material porphyrexide. The target was cooled to about 1° K with pumped liquid helium.

A pair of superconducting coils produced a uniform 25 kilogauss magnetic field at the center of the target. At these low temperatures and high magnetic field, the paramagnetic impurity is highly polarized ($\sim 88\%$). The free protons in the target are not significantly polarized since the proton magnetic moment is approximately 1/1000 that of the paramagnetic center. However, simultaneous spin flips of the free protons (those not bound to other nucleons) and the paramagnetic centers can occur. In fact, it is possible to saturate the transition causing these spin flips by applying a suitable rf siganl. Since the relaxation time of the free proton polarization is long compared to the relaxation time of the paramagnetic centers, it is possible to polarize many protons with a single paramagnetic center. Spin exchange among the free protons helps to propagate the effect of a single paramagnetic center beyond its own locale. Free proton polarization was typically 22% at the beginning of a data run. The polarizable protons are the nuclei of the hydrogen atoms in the target. Those protons in the heavier nuclei are unpolarized due to the difference in their environment (protons paired in the heavier nuclei result in zero net spin). The sample contained about 92% C_2H_5OH and 8% H_2O so that 23% of the protons or 13% of the nucleons were polarizable. The net target polarization is diluted by the unpolarizable nucleons. (See Section

3.6 for a calculation of the effective target polarization.)

Due to the radiation damage to the target, it was necessary to change frequently the section of target being irradiated. At the same time, it was necessary to maintain the target density for a pair of cross section measurements for each asymmetry determination. Thus, after every pair of runs, the target material was raised or lowered by remote control. This motion required only a few seconds and caused no change in the scattering geometry. The targets were generally operated until the polarization was reduced to 60% of the original polarization.

The difference in polarization for the spin up and spin down cross section measurements enters the asymmetry as a normalization factor and had to be measured.

The net target polarization was determined (Section 3.6f) from the free proton polarization which was measured using the proton magnetic resonance signal. The absolute free proton polarization was determined by normalizing the polarized proton signal to the thermal equilibrium proton signal. A discussion of the free proton polarization measurement is given in the thesis of J. Chen.

The average free proton polarization over the entire sample was monitored. Thus, a geometrical correction always had to be applied in order to determine the fraction of target already irradiated. The average polarization in the irradiated section was calculated from the initial and final polarizations thus obtained. The polarization monitor had a long time constant and could not be used to monitor the instantaneous polarization, even of the total sample.

Localized beam heating effects were checked by covering the entire target with beam at the same local current density as was used during the data acquisition. This was accomplished by defocusing the beam and increasing the beam intensity appropriately. Temporary depolarizations were observed, but only at much higher current densities than used for data acquisition. These polarization effects are associated with heating of the target by the beam at a rate greater than could be handled by the helium cooling system.

d) Detection of Scattering Events of Interest.

1) Momentum Counters. The scattering events of interest are those in which an electron of appropriate energy is scattered into the angular acceptance of the apparatus. The first element of an interesting event is a charged particle crossing the focal plane of the half-quadrupole magnet in the appropriate region behind the magnet. A side view of the counters used to establish such a crossing is given in Figure 2.8. A combination of one or more

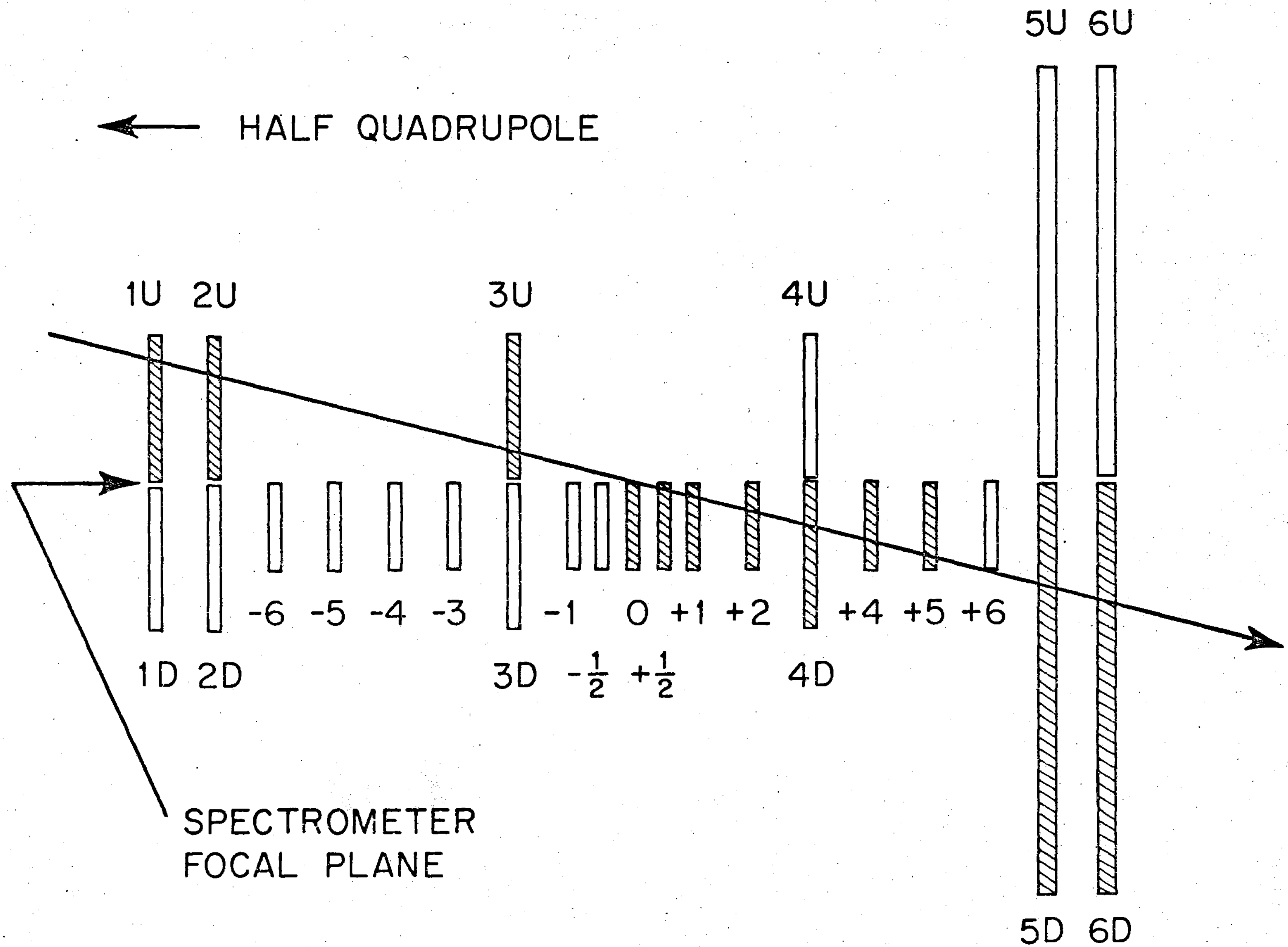

FIG. 2.8

TYPICAL UD TRAJECTORY IN MOMENTUM COUNTERS of the front "up" counters (1U, 2U, 3U, and 4U) with one or both of the back "down" counters (5D and 6D) indicated the possibility of a charged particle crossing the focal plane from top to bottom. Similarly, a coincidence of one or more of the front "down" counters with one or both of the back "up" counters indicated the possibility of a crossing from under to above the focal plane. These two possibilities, referred to as UD and DU trajectories respectively, are the only possibilities since the center of the magnet was plugged.

For every particle focused between 2U(2D) and 5U(5D) at least two up and two down counters should fire. Thus, the triggering system is insensitive to inefficiencies in any one counter or uncorrelated inefficiencies in several counters. This feature was useful here to guard against changes in triggering efficiencies. The acutal efficiency of course, is not particularly important, since the only real requirement of the system is that it select an unbiased sample of electrons with constant efficiency.

The stability of the momentum counters was determined from the inefficiency and overefficiency tests[28] during reanalysis. Inefficiencies were generally less than 1% and overefficiencies, less than 2% except for the 3U, 4U, 5U, and 6U counters which had an extra 3% correlated overefficiency due to recoiling particles from scatterings of the primary scattered electron in the earlier counters.

No changes were observable in the inefficiencies within the statistics of the test and overefficiencies varied about 20 to 30%. The effect of these overefficiencies is primarily a matter of momentum resolution. See Section 2.3d.

An additional feature of this triggering system gives it added flexibility. If one wants to limit the size of the momentum bite accepted, one can remove the 1U, 1D, 2U, and 2D counters from the trigger. Then, only those particles which cross the focal plane between 3U(3D) and 6U(6D) should lead to a trigger. This feature of the apparatus was used in the data runs at the first resonance region. In that case, the scattered electron energy led to a larger momentum acceptance than desired. When the modified trigger was used, 2.6% of the triggers fell into the region before the 3U(3D) counter compared to 31% with the normal full trigger. This triggering rate below the nominal momentum bite is a reflection of the overefficiencies in the 3U(3D) and 4U(4D) counters and agrees with the measured overefficiencies.

Of course, the redundancy of the triggers for particles focused between 3U(3D) and 4U(4D) is lost for the modified trigger.

A more definite identification of the trajectory can be made for those events which are recorded on magnetic tape by the on-line computer. A distinct pattern of counters on and off is associated with each actual trajectory. A typical central trajectory is shown in Figure 2.8. A pattern is designated by the code 00 if it had no apparent excess counters firing in the region where no counters should fire and no counters off where all should be on. A perfect pattern (00) except for one apparently excess counter firing is designated 01 and a perfect pattern except for one apparently inefficient counter, 10. Similarly, the code 11 signifies one excess and one missing counter. The momentum associated with the lowest code is assigned to the event. See Table 2.1 for the density of events by momentum definition code. The data reported in this thesis include codes 00, 01, 10, 02, and 11. A check of the asymmetry for just the first three codes is given as well. See Table 4.2. The asymmetry is clearly not sensitive to the exact code acceptance since the low codes contain a reasonable sample of scattered electrons. We prefer to use codes 00 through 11 as the set least sensitive to instabilities due to changes in random counts and general system preformance while still providing a good sample of true scattered electrons. See Figure 2.17 and Table 2.1.

An ambiguous identification occurs when two different momentum designations fit an event equally well. These events were usually associated with the bins were an excess count was observed in one or another of the "up" counters in the middle of the momentum bite. These events are included in the full resonance region results, but not in the individual bin results. To include ambiguous

TABLE 2.1

MOMENTUM IDENTIFICATION CODES+

$\bar{\theta}_e$ \ CODE	00	01	10	02	11	12**	20	21	22**	77*
7.34	62	13	4	6	1	4	0	0	2	7
7.59	62	10	4	6	0	7	0	0	1	8
9.05	58	11	3	6	1	6	0	0	4	11

+Expressed as % of all triggers above minimum Cerenkov and shower counter pulse heights

*Non-analysable events (not fitting into earlier codes).

**85% of code 12 events and 80% of code 22 events appear in the end bins which were never used for data.

events in the individual bins would require hand scanning of each event or, at least, of a large fraction of the events. Little gain in accuracy would have been obtained by such scanning since the fraction of ambiguous events in the bins involved was on the order of 10% .

2) Cerenkov and Shower Counters. The possibility of random double coincidences causing a trigger was greatly reduced by the Cerenkov and shower counter requirements in the trigger. These counters were used to identify the electrons which crossed the magnet focal plane. Figures 2.9 and 2.10 show the pulse height spectra in each of these counters along with the triggering pulse height and the pulse height required of events in the final analyses. Coincident large pulses in each of these counters serve as a firm identification of an electron. In order to check for charged pion contamination, asymmetry analyses were carried out for several different Cerenkov and shower counter biases. No significant changes were observed in the asymmetry measurements. See Table 4.1.

From the spectrum of pulse heights in the shower counter it is easy to see that slight shifts in gain would have a significant effect on the triggering efficiency, especially for the runs at the first resonance. The stability of the peak location and, we conclude, of the gain of the shower counter system was about 0.5 channel over the course of an

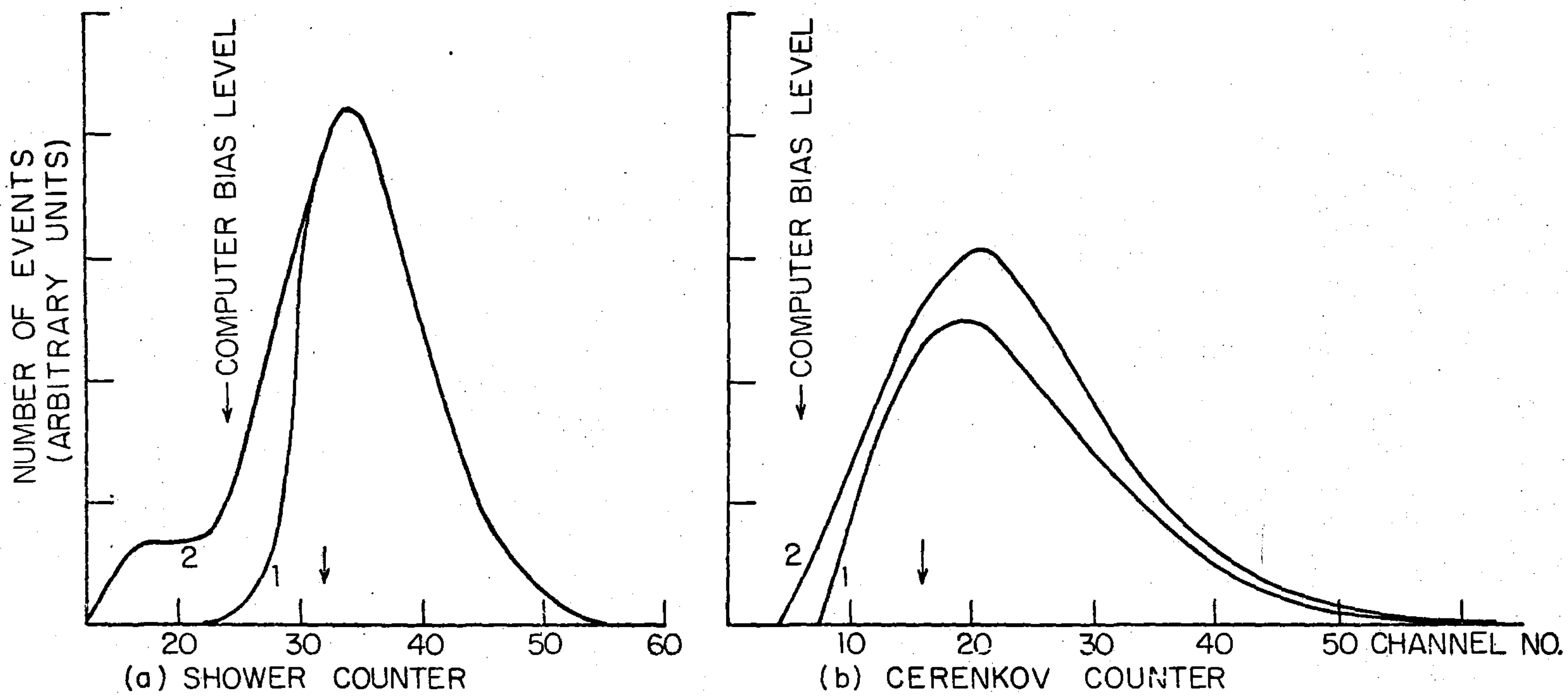

FIG. 2.9 SHOWER AND CERENKOV COUNTERS: TYPICAL SPECTRA FOR LOW ENERGY RUNS, $\bar{\theta}=7.34°$

1. Trigger configuration for data acquisition
2. 6dB removed from before Shower Counter Discriminator and
4dB removed from before Cerenkov Counter Discriminator

High Bias Level Analyses used levels indicated by unlabeled arrows.

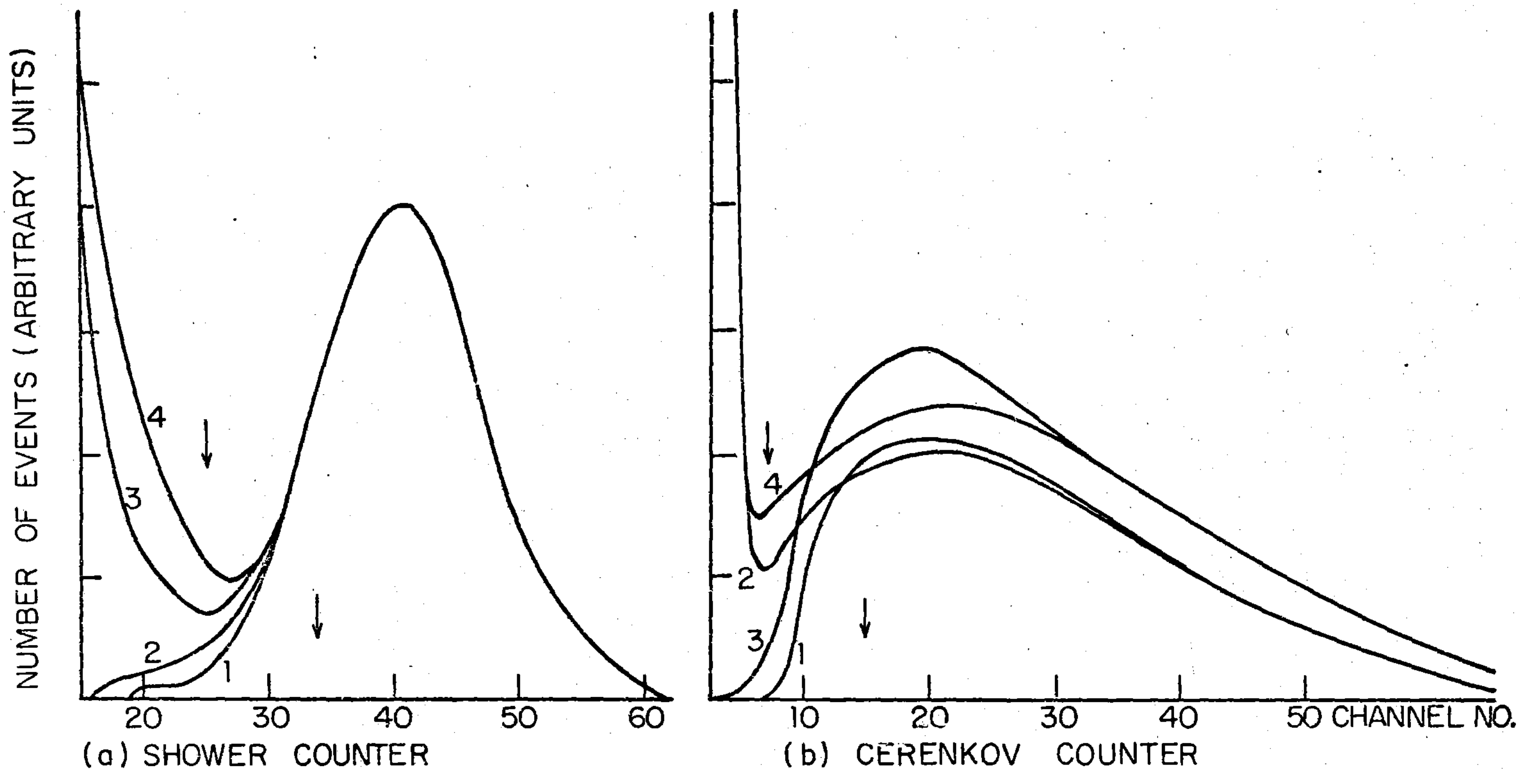

FIG 2.10 SHOWER AND CERENKOV COUNTERS TYPICAL SPECTRA FOR HIGH ENERGY RUNS

1. Both shower and Cerenkov counters required in trigger (Configuration for Data Acquisition at $\bar{\theta}=9.05°$)
2. Only the shower counter requirement in trigger (Configuration for Data Acquisition at $\bar{\theta}=7.59°$)
3. Reduced (6dB) shower counter requirement in trigger.
4. Reduced (6dB) shower and no Cerenkov counter requirements in trigger.

High Bias Level Analyses used levels indicated by unlabeled arrows.

hour. At the first resonance where we were particularly intent on avoiding useless computer triggers, the shower counter discriminator cut significantly into the otherwise acceptable spectrum. From Figure 2.9a, we estimate that over a pair of data runs, the triggering efficiency was only stable to

$$(0.5 \text{ channel/hour})(\tfrac{1}{6} \text{ hour/run pair})(\tfrac{1}{15} \text{ of events}) = 0.6\%/\text{run pair}$$

This is the largest instability at the first resonance for which we do not make any corrections. We trust to the ordering of data acquisition (Section 2.4) to average the effects of these efficiency drifts.

In the higher resonance region runs, the discriminator cut much less severely into the spectrum of otherwise acceptable events. The stability was correspondingly better; i.e., 0.13% per pair of runs. The additional uncertainty due to instability of the computer bias level is insignificant since the computer discrimination level is applied to such a small fraction of the remaining events.

Although the shower counter had eight photomultipliers viewing the lucite sheets, the total system was not entirely free of dependence on the gain of a single photomultiplier. The counter was 35.5 by 44 inches so that the light from a given shower was detected primarily by two of the phototubes. Furthermore, the signals were added actively on the experimental floor. Thus, stability checks on individual phototubes was not possible. Regional checks of uniformity and stability were made by looking at UD (or DU) trajectories which counted in the right or left hand angle counters (counters placed in front of the Cerenkov counter, but not used in this experiment other than for the above checks).

At the high scattered energies detected in this experiment (3.3 to 5.1 GeV), the threshold gas Cerenkov counter could not be operated at near 100% efficiency for electrons and still reject pions. The electron inefficiency of the Cerenkov counter at the higher energies is clear from Figure 2.10b. Nevertheless, the Cerenkov counter was used in the trigger for nearly all of the data except at $\bar{\theta} = 7.59^{\circ}$.

The same stability problem exists for the Cerenkov counter as does for the shower counter. From Figure 2.9b, we conclude that for the first resonance region runs, the Cerenkov counter efficiency was high enough that there is no problem of large numbers of pedestal counts being good events if included. Furthermore, the slight shifts in gain are negligible since the discriminator cut off operates on such a small fraction of the events. Thus, the use of the Cerenkov counter in the trigger served to insure the acceptance of only electrons without adding significant uncertainties due to trigger instability. At the higher energy runs, the problem of Cerenkov counter instability enters at the trigger level ($\bar{\theta} = 9.05^{\circ}$) or at the computer reanalysis level ($\bar{\theta} = 7.59^{\circ}$). Even if we ignore the statistical fluctuations caused by the true electron pedestal events and the random rate probability of pedestal events appearing in the accepted sample, it is difficult to estimate the size of the potential instability. However, we believe that any instabilities are less than 1% over the course of a pair of runs and, as was the case for the shower counter instability in the lower energy runs, trust to the ordering of data acquisition to average out the effects of these efficiency drifts.

Both the shower and Cerenkov counters had considerably wider pulses than the momentum counters. However, the randoms rates in shower and Cerenkov counters were only about 0.3% and 3% respectively. Shifts in the randoms rates were on the order of a factor of two over the course of a weekend of data acquisition. No corrections were applied for such shifts.

3) Prescaling Device. During the runs in the region of the first resonance, a prescaling device was used to reduce the number of potential triggers which reached the

computer. Even at the low beam intensity used, the data rate was high enough that the computer limited the rate of data recording. Thus, the bulk of the data at the first resonance was taken with triggers sent to the computer only for every other potential computer trigger. The reduction in statistical uncertainty with this method of data acquisition is discussed in Section 3.2b.

e) Aperture and Solid Angle.

The aperture was determined at various places beyond the beginning of the magnetic field of the half-quadrupole magnet.[29] The effective geometrical aperture was determined with the use of a computer program (incorporating the CERN subroutine DIFSL4). The target field was approximated by the field of a pair of 9.92 inch diameter Helmholtz coils. It was normalized to the value measured at the center of the target. The results of the ray tracing were also used to determine the physical scattering angle. This result was checked with a geometrical reconstruction using the effective geometrical aperture and making a geometrical correction for the difference in the momenta of the incident and scattered electrons.

The reported scattering angles, $\bar{\theta}$, are weighted averages of the scattering angle across our electron aperture. The weighting function was the elastic electron-proton scattering cross section. The corrections in the scattering angle for each run which were calculated from the output of the split ionization chamber were applied to these angles, $\bar{\theta}$. See Table 2.2 for the scattering angles before and after weighting.

For the scattered electrons, the cryomagnetic field and the target displacement caused a change in the effective aperture from that of the previous experiments with the same spectrometer. The target displacement was particularly important in the 4 GeV runs. In that case, the target was moved beyond the plane of the inside of the flux return piece of the half-quadrupole magnet. The aperture was reduced by 18% relative to the 6 GeV points and 21% relative to the same system without the extra target field and displacement. See Table 2.2.

In spite of this sensitivity to the average position of the scattering center, the slight run to run changes in beam position and direction made only a negligible effect on the solid angle acceptance and, therefore, the measured cross section. No corrections were made for this effect.

f) Incident Charge.

The primary monitor of the incident charge was the Faraday Cup (FC) which also served as the beam dump. The charge collected on the Faraday Cup was discharged by

TABLE 2.2

APERTURE AND SCATTERING ANGLE PARAMETERS

Nominal Floor Angle (degrees)	Geometric Central Angle (degrees)	Weighted Angle $\bar{\theta}$ (degrees)	Incident Energy E (GeV)	Target Displacement (inches)	$\Delta\Omega_e$ (UD + DU) (mstr.)
7.00°	7.54	7.34	4	$2^{15}/64$	1.43
7.86°	7.85	7.59	6	$1^{38}/64$	1.71
9.22°	9.33	9.05	6	$1^{38}/64$	1.71

depositing known amounts of positive charge onto the cup to keep the voltage of the cup at ground.

Past experience with the Faraday cup system indicates that its stability is at least as good as 0.1% over the period of a pair of runs. The stability of the absolute calibration of the integrators was 0.1% over several months.[30]

The duration of each data run was determined by the accumulation of a preset quantity of charge in the Faraday Cup. This was achieved by using a mechanical preset register and, thus, no polarization dependent bias was introduced in the amount of incident charge accumulated for each run. However, we used the measured incident charge for all asymmetry determinations.

A secondary emission monitor (SEM) was placed just upstream of the Faraday Cup hut. This served as a secondary monitor of the incident charge, but was much more sensitive to spray, beam halo, and material in the beam line. Nevertheless, the stability of the ratio of the FC/SEM outputs may be taken as a limit on the FC stability. Previous tests[31] with negligible material in the beam line gave stability of 0.2% for ten minute periods. In this experiment, the ratio was stable to about ½% over the same period.

The aperture of the SEM was larger than that of the

FC. A substantial change in the ratio FC/SEM would have indicated changes in the beam line. No such changes were observed from this ratio.

g) System Improvements.

1) The Counters. Several slight changes were made to the apparatus for this experiment in the general program of system maintenance. In addition to the usual replacement of crazed scintillators and noisy photomultipliers, the lucite light guides for the momentum counters were almost all replaced. The new guides had less than 1/6 the bulk of the former guides and were nearly adiabatic in mapping the scintillator edge onto the surface of the photomultiplier. The reduced mass led to fewer conversions of photons in the guides and less Cerenkov light production. Since the gain of each photomultiplier was raised in order to be efficient in seeing minimum ionizing particles at the far end of the scintillator, the proximity of the Cerenkov light produced in the light guides might easily make up for the reduced intensity of the light and produce random counts. Since the amount of spray in the entire system was greater for this experiment than for any of the earlier work with this apparatus (see Appendix, Section A5), this light guide improvement may not have been negligible.

The improved light collection resulting from the improved design also allowed reduction of the gain on most of the phototubes. The improvement in light transmission was as much as 70%.

The active addition of the signals from the eight shower counter photomultipliers on the floor was another improvement. This change from the former system of passive addition of the signals allowed the timing to be done correctly, reduced the impedance mismatch in the addition, reduced the width of the summed pulse, and, therefore, permitted closer timing and more uniform risetimes for the various parts of the counter.

2) The Logic Circuitry. In order to decrease the intensity dependences in the detection apparatus, two logic circuit changes were incorporated. First, the 4U and 4D counters were added to the trigger as discussed above (Section 2.2d). Secondly, the momentum trigger counters were actively added in Chronetics 118D units for use in identifying crossings of the magnetic focal plane. These units replaced the Chronetics "or" circuits and eliminated their dead time effects.

The use of 100 Mc scalers to monitor the trigger rate was introduced for this experiment. This improvement is discussed in Section 2.3d.

<u>3) The Computer Program.</u> In order to decrease the time lost in data recording, new options were written into the PDP-1 computer program which allowed reduced analysis at the time of data acquisition and attempted to reduce the time lost to running off tape and other problems of imperfect communication between experimenter and computer.

2.3 IMPLICIT PARAMETERS

a) The Incident Electron Energy.

The incident electron energy was controlled by the operators of the CEA. Frequent reports of the parameters[32] which affect the incident energy were requested from the operations engineers. In terms of these parameters, the incident energy of the emergent beam is given by

$$E = \frac{dc}{62.455}\left(1+\frac{\omega^2 T^2}{8}\frac{\Delta T}{T}\right)\left(1-\frac{1}{\alpha}\frac{\Delta\nu}{\nu}\right)\left(1-\frac{\omega^2(\Delta t)^2}{4}\right)$$

$$= \frac{dc}{62.455}\left(1+0.0178\frac{\Delta T}{T}\right)\left(1-\frac{1}{0.031}\frac{\Delta\nu}{\nu}\right)\left(1-\frac{142129}{4}(\Delta t)^2\right)$$

where

T = peaking strip separation in μsec

ΔT = difference from 1000 μsec of T

$\omega = 2\pi\ 60 \times 10^6 = 376.99 \times 10^6\ \mu\text{sec}^{-1}$

dc = dc millivolt reading from shunt

ν = 475.700 Mc

$\Delta\nu$ = frequency difference from 475.700 Mc

Δt = spill time measured from B_{max} (sec)

α = momentum compaction factor[33]

All these parameters except Δt were recorded as reported by the operations engineers. See Figures 2.4 - 2.7. The absolute value of the energy was calculated from the parameters as reported.

The slight run to run <u>variations</u> in incident energy, however, were determined from a nearly independent energy measurement. This measurement uses the average magnetic field in the ring at the time of each event and combines the effect of the dc magnet offset and the last parameter, Δt. One complication arose due to the fact that, for most of the data, the field sampling unit, an integrating device, was triggered from B_{min} rather than from the zero field. Thus, it was necessary to assume a value for the peaking strip separation in order to use the recorded data. We assumed that the peaking strip separation was a constant 1000 μsec for ease of calculation. No significant error arose from this approximation.

The corrections applied due to variations in the incident energy as calculated from the average magnetic field and the rf frequency shifts are discussed in Section 3.4c. No corrections were applied for the variation in the peaking strip separation. See Figures 2.4 - 2.7.

<u>b) The Scattered Electron Energy, E'</u>

The scattered electron energy was determined by the half-quadrupole magnet and counter system. The regulation of the magnet was usually much better than 0.1% over the course of several runs. Furthermore, the spectra were relatively flat (Figures 2.11) and slight shifts in spectrum position in the counter system would not lead to noticeable asymmetries. No corrections were made to the cross sections due to changes in the scattered electron energy.

The spectra of Figures 2.11 make use of the energy widths of the momentum bins defined by the counter system. No new calibration of the bin widths was made for this experiment. The widths used are those of the most recent calibration. A discussion of the method of calibration can be found in the thesis of C. Mistretta.[34] The relative uncertainties in the bin widths are about 5%.

The 25 slat counters which determine the momentum bins were tilted in the horizontal plane to allow for the variation in scattered momentum across the aperture for a constant value of K, the equivalent photon energy. The corrections to the calibration due to variation in the counter bank tilt were applied to the spectra of Figures 2.11.

The value of the centrally focused energy was slightly different from that of previous calibrations of the spectrometer due to the displacement of the target. The corrections due to this effect were less than 0.13%.

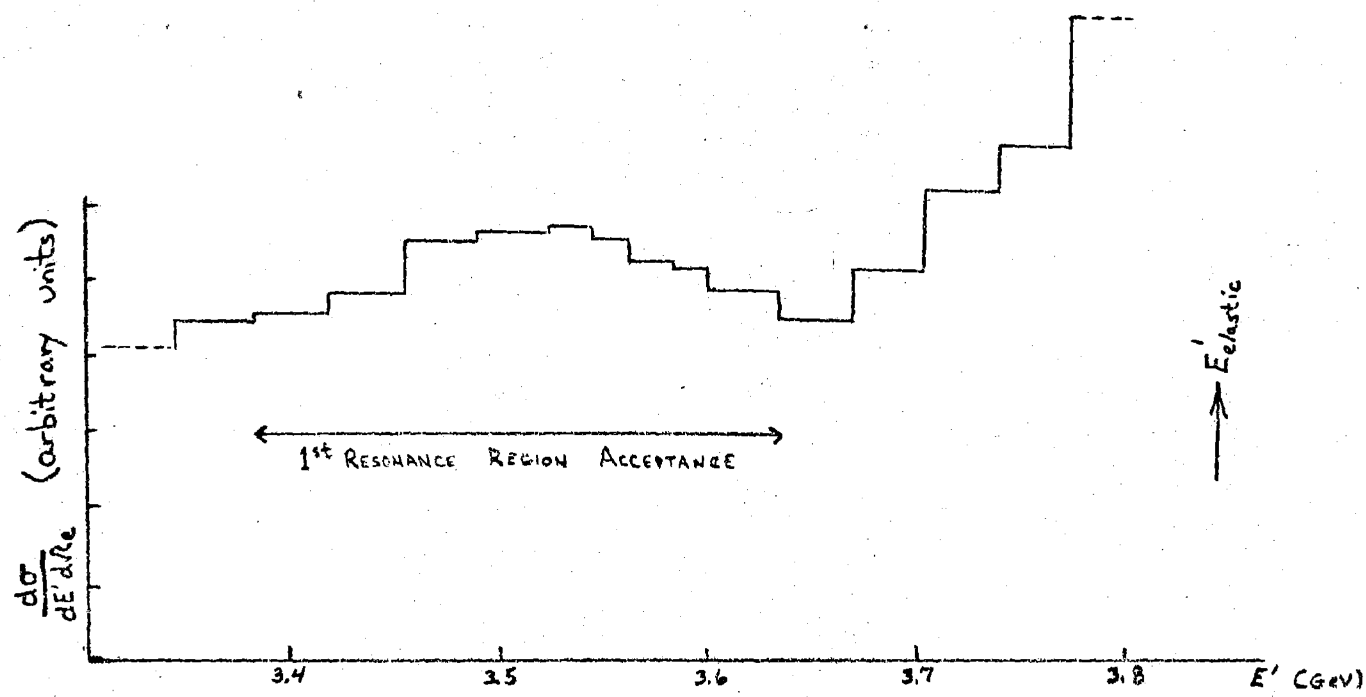

FIG. 2.11a SCATTERED ELECTRON SPECTRUM: E = 4 GeV, $\bar{\Theta} = 7.34°$
Data with regular trigger. Relative Bin Size Uncertainty = 5%

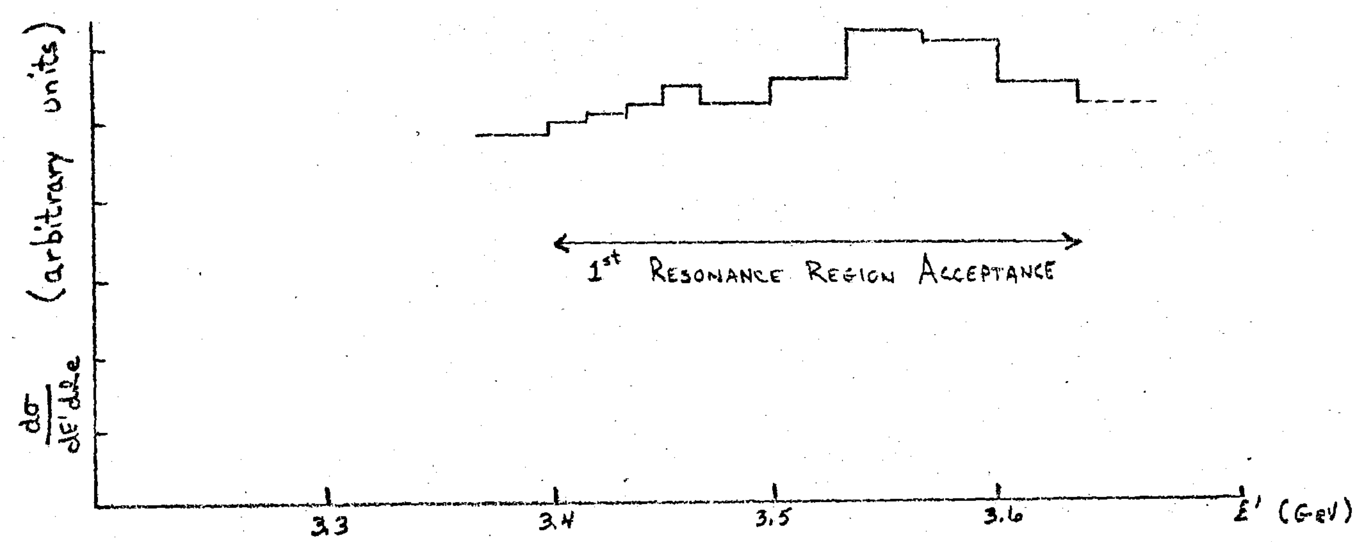

FIG. 2.11b SCATTERED ELECTRON SPECTRUM: E: 4 GeV, $\bar{\Theta}$: 7.34°
Data with modified trigger. Relative Bin Size Uncertainty: 5%

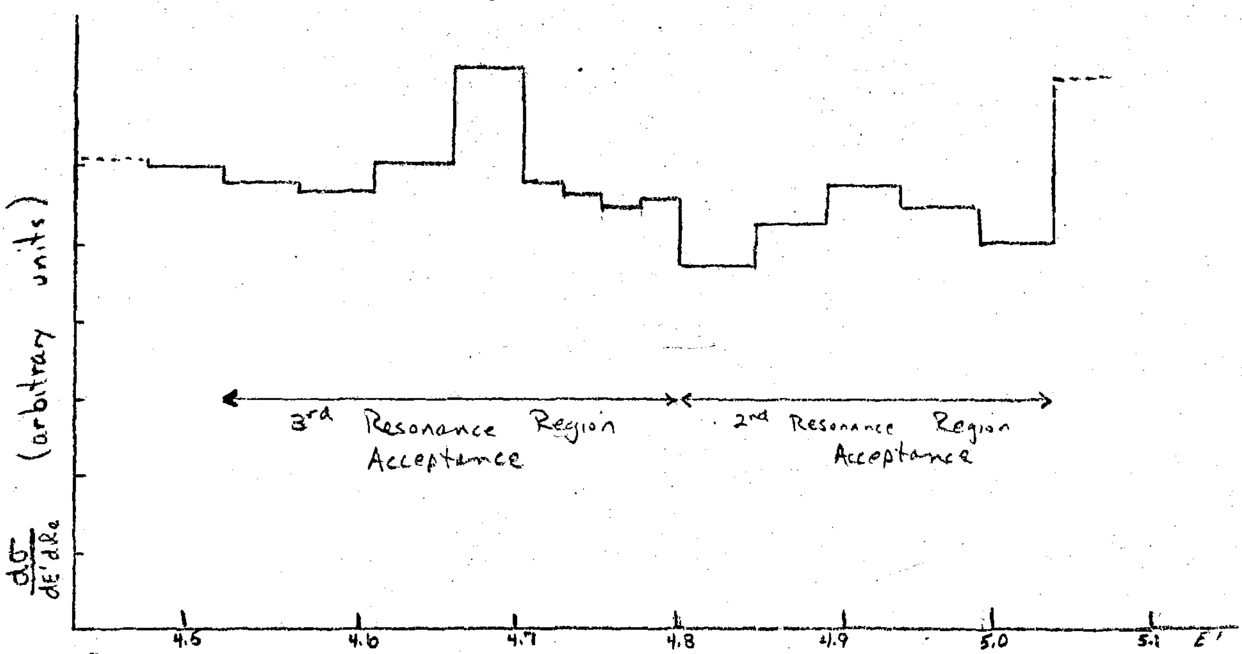

FIG 2.11c SCATTERED ELECTRON SPECTRUM: E = 6 GeV, $\bar{\Theta} = 7.59°$
Relative Bin Width Uncertainty = 5%.

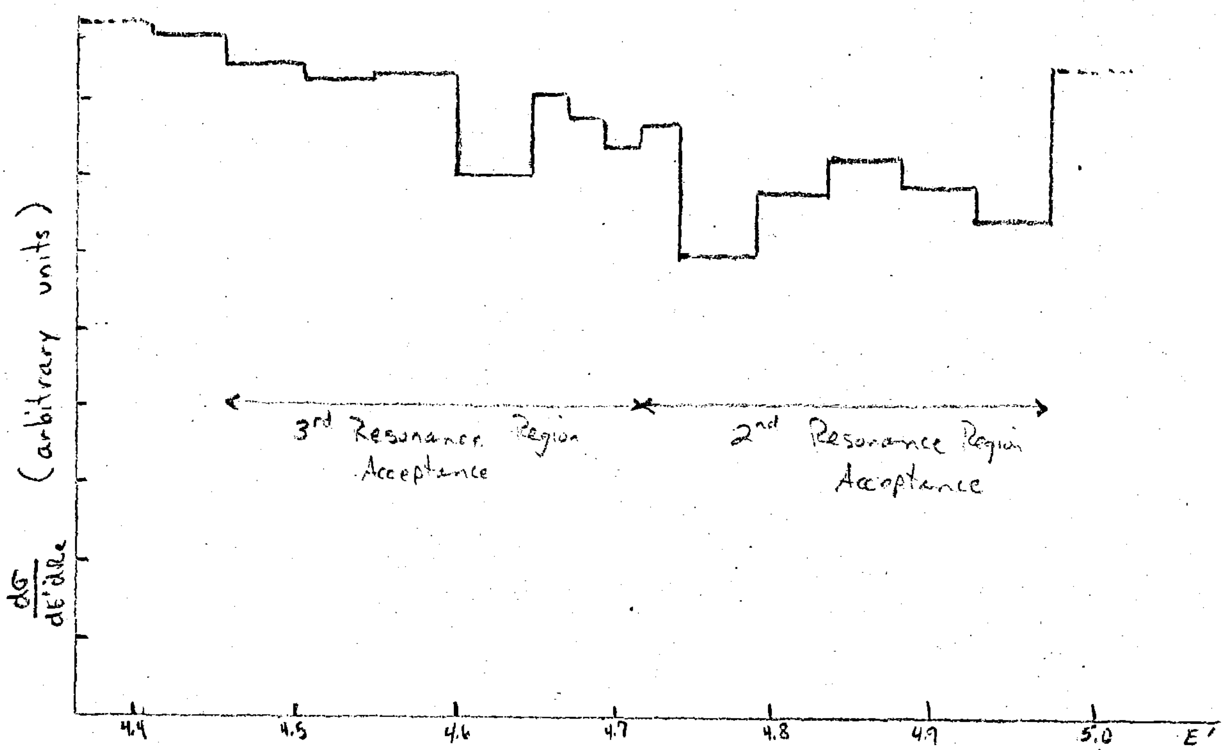

FIG. 2.11d SCATTERED ELECTRON SPECTRUM: E = 6 GeV, $\bar{\Theta} = 9.05°$
Relative Bin Width Uncertainty = 5%

c) Scattering Angle, $\breve{\theta}$.

1) Introduction. When the incident beam was set up, it was directed through the center of the target as discussed in Section 2.2b. For the incident beam passing through the target center, the scattering angle is determined by the target location, the center of the aperture of the electron spectrometer, and the location of the incident beam downstream of the target. Throughout a given set of runs, the spectrometer and target can were located in fixed positions on the floor. Changes in the scattering angle can occur, however, if there are changes in the direction of the emergent beam (even though the beam continues through the target center). The location of the beam at the target was surmised from the scintillation screen just downstream of the target. The TV monitor showing this screen was always in easy sight of the data takers. Any slight changes in beam position at the target were corrected with the presteering magnet. Major drifts led to a check of the transport system monitors. Thus, the position of the beam at the split ionization chamber downstream of the target (Figure 2.1) was the only variable.

The choice of horizontal beam focusing (Section 2.2b) reduced deviations in the horizontal component of the scattering angle. However, the choice of vertical focusing was made at a sacrifice in sensitivity to changes in the vertical component of the scattering angle. Less sensitivity would have been obtained if the beam were focussed at the split ionization chamber as was the case for the horizontal component. Furthermore, since the focus was between the target and the split ionization chamber, the signal at the split ionization chamber could be anti-correlated with the beam position at the target. On occasion, this anti-correlation was observed.[35] However, the scattering angle is not very sensitive to its vertical component for angles away from zero degrees. See Section 2.3c where we discuss corrections for the vertical angle ignoring vertical motion of the beam at the target. Such motion was corrected for when observed on the closed circuit TV view of the target fluorescent screen.

<u>2) The Split Ionization Chamber.</u> The split ionization chamber works on the principle illustrated in the schematic diagrams of the chamber (Figures 2.12) and described here. The electron beam ionizes molecules of gas along its path in the ionization chamber. The number of ions produced is directly proportional to the path length of the electron beam in the gas. The chamber is divided into two independent sections, one each for determining the horizontal and vertical positions of the beam at the chamber. A collector foil separates each section

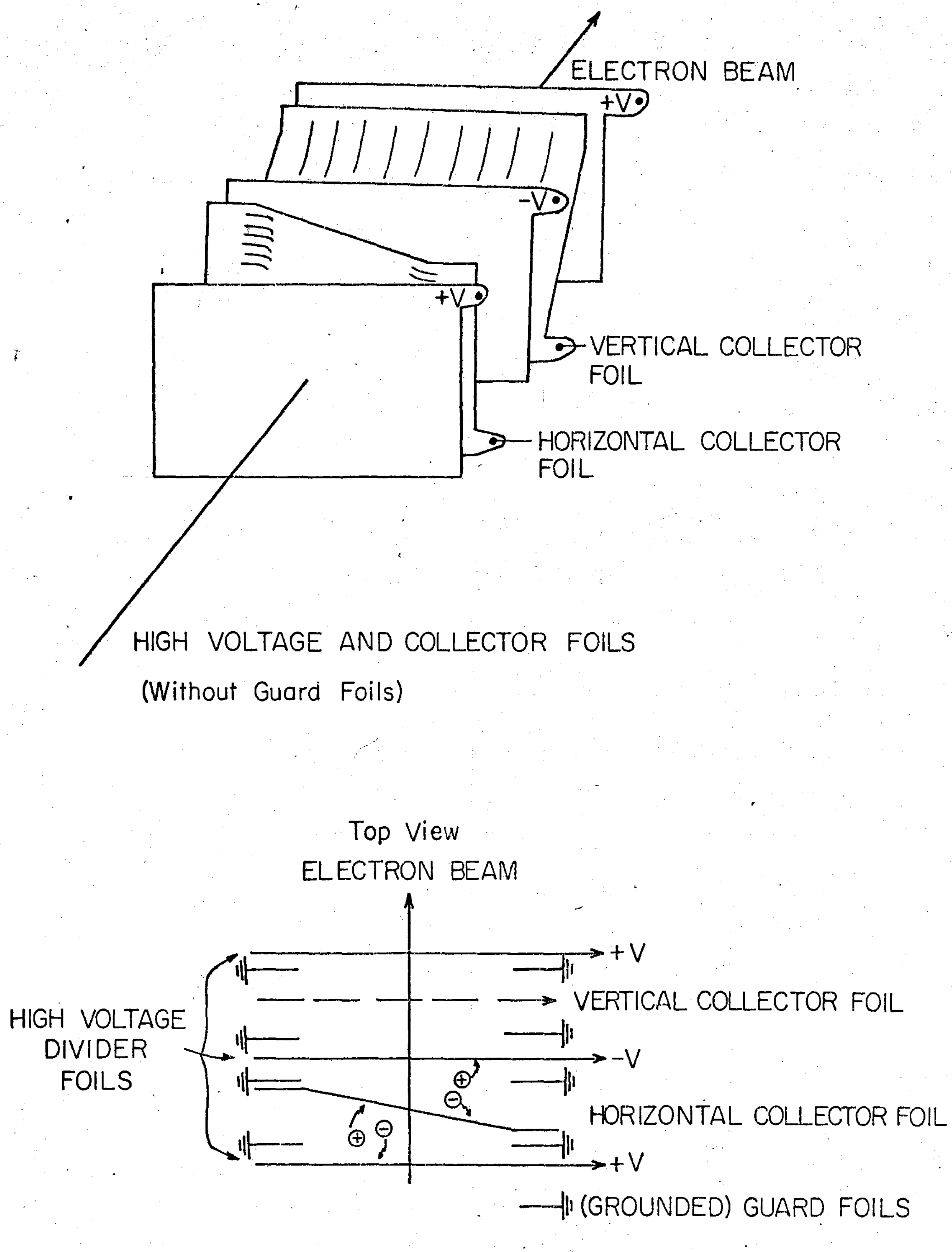

FIG. 2.12 SPLIT IONIZATION CHAMBER

into two parts. Due to the electrostatic potentials applied to the divider foils, the collector foils gather positive charge from one part of the section and negative charge from the other. The collector foils are sloped so that the position of the beam will determine the ratio of positive to negative charge collected. There will be one position of the beam at which the amounts of positive and negative charge will just equalize. This is the nominal center of the chamber. For the horizontal coordinate, it was possible to locate this nominal center by moving the chamber relative to the beam. The position of the chamber was determined with the use of a linear potential divider fixed with respect to the flux return piece of the half-quadrupole magnet. The chamber was calibrated by moving it with respect to the beam in the horizontal direction (Figure 2.13). The vertical position was not movable and the chamber output had a constant offset. The sensitivity of the vertical system was assumed to be identical to the horizontal sensitivity except for the difference due to the difference in the two slopes (7/12 for the horizontal and 7/9 for the vertical).

The chamber was filled with a mixture of 90% He and 10% N_2 at slightly above atmospheric pressure. The windows of the chamber were made of 1½ mil sheets of stainless steel and the foils in the chamber were 1 mil sheets of aluminum.

One would expect an ionization rate of 6×10^{-2} ion pairs/cm/mm Hg pressure/incident electron for the above gas mixture at local fields of 1300 volts/cm.[36] For perfect collection of all ionized particles, one would expect a sensitivity (horizontal) of

$$6 \times 10^{-2} \times 7/12 \times 674 = 24 \text{ ion pairs/cm/incident electron}$$

The measured sensitivity was 19 ion pairs/cm/incident electron, indicating a recombination and collection inefficiency of about 20%. The chamber was operated at $\pm$ 2200 volts, well into the saturated collection region as shown in Figure 2.14.

The output of the chamber was integrated in an RC circuit and the voltage across the capacitor was measured and displayed by a digital voltmeter. The scaler photographs taken at the end of each run include these voltages.

<u>3) Corrections to the Nominal Scattering Angle.</u> The variations in electron scattering angle, shown in Figures 2.15, are dominated by the horizontal component of beam motion. The effect of the horizontal motion on the measured cross section was the same for both the UD and DU trajectories. However, the vertical correction was

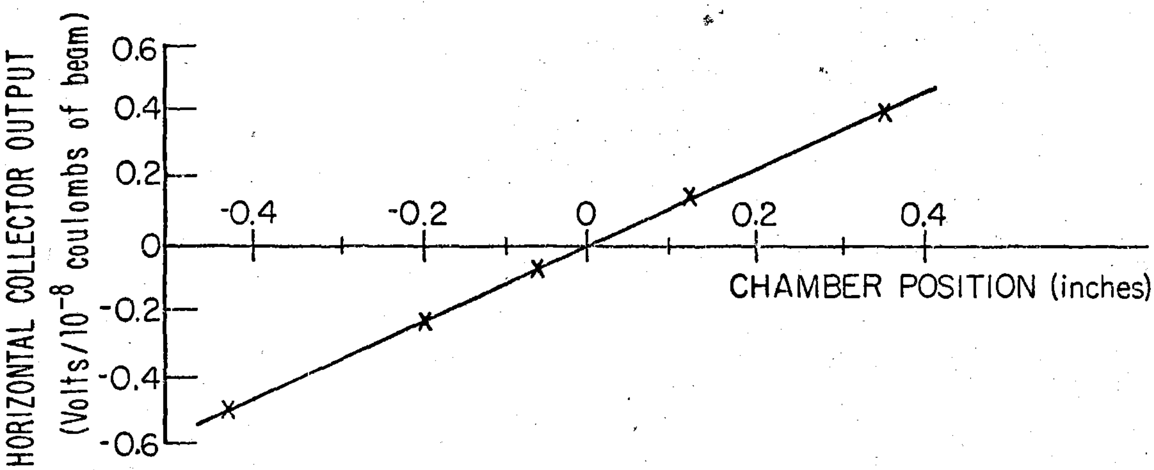

FIG. 2.13 SENSITIVITY CURVE OF HORIZONTAL IONIZATION CHAMBER (Beam intensity = 2×10^{-9} amperes)

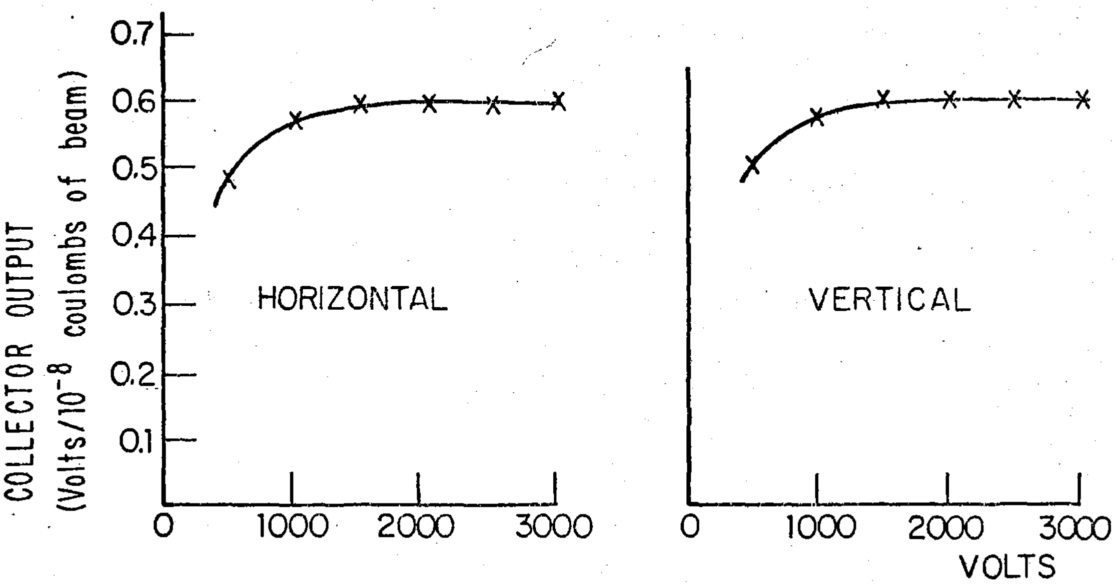

FIG. 2.14 RESPONSE OF IONIZATION CHAMBER VS. HIGH VOLTAGE, V (Beam intensity = 2×10^{-9} amperes)

opposite for the two trajectories. Thus, separate correction factors for each trajectory for each run were applied to the data. See Section 3.4b for a discussion of the corrections.

d) Sensitivity to Beam Intensity.

Beam intensity is a final parameter which is not a part of the calculated asymmetry, but which may affect the asymmetry through its effect on the measured cross-sections. Figures 2.16 and 2.17 show the intensity dependence of the potential computer trigger rate and of the measured cross-section for various momentum definition codes.

The potential trigger rate was monitored separately on a 100 Mc and a 10 Mc set of scalers. Each set scaled separately the trigger rates for potential events with the UD and DU type trajectories, N_{UD} and N_{DU}, as well as the coincidence rate, $N_c = N_{UD} + N_{DU}$, and the total trigger rate $N = N_{DU}$ or N_{UD}. The 100 Mc scalers counted the 50 Mc output pulses from Chronetics 100 Series coincidence units while the 10 Mc scalers counted a stretched pulse. The 10 Mc scalers were, therefore, more sensitive to intensity dependences than were the 100 Mc scalers. We used the 100 Mc scaler outputs for the analysis as described in Section 3.2 and the comparison of the two sets as a monitor of intensity dependence problems.

The randoms rate in the momentum definition counters

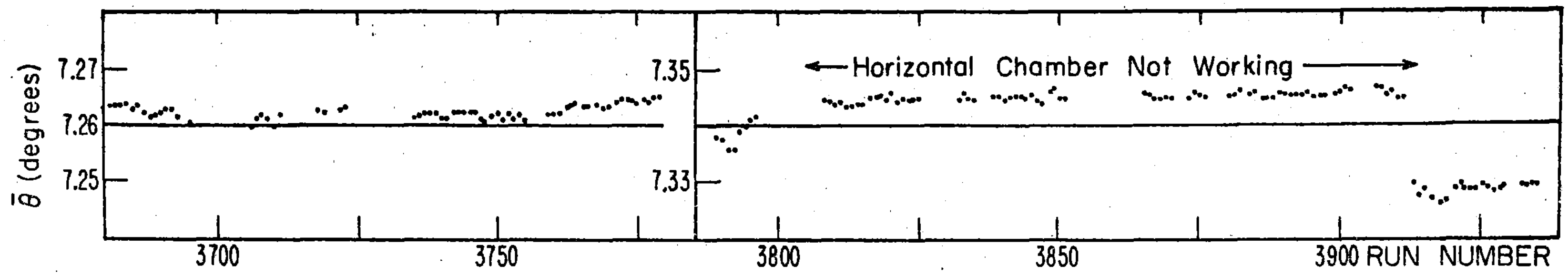

FIG. 2.15a ELECTRON SCATTERING ANGLE, RUN BY RUN: E = 4 GeV $\bar{\theta} = 7.34°$

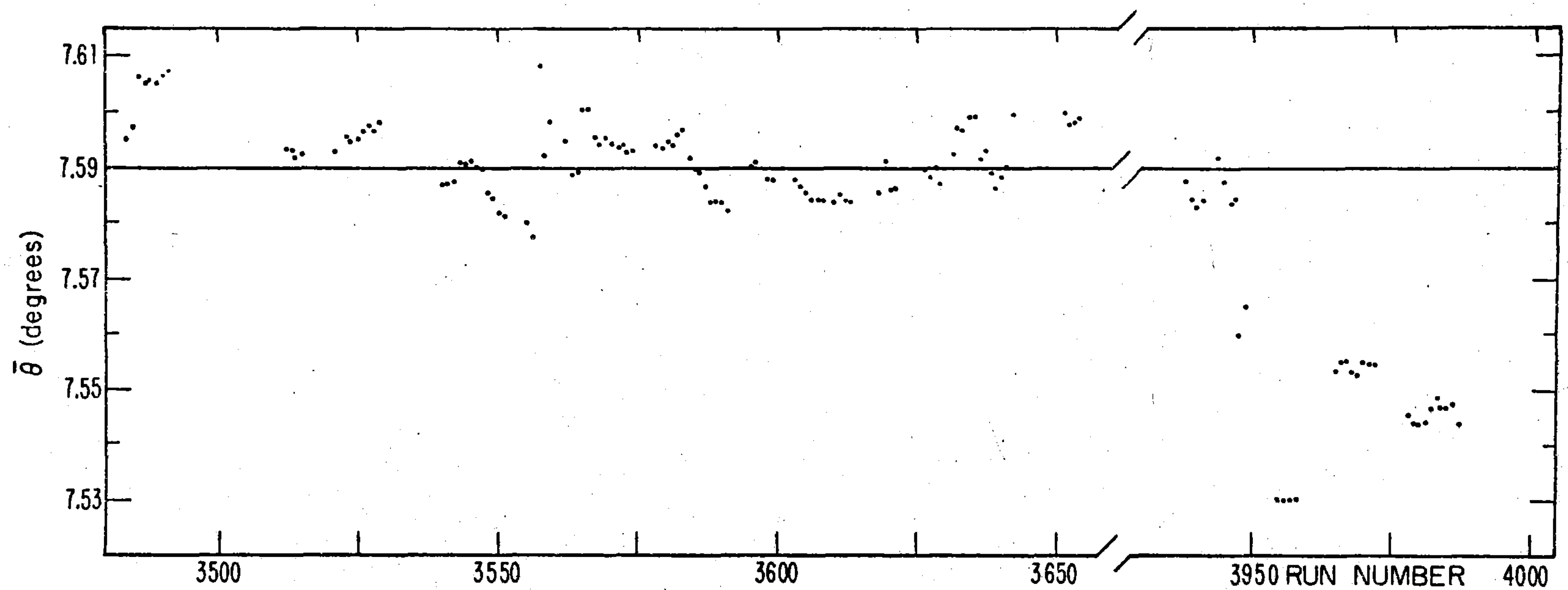

FIG. 2.15b ELECTRON SCATTERING ANGLE, $\bar{\theta}$; RUN BY RUN: E = 4 GeV $\bar{\theta} = 7.59°$

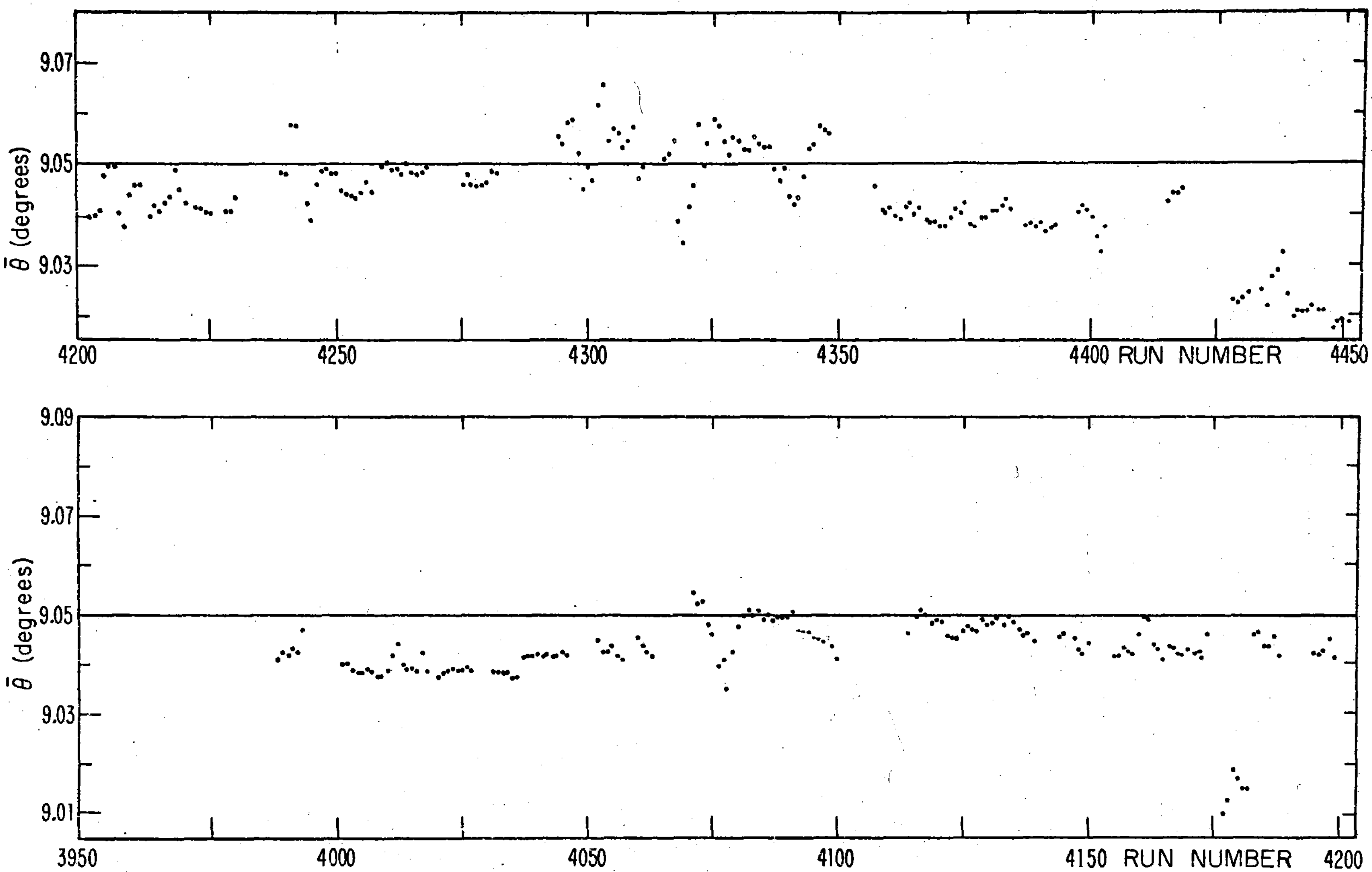

FIG. 2.15c ELECTRON SCATTERING ANGLE, $\bar{\theta}$; RUN BY RUN: E = 6 GeV, $\bar{\theta}$ = 9.05°, PART 1

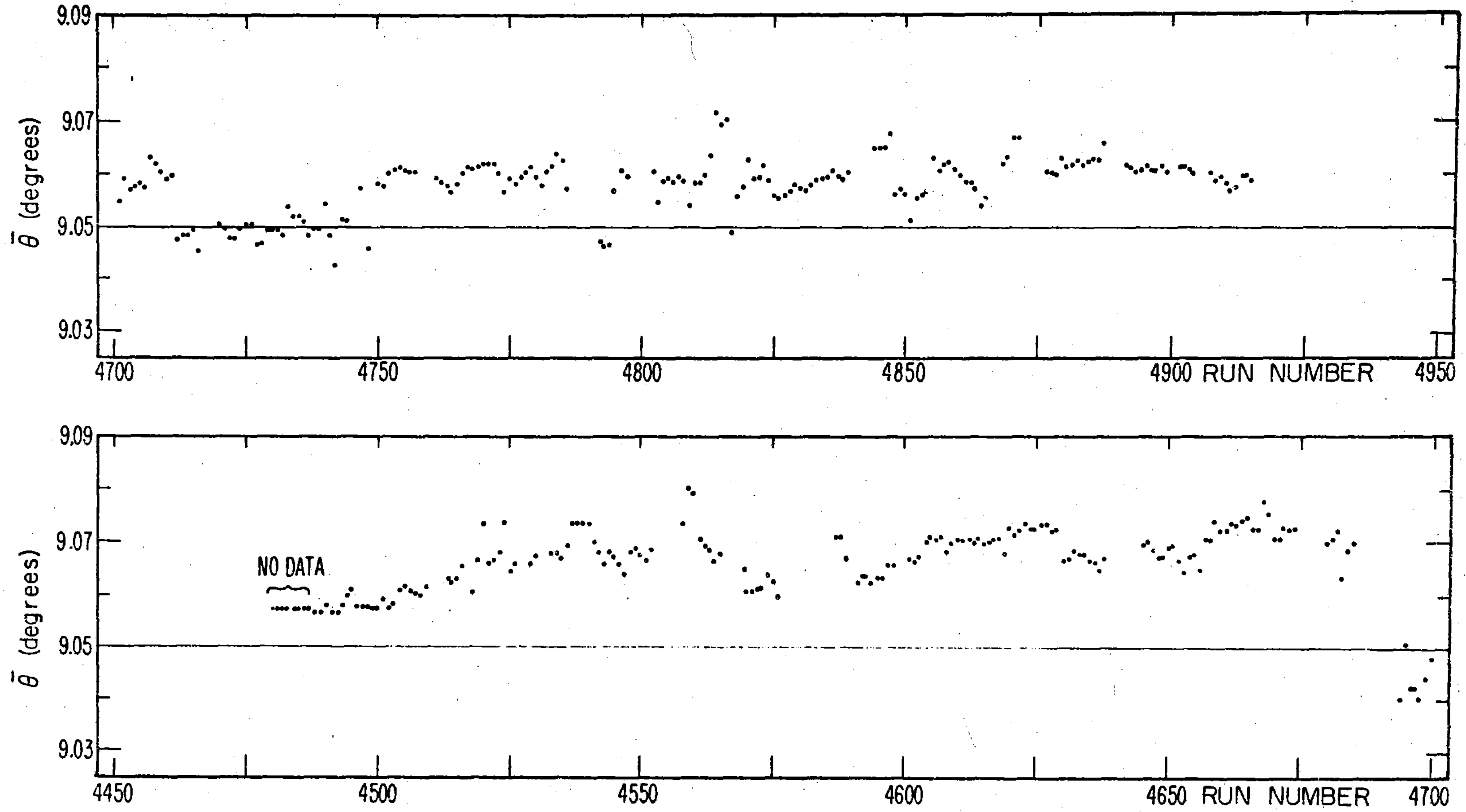

FIG. 2.15d ELECTRON SCATTERING ANGLE, $\bar{\theta}$; RUN BY RUN: E = 6 GeV, $\bar{\theta}$ = 9.05°, PART 2

were particularly sensitive to beam intensity as implied by Figure 2.17. However, as pointed out earlier, inefficiencies in the trigger rate is not a problem and the effect of overefficiencies is merely to smear out the momentum resolution slightly.

Typical intensity variations within a pulse were on the order of 40% while pulse to pulse intensity variations were about 15%. The average intensity over the period of a pair of runs, however, was usually stable to 10%. We believe that our cross-sections were independent of intensity to better than 1% and, therefore, that intensity dependent instabilities were less than 0.2% for a pair of runs. No corrections to the data were applied for such intensity dependences.

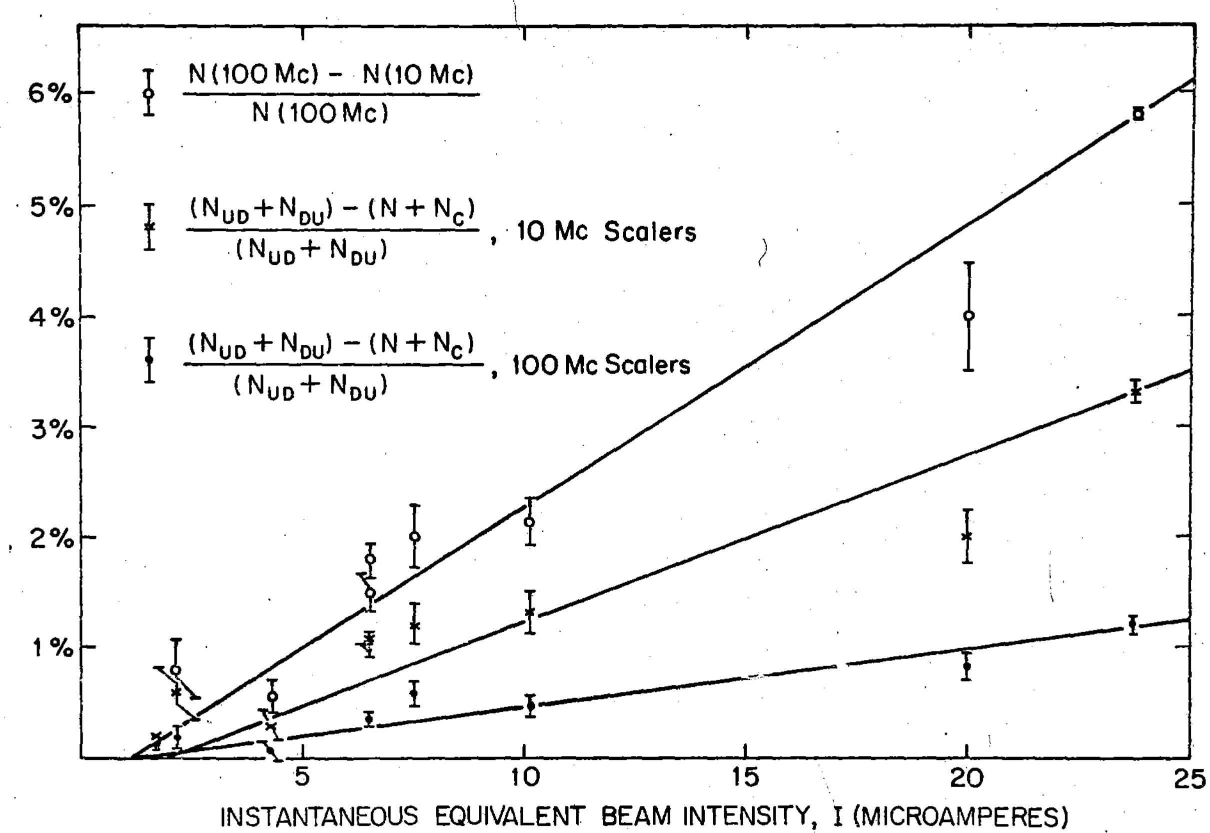

FIG. 2.16 INTENSITY DEPENDENCE OF POTENTIAL COMPUTER TRIGGER RATE (DATA WAS TAKEN WITH I < 5 μAMPS)

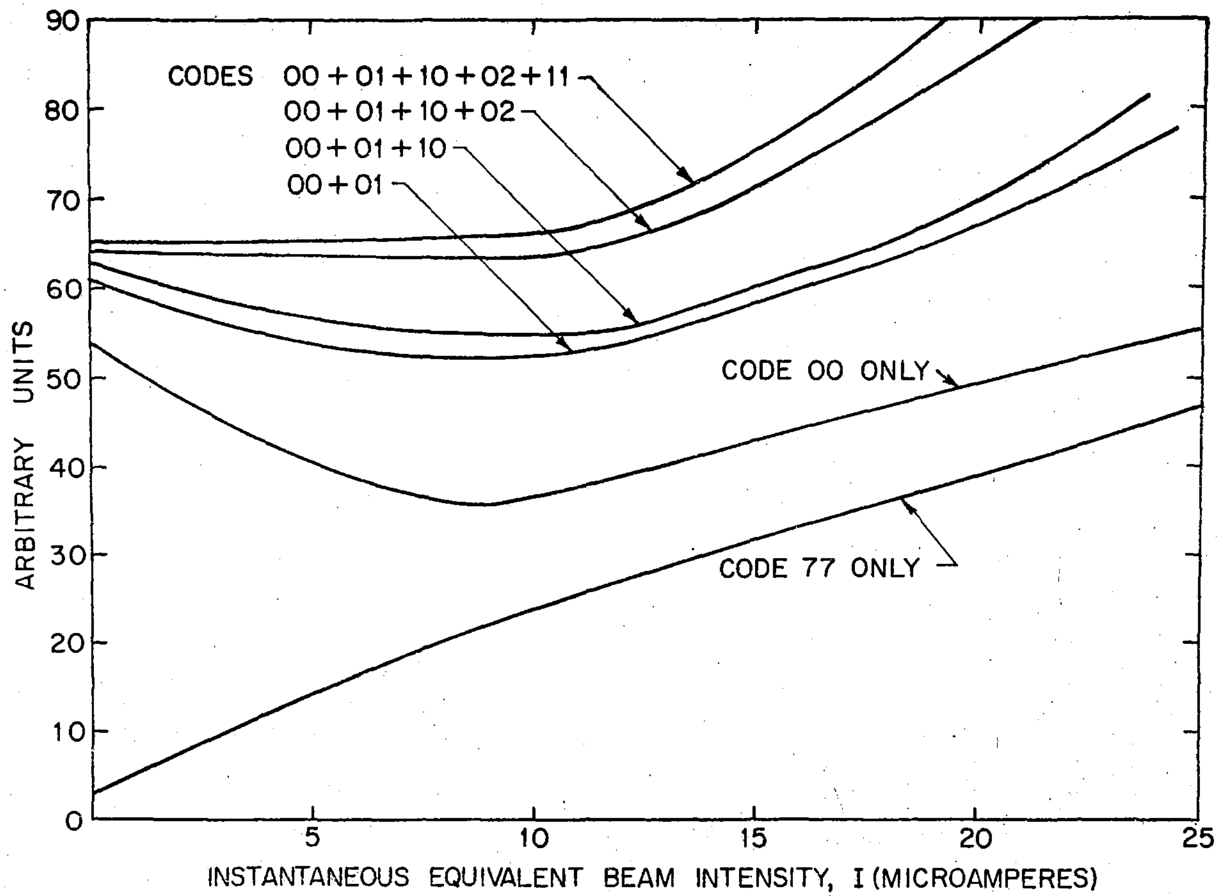

FIG. 2.17 INTENSITY DEPENDENCE OF COMPUTER ANALYZED CROSS SECTIONS (DATA WAS TAKEN WITH I < 5 μAMPS)

2.4 ORDERING OF DATA ACQUISITION

The incident energy and electron scattering angle were monitored as described earlier. Corrections due to changes in these variables have been applied. However, the method of data acquisition was designed to minimize the need for these corrections and other corrections which are less easy to estimate.

First of all, the paired data runs were of short duration, typically three minutes. Time between runs was kept at a minimum, typically ½ minute. The point of this brevity was not only to increase the amount of data taking time, but to minimize the time available for unknown systematic drifts in apparatus behavior.

Secondly, the ordering of runs was designed to cancel first and second order systematic drifts. For most of the data, the ordering was as represented schematically by

$$\ldots \| \uparrow \downarrow | \downarrow \uparrow \| \downarrow \uparrow | \uparrow \downarrow \| \ldots$$

where one or more vertical slashes represent motion of the target in order to expose a new section to the beam. The double slashes are only to aid the eye in seeing the pattern. The symbol $\uparrow(\downarrow)$ represents a cross section measurement with the spin parallel (anti-parallel) to the normal to the scattering plane, $\hat{n}$. An asymmetry was determined from each pair of runs between target motions. Only for the first part of the data taken with a scattering angle $\bar{\theta} = 7.59^\circ$ did we use the less advantageous ordering represented by

$$\ldots| \uparrow \downarrow | \uparrow \downarrow | \uparrow \downarrow |\ldots$$

This ordering fails to cancel second order drifts.

Thirdly, no intentional changes in the apparatus other than the change in polarization were ever made except when the target was also being moved. If a machine control was noted to have drifted or if there were some other reason to change a part of the apparatus, the change was made only after a series of 4 or 8 runs was completed. Never was a change made between two runs which were to be used together for an asymmetry measurement.

CHAPTER 3 DATA ANALYSIS

3.1 INTRODUCTION

The physically meaningful asymmetry, α, is due to the scattering of electrons from 100% polarized protons. For σ_+ (σ_-) representing the doubly differential cross section, $d\sigma/dE'd\Omega_e$, Equation 1.11 gave

$$\alpha = \frac{1}{P} \frac{\sigma_+ - \sigma_-}{\sigma_+ + \sigma_-} \tag{3.1}$$

The measured asymmetry, A, is due to the scattering of electrons from not only polarized protons, but also from other material. This other material included the carbon, oxygen, doping material, and target end walls. If Σ_+(Σ_-) represents the doubly differential cross section for the total scattering material with net polarization positive (negative), the raw asymmetry A is given by

$$A = \frac{1}{P} \frac{\Sigma_+ - \Sigma_-}{\Sigma_+ + \Sigma_-} \tag{3.2}$$

Only scattering events correlated with the sign of the proton polarization remain in the numerators of α and A. The two asymmetries differ, however, in their denominators. The denominator of A contains the events represented by σ's plus the uninteresting scattering from unpolarized material. Given the fraction (1/k) of events coming from free protons, one can determine α from A.

$$\alpha = \frac{1}{P} \frac{\sum_{+} - \sum_{-}}{\frac{1}{k}(\sum_{+} + \sum_{-})} = \frac{k}{P} A \tag{3.3}$$

The following sections discuss the weighted raw asymmetry, A, the normalization k, and the general handling of the data. The free proton polarization, P, is discussed in Section 2.2c and in detail in the thesis of J. Chen.[27]

3.2 THE RAW ASYMMETRY DETERMINATIONS, A^i

The individual measurements A^i are taken from adjacent pairs of data runs in which the polarization of the target is reversed, i.e.,

$$A^i = \frac{1}{p} \left(\frac{N_+ - N_-}{N_+ + N_-} \right) \tag{3.4}$$

where N_+ (N_-) equals the number of accepted counts per incident charge with the polarization vector positive (negative). The positive polarization direction is defined the same as for the normal to the scattering plane, $\hat{n}$.

The numbers $N_{\pm}$ can be taken as the number of potential computer triggers per incident charge, N. This rather crude number may be further refined by looking at the data recorded on magnetic tape and determining the fraction, p, of events which satisfy some specific criteria, i.e., the probability that a given computer trigger will be acceptable. In this case

$$N^i = p\, N \tag{3.5}$$

for N_+ and N_-.

The assumption inherent in this procedure is that the computer is triggered so as to sample the events randomly. That is, the same probability, p, holds for the computer sample and for the total ensemble of events.

The value of p may be very near 1.0 if one uses a tight triggering system for the data of interest. On the other hand, p may be rather small as in the case when interest is centered on some small fraction of the total momentum acceptance. The data is examined using N and various N^i.

In taking data on the region of the first pion-nucleon resonance, a special attempt was made to presort the triggers with the fast logic circuitry so as to produce a tight computer trigger for the momentum bite of interest (and $p \sim 1.0$). Only half the total momentum acceptance was used. Further, only a fraction, f, of the potential triggers were allowed to reach the computer (by using an electronic prescaler, Section 2.2d). When taking data in the second and third resonance regions, the larger momentum acceptance of our spectrometer (14%) was used in order to take data on both regions at once. This procedure typically leads to smaller values of p. The prescaling device was not used in these higher resonance runs.

The reason for this difference in run procedures is explained by the statistical uncertainty in each N^i. The basic aim of the experiment is to obtain a single value of the asymmetry covering a given resonance region. Thus, the values of p can be reasonably close to 0.1. The computer samples fN events of which pfN are acceptable and (1-p)fN are not. The distribution of values for N is Poissonian and for p, binomial. Thus,

$$\left(\frac{\delta N^i}{N^i}\right)^2 = \left(\frac{\delta p}{p}\right)^2 + \left(\frac{\delta N}{N}\right)^2 \tag{3.6}$$

and

$$= \left(\frac{1-p}{pfN}\right) + \left(\frac{1}{N}\right)$$

$$= \frac{1-p+pf}{pfN}$$

or

$$\delta N^i = \left(\frac{1-p+pf}{f}\right)^{1/2} pN \tag{3.7}$$

There are two limits imposed on this uncertainty. One limit is the data recording rate, fN per unit time. The computer will always be a limit at some level. A second limit is due to the maximum acceptable intensity. Either the randoms rates or, in this experiment, beam heating effects pose a limit to the beam intensity available, and thus, to N per unit time. When these two limits are fixed by the experimental situation and apparatus, the value of f is determined. Figure 3.1 gives a plot of the squared fractional uncertainty in N^i as a function of the usefulness of the recorded data, p, for various values of f. It is clearly always an advantage to have the recorded data as useful as possible; that is, the closer p is to

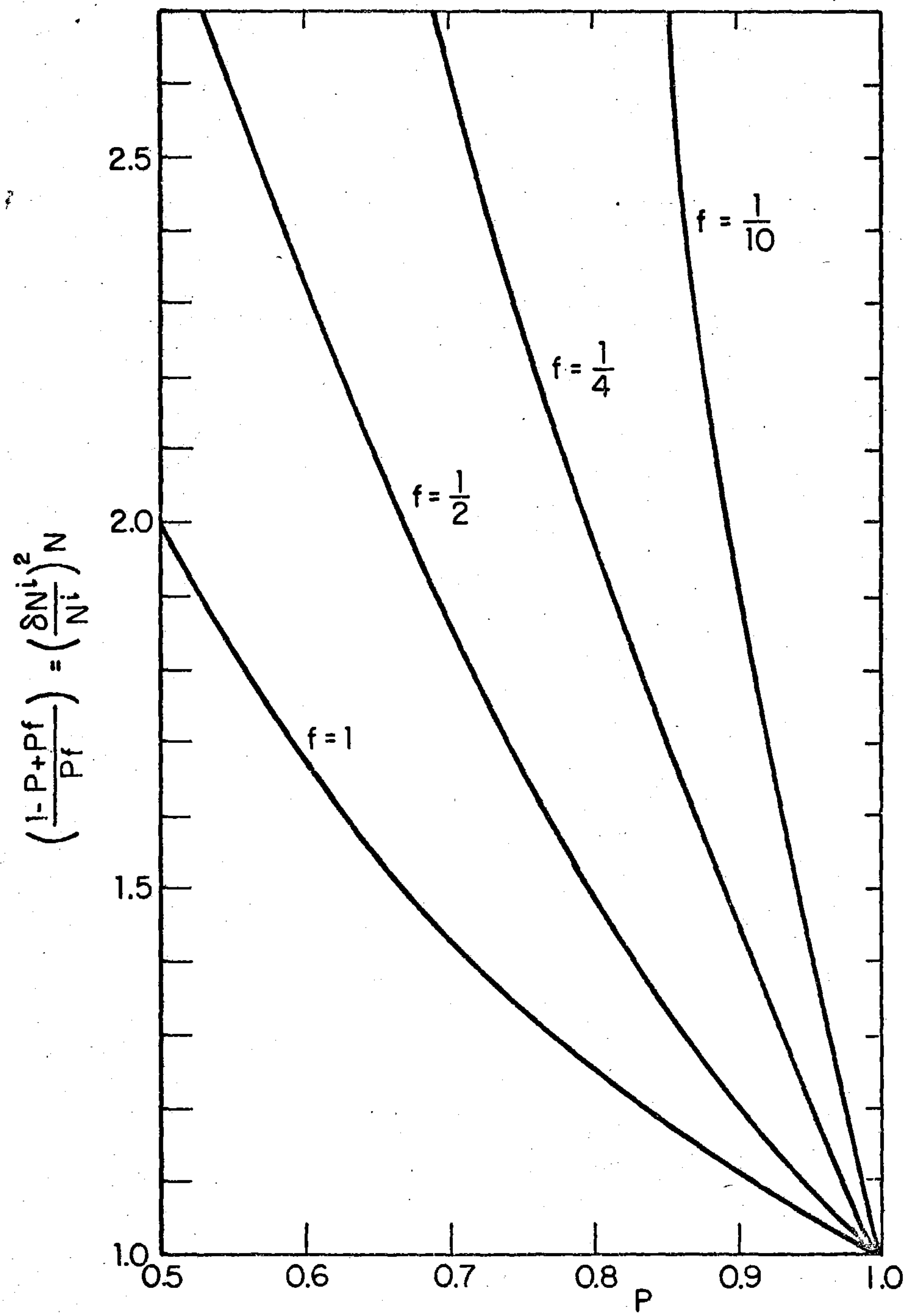

FIG. 3.1 RELATIVE ERROR VS. FRACTION OF TRIGGERS ACCEPTED AS DATA, P, FOR VARIOUS SAMPLING RATIOS, f.

1.0, the less the uncertainty for a given f. Furthermore, the closer to p=1.0, the less important is the fraction of events sampled, f. This is the key to our procedure on the first resonance runs. Table 3.1 gives the values of the parameters p and f and calculates the net uncertainty in the data as recorded and via other possibilities.

At the first resonance, we had the option of reducing the intensity by a factor of two and removing the prescaling device. However, we would have lost up to 30% in the uncertainty. This loss does not include the loss due to radiation damage to the target. However, target changes could be made in about one hour, and we could easily have doubled the target change rate to maintain the higher average polarization of the lower beam intensity method.

Table 3.1 also shows the same argument for the double resonance runs. There, the gain was clearly in favor of taking data on two useful regions at once. This option was not available at the first resonance since the scattered energy had to be lower for the interesting q^2 and the resulting energy bite was too small to include a second resonance or the elastic peak.

Thus, for all our runs, the limit on statistical uncertainty was the beam intensity. Even at the first resonance, we could have further reduced the fraction of events sent to the computer and still reduced the statistical uncertainty.

TABLE 3.1

AVERAGE UNCERTAINTY IN DATA BY PROCEDURE[a]

#	$\bar{\theta}$	Resonance Region	p	f	$\left(\frac{dN}{N^i}\right)^2$ (b)	$\frac{\sqrt{N}}{P/P_o}\left(\frac{dN^i}{N^i}\right)$	Comments	% Loss Compared to Method Used
1	7.34	First	.8	$\frac{1}{2.3}$	$\frac{1.6}{N}$	1.05	Prescaling Device Used, Double Target Change Rate	-17
2	""	" "	.8	$\frac{1}{2.3}$	$\frac{1.6}{N}$	1.26	Prescaling Device Used Data Rate = N/time	-
3	""	" "	.8	$\frac{1}{1.1}$	$\frac{2.6}{N}$	1.61	No Prescaling Device Data Rate = (N/2)/time	28
4	7.59	2nd & 3rd	.4	$\frac{1}{1.5}$	$\frac{2.7}{N}$	1.64	1 Run with Date Rate = N/time (2 resonances) 1 x (2.7 x 1/N) = 2.7/N	-
5	""	" "	.8	$\frac{1}{1.5}$	$\frac{5.6}{N}$	2.37	2 Runs with Data Rate = (N/2)/time per resonance 2x(1.4 x 2/N) = 5.6/N	31
6	9.05	" "	.4	$\frac{1}{1.3}$	$\frac{2.6}{N}$	1.61	1 Run with Data Rate = N/time (2 resonances) 1x(2.6 x 1/N) = 2.6/N	-
7	""	" "	.8	$\frac{1}{1.3}$	$\frac{5.2}{N}$	2.28	2 Runs with Data Rate = (N/2)/time per resonance 2x(1.3 x 2/N) = 5.2/N	29

a) Procedures Used: #'s 2, 4, 6.   b) Taken from Figure 3.1.

3.3 REJECTION OF DATA

Some of the data was not used in the calculation of the final asymmetry due to equipment failures during the runs and various other criteria. Equipment failures included the slow death of the power supply to the trigger counters and bad sections of magnetic tape. Other reasons for rejecting data included the improper ordering of polarization and increased cross sections due to scattering from the target support near the bottom of a target. When rejecting data due to criteria based on the cross section instability, the data was rejected for several runs before the failure was noted. In general, however, the policy was to include as much of the data as possible, both to increase the statistical accuracy of the result and to avoid introducing biases in the rejection procedure. A few pairs of data runs were also lost due to improper transferance of information among the three computers which were used in the analysis.

Only about 1% of the data was lost due to improper data transmission. About 17% of the data was lost due to conditions during the data acquisition itself. See Table 3.2. No extraneous asymmetries are thought to have been introduced due to the rejection of data since

(1) such a small portion of the data was affected and (2) since large sections of continuous runs remained available for analysis.

TABLE 3.2

USAGE OF DATA

$\bar{\theta}$	%Pol'n (free p)	# of Nominal Data Runs	# Runs Used in Analysis	%
7.34	22.5	216	170	79
7.59	14	84	76	
	16	38	20	
	18	16	4	
	20	41	32	
		179	132	74
9.05	7.5	94	86	
	16	211	184	
	17	12	10	
	18	93	80	
	19	242	198	
	22	161	128	
		813	686	84
Total		1,208	988	82

3.4 REFINEMENTS OF THE ASYMMETRIES

a) Introduction.

As already indicated in Section 3.2b, we determined a variety of asymmetries. The crudest form of N^i used in these determinations was just the number of potential computer triggers, N. The first refinement of this value is the setting of various masks in the computer analyses which determined the fractional acceptances, p. The computer masks included minimum pulse heights in the Cerenkov and shower counters and momentum acceptances as defined by the counter array. The importance of using computer refinements to the total trigger rate is shown in the chi squared values of Table 4.2. Once a computer refinement including momentum definition was used, the results were insensitive to the exact specification of these biases (Section 4.2b). There are two other basic refinements we applied in the calculations for values of N^i. These are the corrections to the counting rate due to changes in the scattering angle, $\bar{\theta}$, and changes in the incident electron energy, E.

b) Corrections Due to Changes in $\bar{\theta}$.

The mean scattering angles were calculated for each run from the output of the split ionization chamber as explained in Section 2.3c. An angular correction factor was then applied to each run in the form $C_\theta = (\bar{\theta}_{measured}/\bar{\theta}_{nominal})^n$ where the value of n was selected as described below.

At the first resonance, the angular dependence of the counting rate was taken from the product $\Gamma_T\ \sigma_T$ where[36a]

$$\Gamma_T = \frac{\alpha}{4\pi}\,\frac{K}{q^2}\,\frac{E'}{E}\left(2 + \frac{\cot^2\frac{\theta}{2}}{1+\tau}\right)$$

and

$$\sigma_T = (560\,\mu\,\text{barn})(e^{-1.36\,q^2})$$

For our kinematic situation, this leads to n = 6.1. For the higher resonance region data, the angular dependence of the counting rate is not as well known. However, since the size of the typical run to run correction due to changes in the scattering angle was less than 0.01%, we feel confident that using n=0 and 7.5 give reasonable limits on the effect of angular drifts. Using n=7.5, the net effect of the angular corrections is less than 1/10th of a standard deviation compared to the result with n=0 (i.e., no angular corrections). We used n=4 for the final asymmetry calculations for the higher resonance regions.

c) Corrections Due to Changes in E.

Corrections due to changes in the incident energy, E, were applied to the counting rate for each run in the form of a correction factor, $C_E = (E_{measured}/E_{nominal})^n$. All data was corrected with n=4.

The correction was determined from the average accelerator field at the time of spill as explained in Section 2.3a. The data on the accelerator rf (Figures 2.4 - 2.7) did not permit additional run to run corrections due to changes in this parameter. However, average changes in the rf corresponded to energy changes of less than 0.05%.

3.5 THE WEIGHTED RAW ASYMMETRY

The experiment yielded a large number of determinations of the raw asymmetry, A^i, whose precision is dominated by statistical errors. A weighted average of these moderate accuracy measurements is used to obtain a statistically more meaningful value of A.

For the data in this experiment, the values of N_+ and N_- were independently determined so that

$$(\delta A^i)^2 = \left(\frac{2N_-}{(N_+ + N_-)^2}\right)^2 (\delta N_+)^2 + \left(\frac{2N_+}{(N_+ + N_-)^2}\right)^2 (\delta N_-)^2 \qquad (3.8)$$

The uncertainties δN_+ and δN_- are given in Equation 3.7. In the limiting case where p = 1.0, the formula reduces to

$$(\delta A_i)^2 = (1 - A_i^2)/(N_+ + N_-) \qquad (3.9)$$

Since $\delta N_\pm = N_\pm$. And for $N_+ = N_- = N/2$,

$$(\delta A_i^2) = \frac{1}{N} \qquad (3.10)$$

3.6 NORMALIZATION OF THE ASYMMETRY, k

a) Introduction.

As discussed in the introduction to Chapter 2, the normalization was not a matter of critical importance in this experiment. We aim at a 20% value for k knowing that the error involved is insignificant compared to the statistical uncertainty. To get the asymmetry for a 100% polarized free proton target, we need to correct for (1) the scattering from target material other than free protons, (2) scattering from material other than the target, (3) lack of exact orthogonality of the polarization vector and the scattering plane, and (4) resolution and radiative corrections. We discuss each of these in turn.

b) Fraction of Free Proton Target Scattering.

Using the impulse approximation, we consider each nucleon in the target to be independent of its environment. Thus, each nucleon contributes incoherently to the total scattering cross section. A dilution factor, k_1, is calculated assuming that, at the angles of interest, each of the neutrons contributes $(80 \pm 15)\%$ of the cross section due to a single proton.[37] Thus,

$$k_1 = \frac{26 + (.80 \pm .20) \times 20}{6} = 7.0 \pm 0.7$$

for a target of ethanol or its equivalent.

c) Non-target Scattering.

Non-target materials from which electrons scattered included the 0.3 inches of cooling helium and several containing walls. The total mass-thickness of this extraneous material was 13% of the target mass thickness. Thus, an additional dilution factor, k_2, is required, *i.e.*,

$$k_2 = 1.13$$

d) Non-orthogonality of Polarization and Scattering Plane.

The electron spectrometer utilized a quadrupole magnet with its center plug at beam height. Thus, the UD and DU apertures were respectively above and below beam height. This caused a tilt in the scattering plane relative to the horizontal plane. The angle of tilt is called ω. Since the protons in the target were polarized in the vertical direction, the polarization vector was not orthogonal to the scattering plane. This effect served to further dilute the effective polarization. Table 3.3 gives the various dilution factors, k_3, which correct for

TABLE 3.3

NORMALIZATION FACTORS

Electron Scattering Angle, $\bar{\theta}$	Resonance Region	k_1	k_2	k_3	k_4	k
7.34	1^{st}	7	1.13	1.052	1.08	8.99
7.59	2^{nd} & 3^{rd}	7	1.13	1.051	1.14	9.47
9.05	2^{nd} & 3^{rd}	7	1.13	1.032	1.14	9.31

this effect.

$$k_3 = \frac{1}{\hat{n} \cdot \hat{p}} = \frac{1}{\cos \omega}$$

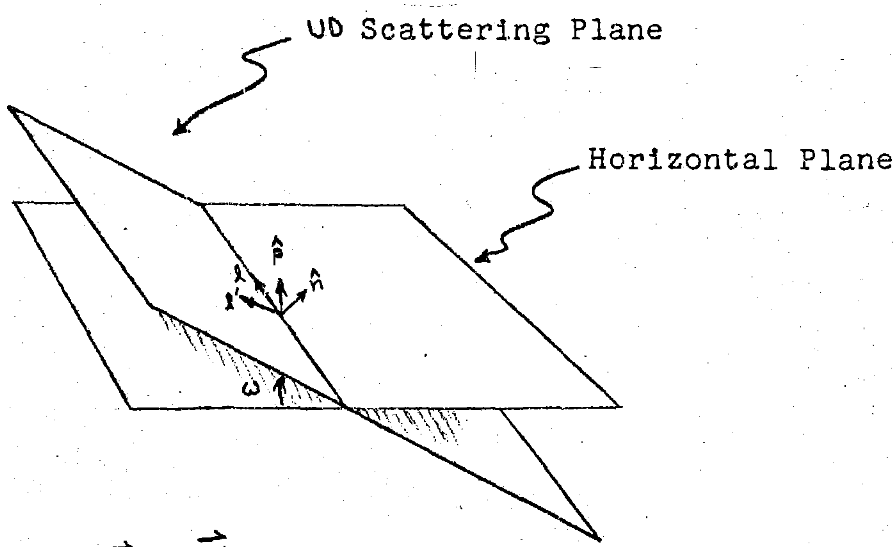

$$\hat{n} = \frac{\vec{l} \times \vec{l}'}{|\vec{l} \times \vec{l}'|}$$

Figure 3.2 Non-Orthogonality of Polarization Vector, $\hat{p}$, and the Scattering Plane.

e) Resolution Phenomena.

Every process of interest has a scattered electron energy associated with it. We detected electrons of that energy and consider them to be an indication of the process of interest. However, some of the detected electrons came from other processes. Events connected with (1) the tails of the spectrometer resolution function, (2) radiative corrections, and (3) the tails of the nuclear Fermi momentum smearing function are all of concern in this respect.

When the process of interest is well understood, corrections for the above resolution problems are usually calculable. For example, since no polarization asymmetry is expected for elastic scattering, we correct for all elastic and quasielastic scattering events which appear in our acceptance due to radiation losses and Fermi momentum smearing.

Furthermore, once it is established that no asymmetry effects appear at the first resonance, it is necessary to correct for the appearance of such events in the deeper inelastic regions. However, instead of taking the view that we have proved that there are no T violation effects at the first resonance, we assume that any T violation effects are smoothly varying functions. In that case, resolution problems are less serious since events lost and gained have similar T violation properties. The only differences are due to the variations in the cross section; i.e., the difference between the numbers of events gained and lost in our energy bite. We apply a uniform 10% normalization correction due to this last resolution problem; i.e., we lose 10% more events than we gain.

Taking the above discussion into account and feeling that we do not have a compelling model for a violation of T, we apply only the correction due to elastic and quasi-elastic scattering and the uniform 10% resolution correction for the deep inelastic regions. See Table 3.3 for these corrections, k_4. Any use of the data presented here for the purpose of investigating a model which predicts rapidly varying asymmetries as a function of E' must reevaluate the resolution corrections for the specific model.

f) Net Target Polarization

The net normalization factor, k, is just the product of the above four factors, k_i. As we have implied, it is useful to view the normalization in terms of a net target polarization dilution factor. Thus, a 20% free proton polarization corresponds to a net (20/k)% target polarization. In this vein, our typical target polarization was about 2%. Thus, all raw counting asymmetries must be multiplied by a factor on the order of 50 in order to get the physically meaningful asymmetry, α.

3.7 SEPARATION OF UD AND DU TRAJECTORY DATA

The computer analysis distinguishes between the UD and DU trajectories according to their pattern in the momentum defining counters. In addition, we scaled the potential computer triggers for the UD and DU trajectories separately, *i.e.*, N_{UD} and N_{DU} (as well as their inclusive "or", N). If we knew the number of UD and DU computer triggers, we could have done completely independent asymmetry measurements for each trajectory. Early in the set up of the electronic circuitry, an appropriate pair of computer bits was reserved for this purpose. However, before the data acquisition began, these bits were destroyed in favor of some less useful information.

It is possible, nonetheless, to do separate analyses for the UD and DU trajectories. In using the computer to determine the fraction of acceptable events, p, one merely uses the additional requirement that an event correspond to the appropriate trajectory. Had we included a bit to identify the trigger for each event, the appropriate number of computer triggers, T_{UD} or T_{DU}, would have been used to calculate p. Instead, we were forced to use the total trigger rate, T. For N_a equal the number of acceptable events for a given trajectory, we would have had

$$P = \frac{N_a}{T_{UD}} \quad \text{or} \quad \frac{N_a}{T_{DU}} \ ,$$

but we had to use

$$P = \frac{N_a}{T} \ .$$

In the former case, p might have been close to 1.0. In the later case, the value of p is about half what it might have been. This distinction is particularly important at the first resonance as discussed in Section 3.2. For all the data, using the full trigger rate leads to less sensitivity than might have been obtained for the separate tarjectory analyses.

Using the second method of analysis as described above, we examined the data for UD, DU, and summed cross sections. Asymmetries were calculated for each of these three types of cross section. Any differences in the results for the UD and DU asymmetries could be attributed to one of two causes; (1) vertical beam motion or other (unknown) systematic effects which affect the trajectories differently or (2) effects proportional to the polarization parallel to the scattering plane. Both of these effects should tend to cancel in the summed cross section asymmetries. We included corrections due to the vertical beam motion as described in Sections 2.3c and 3.4. However, these corrections were negligible. The results of the separate trajectory analyses are given in Section 4.2d.

CHAPTER 4 DATA AND CONCLUSIONS

4.1 INTRODUCTION

In this chapter, we present the results of the asymmetry measurement, check the reliability of the data, and interpret the results in terms of the two possible T violation models discussed in Chapter 1.

We find that the result is insensitive to the particular biases selected in analyzing the data and that there are no statistically significant variations of the asymmetry as a function of scattered electron energy (or hadron final state energy) in any of the resonance regions. The final results are shown to behave as expected for data whose principal uncertainty is statistical. The asymmetry results which are sensitive to the time reversal violation effect are shown to behave similarly to the series of specially constructed asymmetries which are insensitive to such an effect.

In the final section, we show what limit is placed on the relative phases of the scalar and transverse amplitudes in the two models discussed in Section 1.3.

In the various tables of this chapter, we use the notation developed in Chapters 2 and 3. Thus, N refers to the asymmetries which have been calculated from the potential computer trigger rate alone; pN to the potential trigger rate corrected for the acceptability of the typical trigger. Additional factors C_θ and C_E imply the application to the counting rate of run to run corrections due to changes in electron scattering angle and incident electron energy before calculation of the asymmetries. Chi squared per degree of freedom when the mean asymmetry is forced to be zero is called χ^2_0. χ^2_α is the value when the mean asymmetry is allowed to take its calculated value.

4.2 ASYMMETRY RESULTS SENSITIVE TO T VIOLATIONS

a) Final Values and the Effect of Various Corrections.

The final values of the asymmetry are listed in Table 4.1 along with the asymmetries calculated from the data using various corrections. As is evident from these tables, the fluctuations of the incident energy and electron scattering angle are nearly negligible. The effect of the angular and energy corrections for run to run variations not only tend to cancel due to their randomness, but also are very small compared to the dominant statistical uncertainty of each run. These conclusions were shown to be insensitive to the exact angular and energy dependences used in correcting the observed counting rate.

The application of computer analysis, however, is quite significant. Even though the computer triggering system had fairly rigid requirements, sufficient latitude remained that a significant improvement in chi squared per degree of freedom was obtained by post-run computer analysis of the recorded data.

b) Various Computer Analysis Requirements.

The most significant part of the computer analysis is the requirement of an identifiable single particle trajectory in the momentum defining counters. (Table 4.2 and Figure 4.1.) The standard set of biases used for the Cerenkov and shower counters contained little additional pulse height requirements above those of the initial triggering circuitry (Figures 2.9 and 2.10). However, an immediate improvement in chi squared per degree of freedom occurs when momentum definition is required This improvement is insensitive to which particular set of momentum definition codes (Section 2.2d) one uses. The important point is that the effects of general spray and random end bin triggers are reduced. Adding higher Cerenkov and shower counter pulse height biases have little effect on the asymmetry. These effects can be understood if the unacceptable computer triggers are associated with sprays of particles. Multiple particles with low energy can look like a single high energy particle in the Cerenkov and shower counters, but be excluded by their unrecognizable pattern in the momentum defining counters. Furthermore, the singles rates in the momentum definition counters were significantly higher in this experiment than in any previous experiment with the same detection apparatus. The singles rates in the trigger counters were on the order of 1 Mc. To reduce the random coincidence trigger effects only data for events with a particle apparently focused between the -6% and +6% counters (Figure 2.8) were used in the computer analysed data.

The cause of the high singles rates in the counters was the spray of low energy particles resulting from the large magnetic field at the target. (Section A.5.) Nevertheless, we feel that the combination of momentum definition and Cerenkov

TABLE 4.1

FINAL VALUES AND EFFECT OF RUN TO RUN CORRECTIONS[†]

RESONANCE REGION	$\bar{\theta}$ (degrees)	NUMBER OF MEASUREMENTS	TYPE OF N^{λ} USED FOR α	α	$\delta\alpha^*$	χ_0^2	χ_α^2
FIRST	7.34	85	N	.079	.024	2.77	2.64
			$NC_\theta C_E$	.080	.024	2.70	2.57
			pN	.034	.041	1.51	1.50
			pNC_θ	.034	.041	1.50	1.49
			$pNC_\theta C_E$	.035	.041	1.50	1.49
SECOND	7.59	66	N	-.100	.050	3.01	2.95
			$NC_\theta C_E$	-.099	.050	3.07	3.01
			pN	-.140	.124	1.13	1.11
			pNC_θ	-.145	.125	1.12	1.10
			$pNC_\theta C_E$	-.142	.124	1.13	1.11
	9.05	343	N	.008	.030	1.40	1.40
			$NC_\theta C_E$	.008	.030	1.36	1.35
			pN	-.004	.063	1.10	1.10
			pNC_θ	-.005	.063	1.10	1.10
			$pNC_\theta C_E$	-.005	.063	1.10	1.10
THIRD	7.59	66	N	-.100	.050	3.01	2.95
			$NC_\theta C_E$	-.099	.050	3.07	3.01
			pN	-.007	.109	1.21	1.21
			pNC_θ	-.006	.110	1.19	1.19
			$pNC_\theta C_E$	-.006	.109	1.19	1.19
	9.05	343	N	.008	.030	1.40	1.40
			$NC_\theta C_E$	.008	.030	1.36	1.35
			pN	-.022	.054	1.04	1.04
			pNC_θ	-.023	.054	1.04	1.04
			$pNC_\theta C_E$	-.023	.054	1.04	1.04

† FINAL VALUES ARE THOSE LISTED AS $pNC_\theta C_E$

* STATISTICAL UNCERTAINTY ONLY

TABLE 4.2

EFFECT OF COMPUTER BIASES ON ASYMMETRY

RESONANCE REGION	$\bar{\theta}$ (degrees)	CERENKOV & SHOWER CTR. LEVELS	MOMENTUM DEF. CODES ACCEPTED	α	$\delta\alpha$*	χ^2_0	χ^2_α	NUMBER OF MEASUREMENTS
FIRST	7.34	potential trigger rate		.080	.024	2.20	2.57	85
		standard	00-11	.035	.041	1.50	1.49	"
		"	00-10	.028	.043	1.55	1.55	"
		high	00-11	.083	.067	2.13	2.11	73
SECOND	7.59	potential trigger rate		-.099	.050	3.07	3.01	66
		standard	00-11	-.142	.124	1.13	1.11	"
		"	00-10	-.166	.128	1.12	1.10	"
		high	00-11	-.054	.145	1.39	1.39	61
	9.05	potential trigger rate		.008	.030	1.36	1.35	343
		standard	00-11	-.005	.060	1.10	1.10	"
		"	00-10	-.039	.066	1.12	1.12	340
		high	00-11	-.078	.083	1.08	1.07	285
THIRD	7.59	potential trigger rate		-.099	.050	3.07	3.01	66
		standard	00-11	-.006	.109	1.19	1.19	"
		"	00-10	.012	.112	1.20	1.20	"
		high	00-11	.052	.130	1.43	1.43	61
	9.05	potential trigger rate		.008	.030	1.36	1.35	343
		standard	00-11	-.023	.054	1.04	1.04	"
		"	00-10	-.023	.056	1.00	0.99	340
		high	00-11	-.041	.073	1.14	1.14	285

* STATISTICAL UNCERTAINTY ONLY

Footnotes for Figures 4.1

The measurements appearing in the histograms are

(a) Final asymmetry values.
(b) Asymmetries calculated from the potential trigger rates, N.
(c) Asymmetries accepting only the three lowest momentum definition codes, 00-10.
(d) Asymmetries calculated from the data with high Cerenkov and shower counter biases.

The numbers in parentheses on the sides of the histograms are the number of measurements which are beyond the range of the part of the histogram shown.

The dashed curves are for a gaussian distribution.

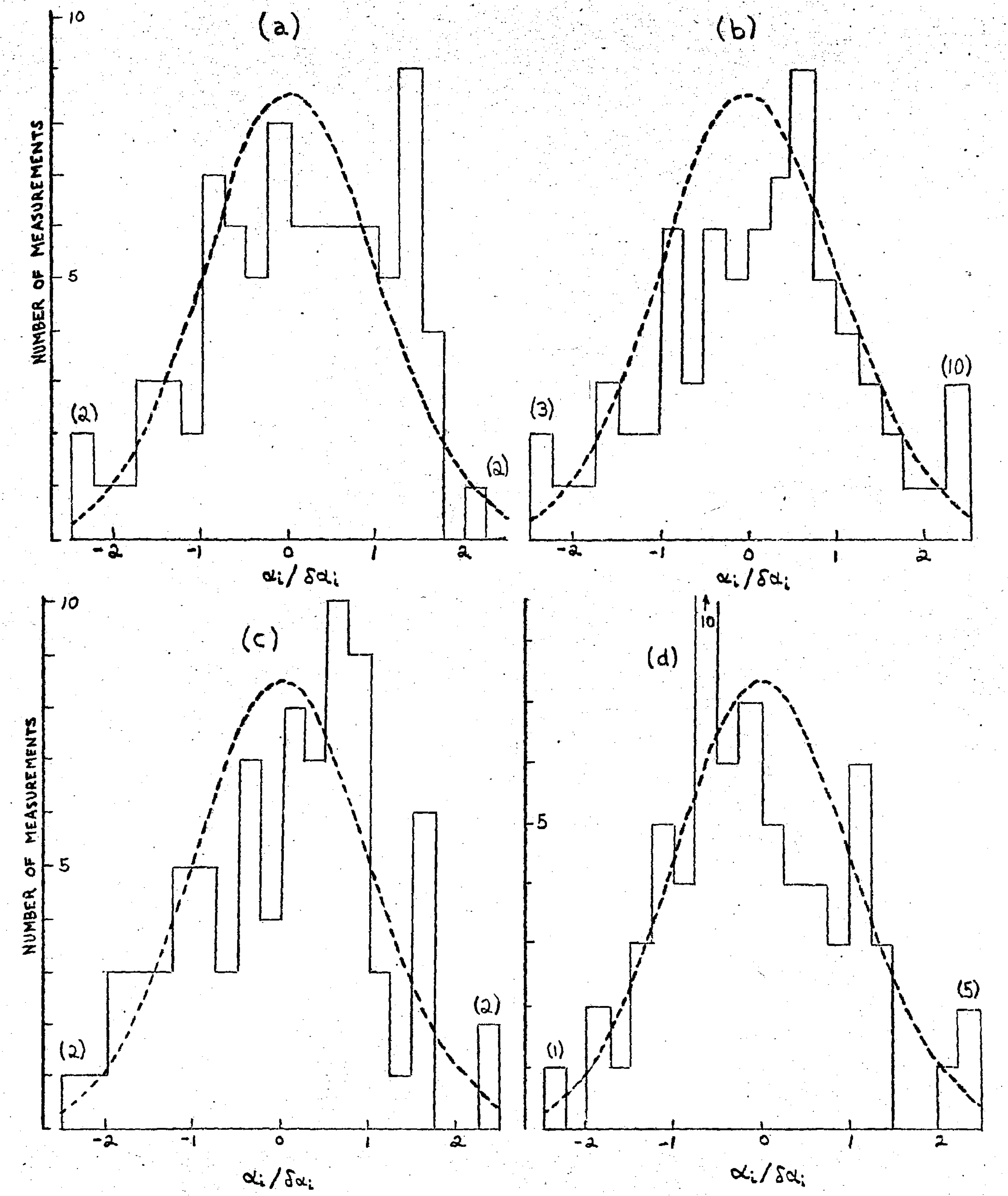

FIG. 4.1a HISTOGRAMS OF ASYMMETRY MEASUREMENTS, FIRST RESONANCE REGION
$E = 4$ GeV, $\bar{\theta} = 7.34°$

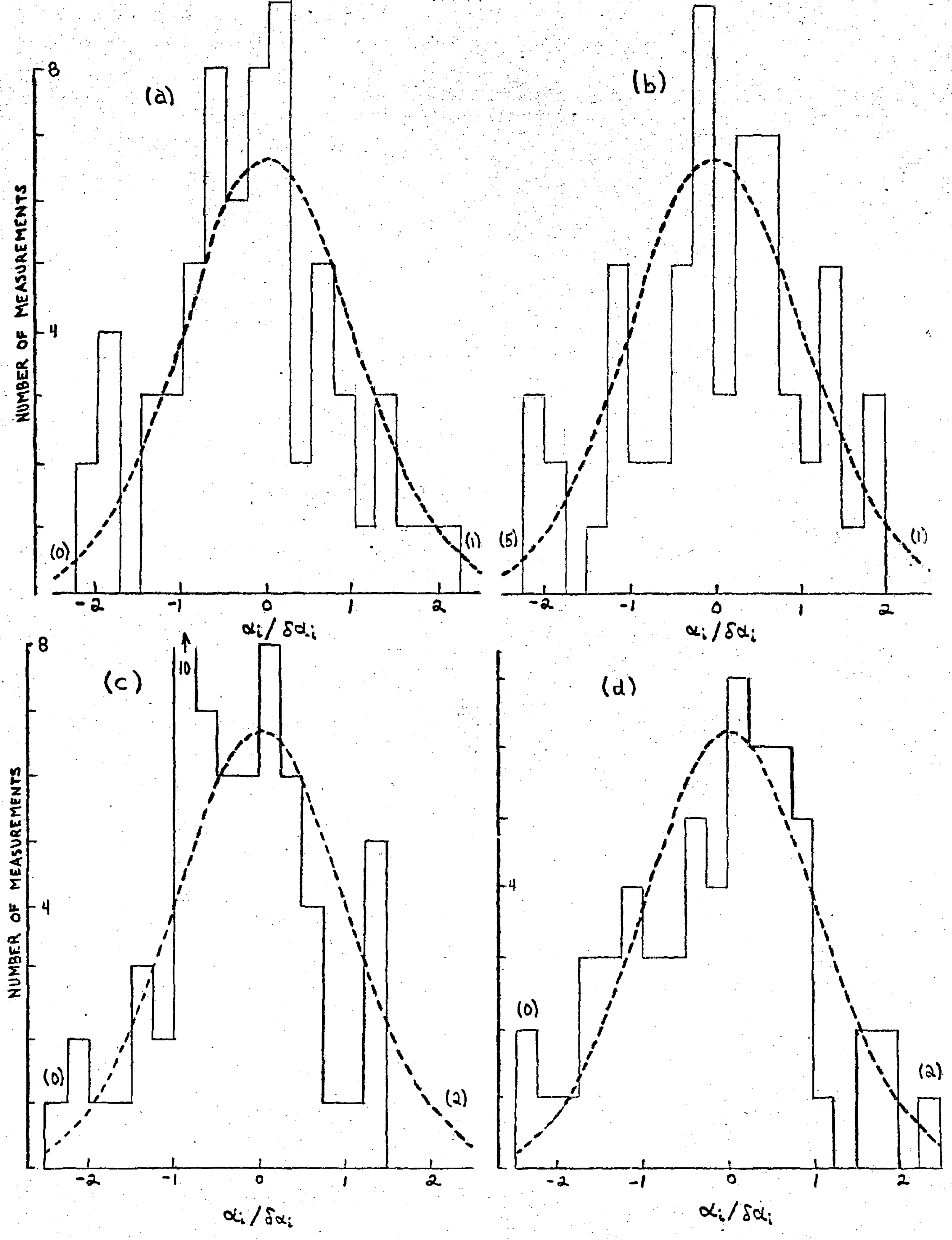

FIG. 4.1b HISTOGRAMS OF ASYMMETRY MEASUREMENTS, SECOND RESONANCE REGION
E = 6 GeV, $\bar{\Theta}$ = 7.59°

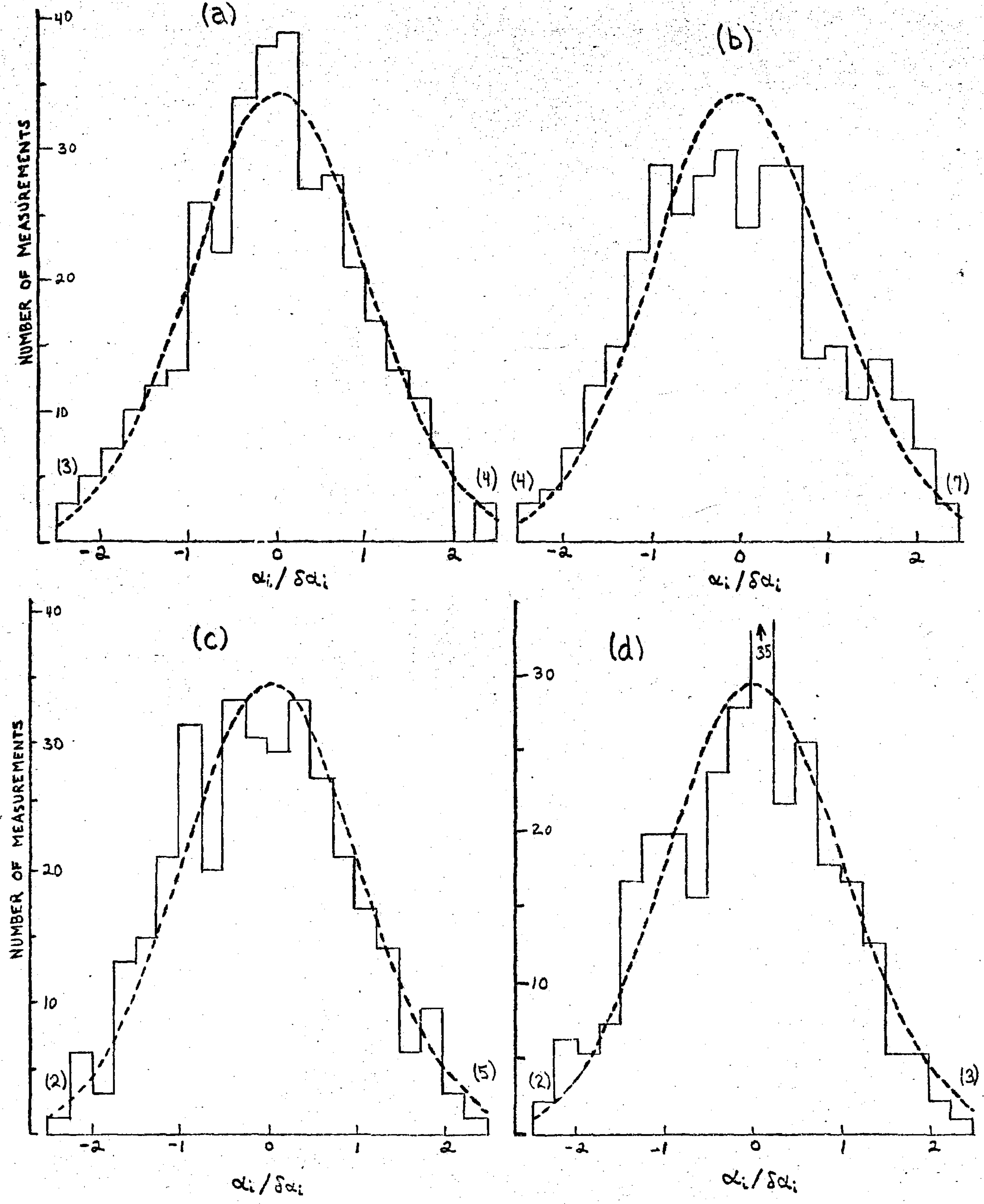

FIG. 4.1c HISTOGRAMS OF ASYMMETRY MEASUREMENTS, SECOND RESONANCE REGION
$E = 6$ GeV, $\bar{\Theta} = 9.05°$

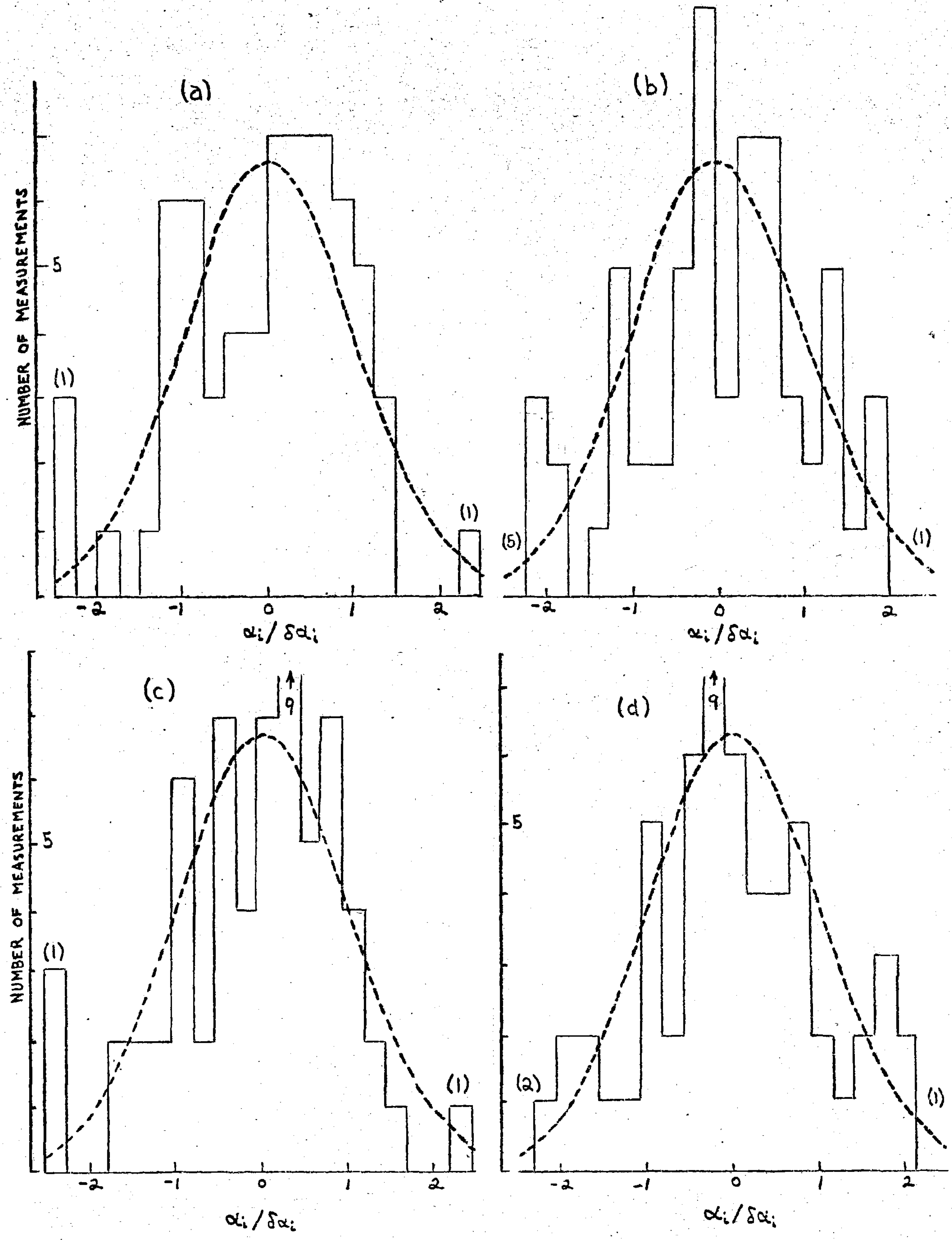

FIG. 4.1d HISTOGRAMS OF ASYMMETRY MEASUREMENTS, THIRD RESONANCE REGION
E = 6 GeV, $\bar{\theta}$ = 7.59°

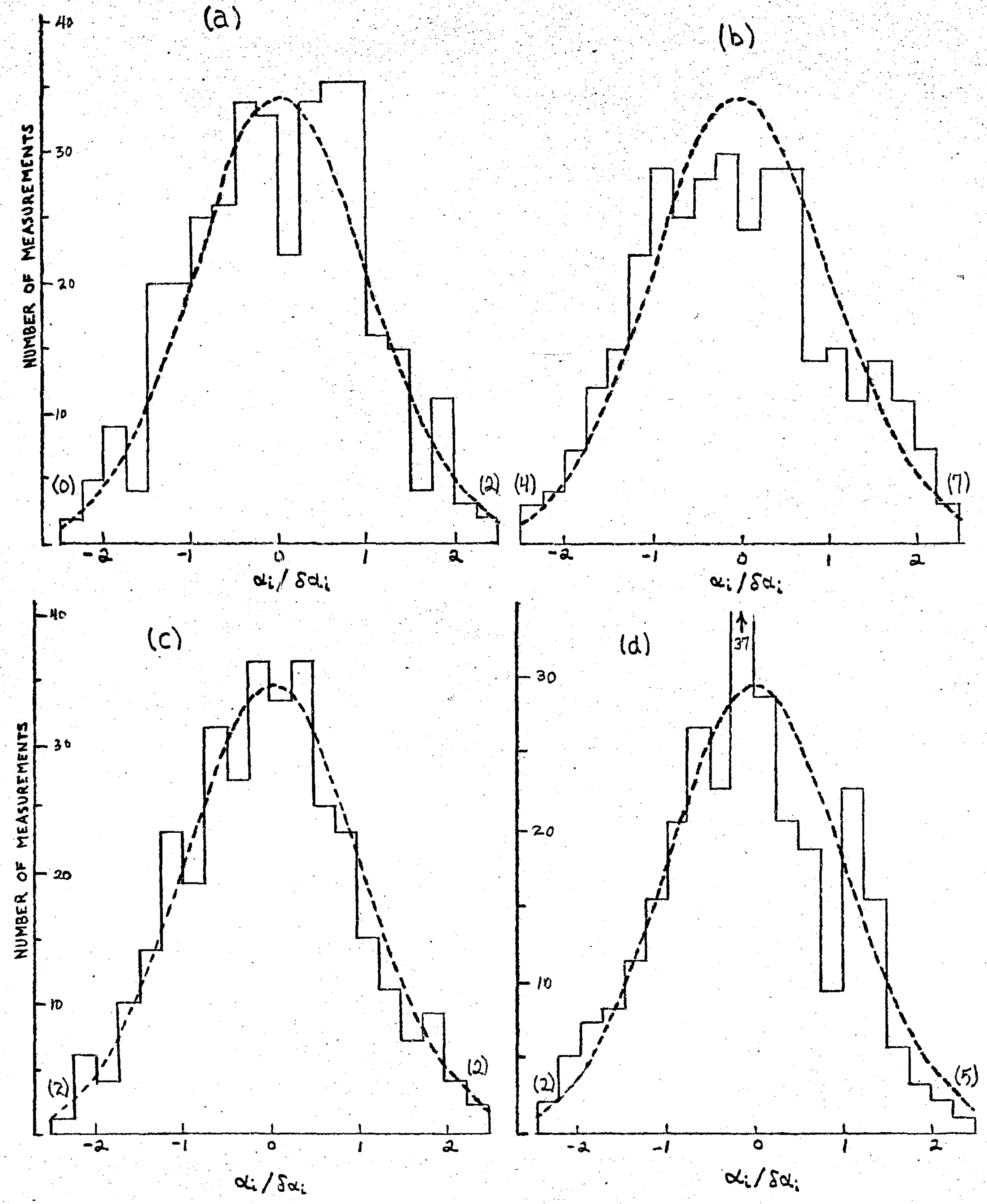

FIG. 4.1e HISTOGRAMS OF ASYMMETRY MEASUREMENTS, THIRD RESONANCE REGION
E = 6 GeV, $\bar{\theta} = 9.05°$

and shower counter requirements was sufficient to provide an unbiased sample of scattered electron events. We operated at intensities where the detection system behaved in a generally unambiguous and stable mode.(Figures 2.16 and 2.17).

c) Asymmetry Spectra.

The asymmetry as a function of scattered electron energy, E', and hadron center-of-mass energy, W, is given in Figures 4.2 and Tables 4.3. In interpreting these spectra it should be remembered that the scattered electron energy resolution (FWHM) was about 4%. Thus, the abrupt irregularities in the middle of the spectrum at $\bar{\theta} = 7.59^{o}$ are unphysical.

No structure is evident in these spectra and, therefore, the resonance region asymmetries are good indications of the limit placed on the T violation effect consistent with the resolution of the detection system. Furthermore, none of the models which inspired this experiment have rapid variation of the asymmetry as a function of hadron energy.

d) Trajectory Separation.

The results of the separate analyses (Section 3.7) of the data from the UD and DU trajectories are shown in Table 4.4. As is clear from the table, the UD and DU data tend to give opposite signs of the calculated asymmetry. This is particularly true for the data at the third resonance region for the largest scattering angle.

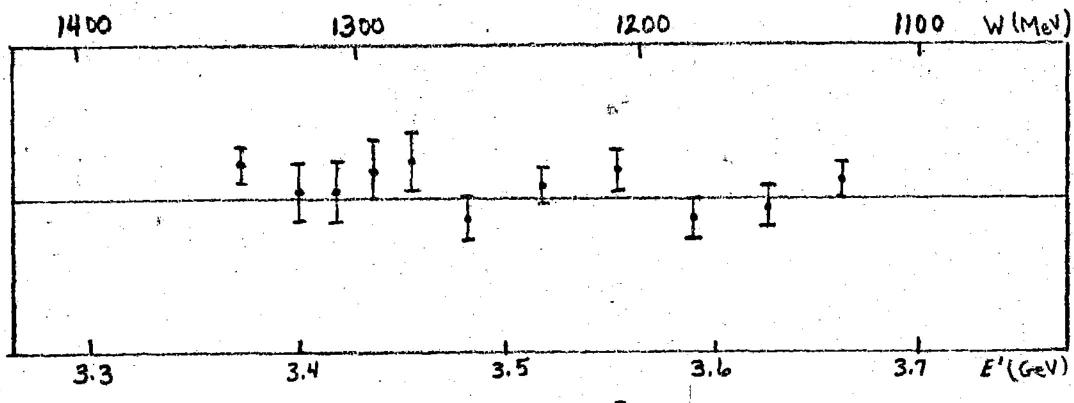

FIG. 4.2a ASYMMETRY SPECTRUM, $\bar{\theta} = 7.34°$

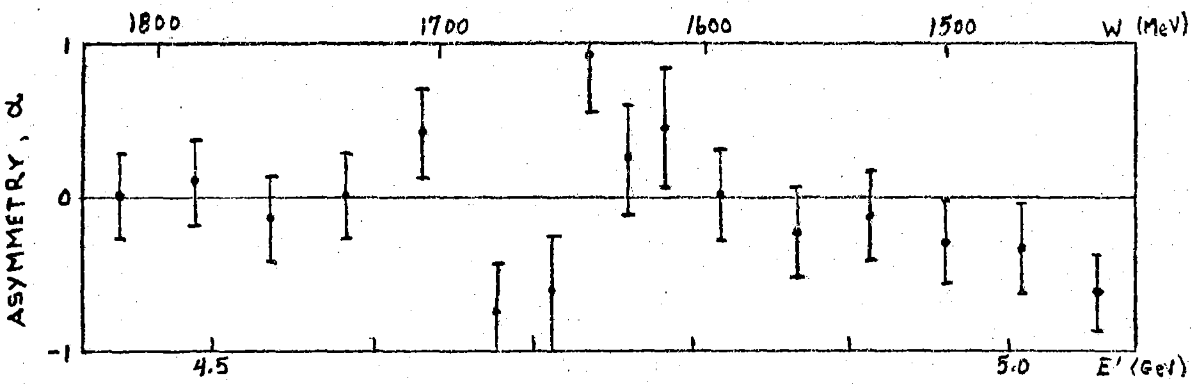

FIG. 4.2b ASYMMETRY SPECTRUM, $\bar{\theta} = 7.59°$

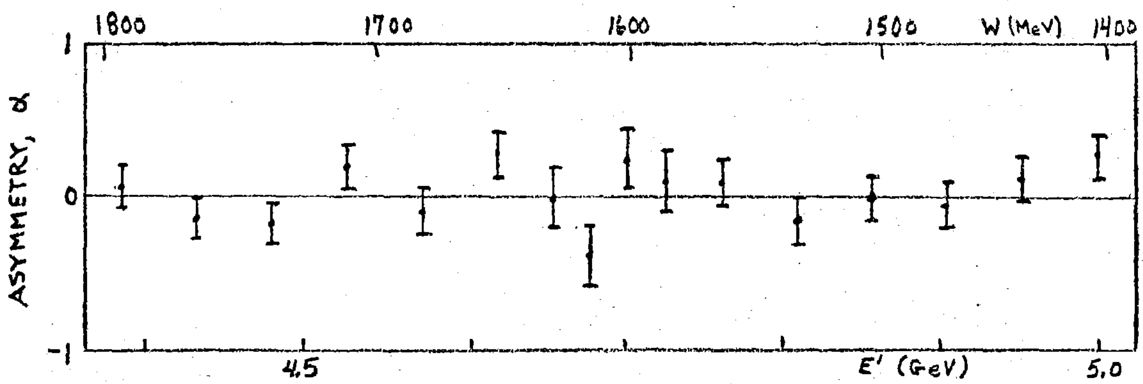

FIG 4.2c ASYMMETRY SPECTRUM, $\bar{\theta} = 9.05°$

TABLE 4.3a

Asymmetry Spectrum, First Resonance Region

E' (GeV)	K (GeV)	W (GeV)	α	$\delta\alpha$ *	χ_o^2	χ_α^2
3.38	484	1337	.252	.160	1.19	1.15
3.40	458	1318	.061	.211	0.84	0.84
3.42	440	1306	.067	.209	1.24	1.24
3.44	422	1294	.202	.203	1.06	1.04
3.45	404	1281	.241	.203	0.95	0.93
3.48	378	1265	-.133	.140	1.08	1.07
3.52	343	1234	.092	.141	1.02	1.01
3.55	308	1206	.196	.139	1.00	0.97
3.59	272	1178	-.123	.134	1.20	1.19
3.62	236	1150	-.046	.138	0.95	0.95
3.65	200	1121	.105	.123	0.87	0.87

* Statistical Uncertainty Only

TABLE 4.3b

Asymmetry Spectrum at $\bar{\theta} = 7.59^{o}$

E' (GeV)	K (GeV)	W (GeV)	α	$\delta\alpha$ *	χ_o^2	χ_α^2
4.44	1281	1814	-.001	.268	.98	.98
4.49	1231	1787	.091	.285	1.32	1.31
4.54	1181	1759	-.151	.279	1.20	1.19
4.59	1131	1732	.005	.279	.83	.83
4.63	1081	1706	..417	.289	1.21	1.17
4.68	1030	1678	-.736	.306	1.02	.93
4.73	992	1657	-.617	.378	1.12	1.08
4.76	967	1643	.920	.382	.89	.80
4.78	942	1628	.238	.376	1.02	1.01
4.81	917	1614	.445	.385	.89	.86
4.83	880	1591	.010	.296	1.01	1.01
4.88	830	1561	-.224	.292	1.15	1.14
4.92	779	1530	-.123	.294	1.07	1.07
4.97	729	1500	-.290	.282	.87	.86
5.02	679	1468	-.336	.288	.90	.88
5.06	629	1435	-.630	.247	1.16	1.06

* Statistical Uncertainty Only

TABLE 4.3c

Asymmetry Spectrum at $\bar{\theta}$ = 9.05°

E' (GeV)	K (GeV)	W (GeV)	α	$\delta\alpha$*	χ_o^2	χ_α^2
4.38	1238	1791	.069	.135	1.03	1.03
4.43	1192	1764	-.142	.144	.93	.92
4.48	1137	1737	-.174	.143	1.01	1.01
4.53	1086	1709	.194	.143	1.06	1.05
4.58	1036	1680	-.098	.149	1.01	1.01
4.62	985	1645	.278	.162	1.10	1.09
4.67	948	1631	-.017	.193	1.01	1.01
4.69	922	1615	-.395	.197	.96	.94
4.71	897	1601	.245	.193	1.08	1.07
4.73	872	1587	.107	.198	1.01	1.01
4.76	833	1565	.097	.161	1.05	1.05
4.81	783	1534	-.169	.156	1.13	1.12
4.86	732	1503	-.019	.159	.95	.95
4.90	681	1470	-.061	.153	1.08	1.08
4.95	631	1437	.128	.156	1.18	1.17
5.00	580	1403	.266	.135	.99	.98

* Statistical Uncertainty Only

We have less than a 33% sensitivity to physical correlations of the counting rate with the polarization parallel to the scattering plane. Thus, our data is consistent with large counting rate correlations. Nevertheless, these effects are not significant for the T violation result.

Since the UD and DU apertures are symmetric with respect to the scattering plane, the summed counting rate is potentially less sensitive to instabilities than either of the separate trajectory rates. However, the values of chi-squared per degree of freedom show only small and inconsistent differences for the separate and summed trajectory data. Furthermore, no systematic differences in the handling of the UD and DU events have been discovered.

Even the separate trajectory asymmetries taken alone do not show significant T violation effects. Thus, we ignore the differences and quote the summed results for our final values.

TABLE 4.4

TRAJECTORY SEPARATION

RESONANCE REGION	$\bar{\theta}$ (degrees)	TYPE	α	$\delta\alpha$ *	χ^2_0	χ^2_α
FIRST	7.34	UD + DU	.035	.043	1.50	1.49
		UD	-.031	.068	0.96	0.95
		DU	.093	.065	1.35	1.33
SECOND	7.59	UD+DU	-.142	.124	1.13	1.11
		UD	-.278	.181	1.16	1.13
		DU	-.007	.177	1.03	1.03
	9.05	UD + DU	-.005	.063	1.10	1.10
		UD	.046	.093	1.02	1.01
		DU	-.051	.090	1.04	1.04
THIRD	7.59	UD+DU	-.006	.109	1.19	1.19
		UD	-.021	.160	0.84	0.84
		DU	.007	.156	1.14	1.14
	9.05	UD+DU	-.023	.054	1.04	1.04
		UD	-.181	.079	1.00	0.98
		DU	.132	.078	1.01	1.01

* STATISTICAL UNCERTAINTY ONLY

4.3 SYSTEMATIC CHECKS INSENSITIVE TO T VIOLATIONS

a) Introduction.

In order to check possible systematic biases and to see what general behavior may be ascribed to the electron beam and detection system, we have calculated two types of asymmetry which are insensitive to the T violation effect. These specially constructed asymmetries are made insensitive to the T violation effect by averaging out effects which are correlated with the sign of the target polarization.

b) Chronologically Ordered Asymmetry.

The chronologically ordered asymmetry was obtained by taking the first minus the second cross section measurement of each pair at a given target position. This difference divided by the sum of cross sections gives an asymmetry in which, for the pattern given in Section 2.4, spin correlated effects will average to zero. However, this asymmetry will be sensitive to linear drifts in the system.

c) Double Target Position Averaged Asymmetry.

The double target position averaged asymmetry was obtained by pairing runs from adjacent target positions as indicated by the horizontal brackets in the drawing below.

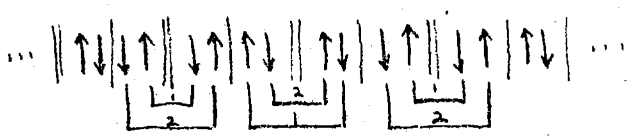

The sum of cross sections from the paired runs was calculated.

The first sum minus the second, divided by the sum of all four cross sections, gives an asymmetry which is independent of polarization correlated effects and, for the sequence drawn above, linear drift effects, too. Furthermore, this asymmetry is moderately insensitive to target thickness effects since adjacent target positions have about 2/3 of the beam going through identical locations for both positions.

d) Conclusions.

The specially constructed asymmetries of this section (Table 4.5) are most useful as indicators of the performance of the experimental apparatus independent of any polarization effects. Thus, the most significant conclusion of this section is that the statistical behavior of the results is independent of the polarization. For example, the somewhat improbable chi squared per degree of freedom for the results in the first resonance region carry over from the T violation asymmetry to the special asymmetries of this section. Thus, the T violation sensitive results are essentially indistinguishable from the other asymmetries.

TABLE 4.5

SYSTEMATIC CHECKS

RESONANCE REGION	$\bar{\theta}$ (degrees)	NUMBER OF MEASUREMENTS	TYPE OF α	α	$\delta\alpha$*	χ_0^2	χ_α^2
FIRST	7.34	85	Regular	.035	.043	1.50	1.49
		"	Chron.	-.009	.043	1.50	1.50
		37	Double Posn Avg.	-.012	.044	1.78	1.78
SECOND	7.59	66	Regular	-.142	.124	1.13	1.11
		"	Chron.	.080	.124	1.13	1.12
		20	Double Posn Avg.	-.083	.159	1.56	1.54
	9.05	343	Regular	-.005	.063	1.10	1.10
		"	Chron.	-.032	.063	1.10	1.10
		153	Double Posn Avg	-.129	.068	1.06	1.04
THIRD	7.59	66	Regular	-.006	.109	1.19	1.19
		"	Chron.	-.064	.109	1.19	1.19
		20	Double Posn Avg.	.099	.139	1.09	1.09
	9.05	343	Regular	-.023	.054	1.04	1.04
		"	Chron.	-.013	.054	1.04	1.04
		153	Double Posn Avg.	-.007	.058	1.07	1.07

* STATISTICAL UNCERTAINTY ONLY

4.4 POSSIBLE PION CONTAMINATION

Pion contamination of the scattered electrons is one possible asymmetry producing background in this experiment. As discussed for single pion production in Sections 1.2 and A.2, a polarization asymmetry is expected for detection of a restricted hadron phase space associated with a given scattered electron energy. Pion contamination in this experiment would be the result of such a restricted pion acceptance, but would be integrated over all (undetected) scattered electron energies.

As a check of neutral pion initiated events (and general spray), we took short runs with the polarity of the half-quadrupole magnet reversed. The results are shown in Table 4.6.

TABLE 4.6

Reversed Field Runs

$\bar{\theta}$ (degrees)	Reversed Field Rate/Scattered Electron Rate N	p'N	pN
7.59	7%	0.7%	0.4%
9.05	1.2%	0.9%	0.4%

Assuming that an equal number of apparent positron and electron events result from neutral pion decay, we find that these events accounted for less than 0.5% of the accepted electron events. Even for a maximum polarization correlation for this contamination, the effect on our final result would be less than 1/10 of a standard deviation.

As evidence that we were not detecting a significant number of charged pions whose intensity might be correlated with the target polarization, we note the lack of significant change in the resultant asymmetry when the Cerenkov and shower counter bias requirements were significantly raised. We did not perform any lead filter tests which could be analysed to give a useful limit to the charged pion contamination of the scattered electron sample.

We take the two evidences which we do have as sufficient indication that the results of this experiment are not affected by any possible pion contamination remaining in our accepted sample. No subtractions or increases in uncertainty were made due to possible pion contamination.

4.5 INTERPRETATION OF RESULTS

a) First Resonance Region.

1) Maximal Effect. Assuming that both resonant and non-resonant amplitudes contribute to a time reversal violation asymmetry, we obtain an estimate of the maximal effect possible for this experiment. We need estimates of the A and R (Eq. 1.16) to determine the phase angle δ between the potentially interfering scalar and transverse amplitudes in this model. Lynch, Allaby, and Ritson[38] and Bartel, et. al.[39] have separated the scalar and transverse contributions to the cross section in the kinematic range of interest to us. From their values (Table 4.7) we calculate $R = (\sigma_o/\sigma_T)^{1/2}$.

TABLE 4.7

First Resonance Region R Values

q^2 $(GeV/c)^2$	$\sigma_T(q^2)$ μb	$\sigma_o(q^2)$ μb	Ref.	R
0.1	530 ± 52	62 ± 27	38	$0.34\,^{+.08}_{-.18}$
0.2	444 ± 13	88 ± 23	38	
	436 ± 23	115 ± 37	39	
	442 ± 11	95 ± 20	Average	$0.46\,^{+.05}_{-.06}$
0.3	393 ± 14	144 ± 31	38	
	402 ± 18	81 ± 34	39	
	396 ± 11	115.4 ± 23	Average	$0.54\,^{+.05}_{-.06}$

For our $q^2 = 0.23$, we use $R = 0.5$.

Since the transverse pion production amplitudes in this region are dominated by the resonance, we use the value of A obtained from the resonant amplitude only. For the resonant magnetic dipole excitation,[40]

$$F_+ = \sqrt{3}\, F_- \quad \text{and} \quad A = 1/2.$$

From Eq. 1.16a, we get

$$\sin \delta = \frac{\alpha (1 + R^2)}{2\, A\, R} = 2.5\, \alpha$$

which leads to $\delta = (4.9 \pm^{6.2}_{5.9})^{\circ}$.

2) Pure Resonant Effect. If one assumes that a T violation effect occurs in the resonance alone, i.e., only the resonant part of F_- interferes with only the resonant part of F_z, one gets a slightly less restrictive limit on $\sin \delta$. A maximal effect within the confines of the purely resonant model occurs if all the scalar amplitude is resonant (in agreement with the tentative results of Mistretta, et. al.[62] for the π^0, but not including all parts of the pion pole contribution for π^+ production). Further, we extend the result of photoproduction by taking 75% of the transverse production as resonant,[41] then

$$f_1 = \sqrt{0.75} \quad \text{and} \quad f_2 = 0.1$$

so that

$$\sin\delta = \frac{\alpha(1 + R^2)}{2\ f_1\ f_2\ A\ \ R} = 2.9\,\alpha$$

and

$$\delta = (\ 5.8 \pm {}^{7.2}_{6.9}\ )^{\circ}$$

b) Second Resonance Region.

1) Maximal Effect. From a recent data compilation of photoproduction data,[42] the total γp cross section is about 125 μb in the region of the second resonance. If we take this value for $\sigma_T(q^2 = 0)$ and apply a q^2 dependence of the form $G_{MP}(q^2)/G_{MP}(0) = \left\{1/(1 + q^2/0.71)^2\right\}$, we obtain values for the transverse cross section $\sigma_T(q^2)$ in the regions of our measurements. Taking the value of the total cross section from Cone, et. al.[43] at $q^2 = 0.79\ (\text{GeV}/c)^2$ and $\epsilon = .72$ as appropriate to both our experimental points, we obtain the value of the total scalar cross section σ_0 from

$$\sigma = \sigma_T + \epsilon\sigma_0$$

TABLE 4.8

Second Resonance Region R Values

q^2 $(GeV/c)^2$	$\sigma_T(q^2)$ (μb)	σ (μb)	σ_0 (μb)	R
0.52	42	120	108	1.6
0.72	31	120	123	2

The resonance does not contribute to the numerator of A since $(F_-)_{resonance} = 0.$[44] Thus, even a maximal effect includes only interferences of the resonant and nonresonant scalar amplitudes with part of the nonresonant transverse amplitudes. Thus, in order to obtain an estimate of the maximal asymmetry consistent with current knowledge, we assume that (1) $(F_+)_{\text{NONRES.}} = 0$ and (2) all scalar amplitudes participate in the interference. Thus,

$$f_2 = 1$$

and from the data of Cone, et. al.,

$$Af_1 = 0.6$$

Thus, for $q^2 = 0.52\ (GeV/c)^2$

$$\sin \delta = (1.9)\,\alpha$$

and

$$\delta = \left(-16 \,{}^{+14}_{-15}\right)^{\circ}$$

and for $q^2 = 0.72\ (\mathrm{GeV}/c)^2$

$$\sin \delta = (2.1)\,\alpha$$

and

$$\delta = (-0.6 \pm 7.6)^{\circ}$$

<u>2) Pure Resonant Effect.</u> For $(F_-)_{res} = 0$ as discussed above, there can be no purely resonant T violation effect evident in this experiment.

<u>c) Third Resonance Region.</u>

Data on the third resonance region is even more sparce than it is for the second resonance region. Thus, in order to make an estimate of $\sin\delta$ from our value of α, it is necessary to make some even more unjustified extrapolations. From the indications that $(F_-)_{1688}$ resonance = 0,[45] we assume that the third resonance region is similar to the second and take over the maximum effect model discussed for that region. Thus,

$$f_2 = 1$$

and from the data of Cone, <u>et</u>. <u>al</u>.

$$A\, f_1 = 0.5.$$

Furthermore, we use the value of $\left(\frac{1 + R^2}{R} \right)$ which occurred for both other resonance regions. Thus

$$\sin \delta = (2.5)\,\alpha$$

and at $q^2 = 0.49$

$$\delta = \left(-1 \pm {}^{14}_{17}\right)^{\circ}$$

and at $q^2 = 0.68$

$$\delta = (-3.3 \pm 7.8)^{\circ}$$

4.6 CONCLUSIONS

The results of this experiment are summarized in Table 4.9, below.

TABLE 4.9

Summary

Resonance Region	$\bar{\theta}$ (degrees)	α	Model	$\sin\delta$	δ (degrees)
First	7.34	.035 ± .043	Max. Eff.	.088 ± .105	$4.9^{+6.2}_{-5.9}$
			Pure Res.	.102 ± .119	$5.8^{+7.2}_{-6.9}$
Second	7.59	-.142 ± .124	Max. Eff.	-.270 ± .236	-16^{+14}_{-15}
	9.05	-.005 ± .063	Max. Eff.	-.010 ± .132	-0.6 ± 7.6
Third	7.59	-.006 ± .109	Max. Eff.	-.015 ± .272	-1^{+14}_{-17}
	9.05	-.023 ± .064	Max. Eff.	-.057 ± .135	-3.3 ± 7.8

Values of δ away from 0 imply violation of T invariance.

From these results, it is clear that any T violation is less than maximal for the regions studied in this experiment. Furthermore, there is no evidence of any T violation outside the precision of this experiment.

In order to explain the magnitude of the observed CP violation in the decay of the long lived neutral K meson via the electromagnetic Hamiltonian, a nearly maximal T violation in the electromagnetic Hamiltonian was assumed. We find no such maximal violation evident and, therefore, no evidence for the hypothesized T even current K_μ suggested by Bernstein, Feinberg, and Lee.[2]

APPENDIX COINCIDENCE EXPERIMENT ATTEMPT

A.1 INTRODUCTION

In the early days of the Time Reversal Experiment, a limited effort was devoted to a coincidence experiment. As explained in Section 1.4a, the Time Reversal Experiment demands an integration over the hadron final states. To do otherwise, as by detecting some of the recoiling particles, could lead to an asymmetry due not to Time Reversal non-invariance, but due to the nature of the pion-nucleon interaction. The coincidence work was an attempt to measure this other effect, the interference between various components of the single pion electroproduction matrix.

The expectation was that data could be taken on line to the PDP-1 computer triggered on the electron arm alone. A later analysis would have separated out the coincidence events of interest for further study.

The extent of the limitation of effort was determined primarily by the time schedule for the Time Reversal Experiment. When it was discovered that the additional apparatus required to do the coincidence experiment included more than simple scintillation and plastic Cerenkov counters, the effort was cut out completely.

This appendix will discuss topically some of the thoughts and lessons which resulted from these early efforts.

A.2 PURPOSE OF THE COINCIDENCE EXPERIMENT AND RELATION TO OTHER MEASUREMENTS

a) Introduction

By its very nature, a coincidence polarization asymmetry measurement is a refined tool. Since it is a measure (as we shall see) of the imaginary part of an interference between different amplitudes, it is most useful when enough information already exists to predict what amplitudes are involved. To say that there is a large polarization asymmetry may contain no more information that that there exist two or more amplitudes with differing phases. (It is just this sort of information which is of interest in the Time Reversal Experiment. See Chapter 1.) In this appendix we will be concerned primarily with single pion electroproduction in the region of the first pion-nucleon resonance since it is only here that enough is known to interpret results meaningfully. Experimentally, this means measuring in kinematic regions where there is negligible contamination due to multiple pion production, typically below 1350 MeV for the pion-nucleon state energy in its own center of mass.

b) Theoretical Framework of Single Pion Electroproduction.

The notation used throughout this thesis is defined in Figures A.1 and A.2 and Table A.1. We maintain a close connection with the notation of Mistretta[50] who should be consulted for a more detailed discussion of some of the points which are only mentioned briefly here. Note that the four-momentum of the virtual photon is q, not k, as is common in some of the literature; and the pion momentum is $\vec{\pi}$, not $\vec{q}$. Starred quantities are evaluated in the center of mass system of the pion-nucleon final state and unstarred quantities, in the laboratory system.

In the one photon exchange approximation (Figure A.1), Lorentz invariance and conservation of the electromagnetic current allow the cross section to be expressed in terms of six complex amplitudes, $\mathcal{F}_i$.[51,52] The cross section (as given in Equation A.1) includes polarization effects due to target nucleons of polarization normal to the scattering plane, P. The selection of the particular six amplitudes above allows one to separate out the non-transverse parts of the total amplitude and to maintain a parallel with photoproduction for the four transverse amplitudes. The six amplitudes are functions of q^2, W, and θ_π^*. A further decomposition of the amplitudes in terms of the various multipole amplitudes allows one to separate out the θ_π^* dependence and the multipole amplitudes are functions of q^2 and W.[52] See Equation A.2. The advantage of the multipole decomposition in this energy region is that s and p pion-nucleon partial waves have been found sufficient to explain all but the pion pole term.[53] This part of the cross section is believed to be well described by the Born type amplitude which can be reliably calculated. Forthermore, the phases of the multipole amplitudes are equal to the corresponding pion-nucleon scattering phase shifts.[54] Near resonance, the W dependence of the multipole amplitudes may be isolated in the form $\sin\delta \; e^{i\delta}$ where $\delta(W)$ is the relevant pion-nucleon phase shift.

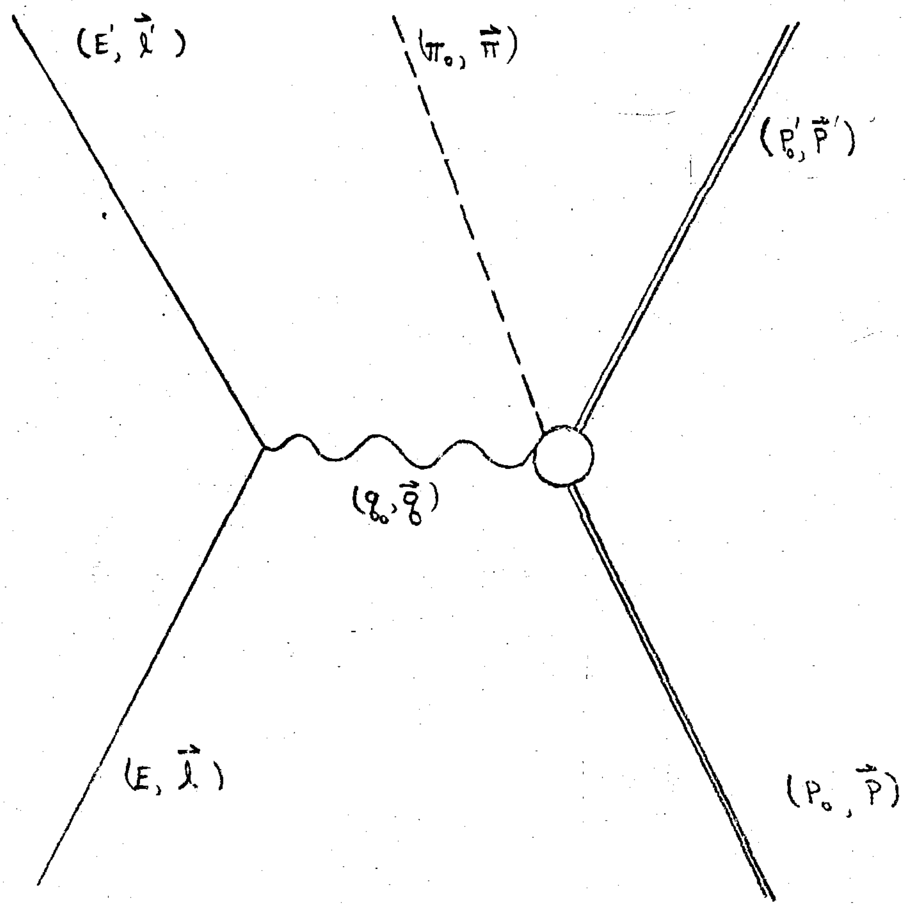

Single Photon Exchange
Diagram

FIG. A.1

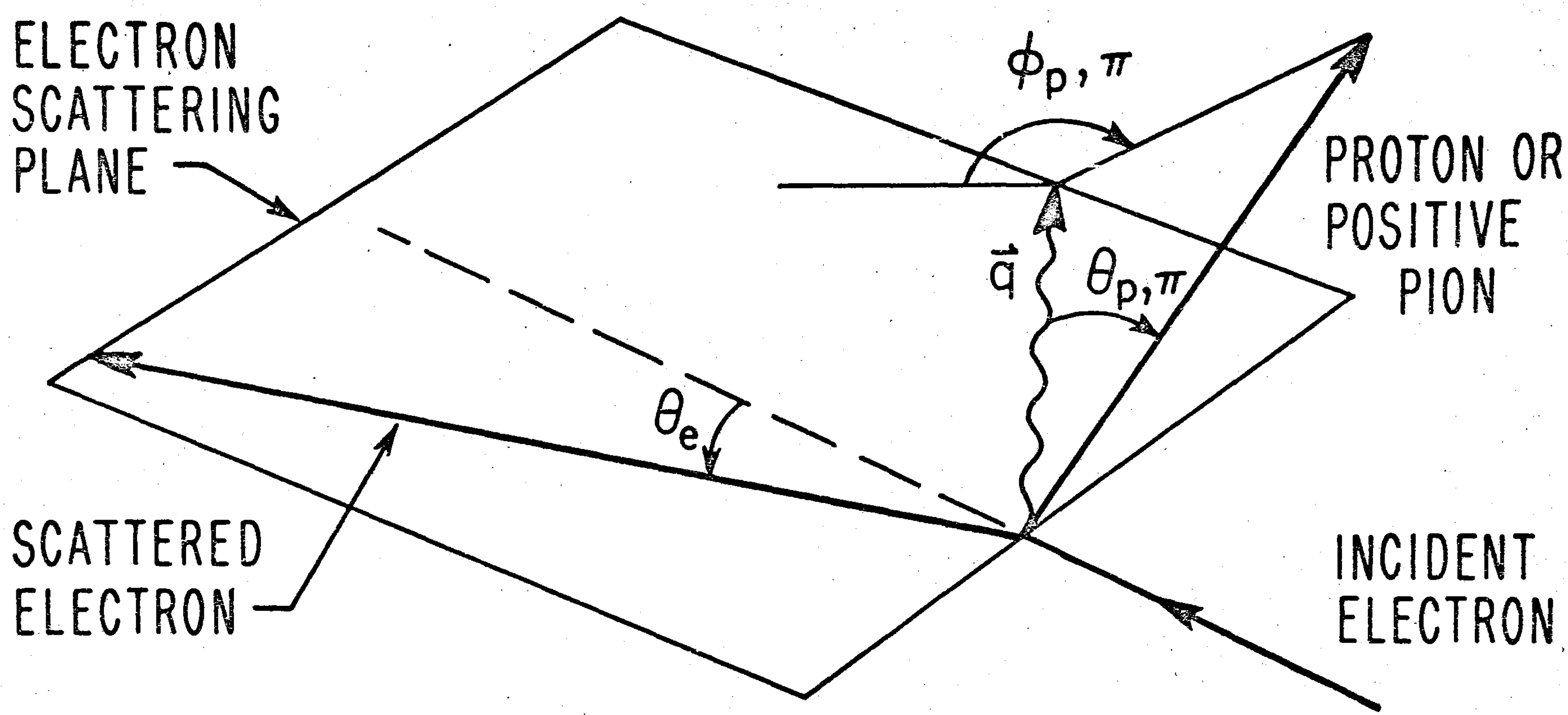

FIG. A.1. SINGLE PION PRODUCTION KINEMATICS

TABLE A.1

NOTATION

Invariant four momentum transfer $\quad q^2 \equiv |\vec{q}|^2 - q_0^2 = 4EE' \sin^2 \frac{\theta_e}{2}$

Energy transfer in the laboratory $\quad q_0 = E - E'$

Proton mass $= M$ $\qquad$ Pion mass $= \mu$

Equivalent photon energy $\quad K = q_0 - q^2/2M$

Scattered electron energy $\quad E' = (E-K)/(1 + \frac{2E}{M} \sin^2 \frac{\theta_e}{2})$

π- N center - of - mass energy $\quad W = (M^2 + 2MK)^{1/2}$

Pion momentum in π-N c. of m. system $\quad |\vec{\pi}^*| = \left[\frac{(W^2 + M^2 - \mu^2)^2}{2W} - M^2\right]^{1/2}$

$$\tau \equiv q_0^2/q^2$$

Angle between pion and $\vec{q}$ in π-N c. of m. system $\quad \theta_\pi^*$

$$z \equiv \cos \theta_\pi^*$$

Normal to the scattering plane $\quad \hat{n} \equiv (\vec{\ell} \times \vec{\ell}')/|\vec{\ell} \times \vec{\ell}'|$

Polarization normal to the scattering plane $\quad P = \vec{p} \cdot \hat{n}$

Eqn's. A.1

$$\frac{d\sigma}{d\Omega_e\, dE'\, d\Omega_\pi^*} = \Gamma_T \left[\frac{d\sigma_T}{d\Omega_\pi^*} + \epsilon \frac{d\sigma_0}{d\Omega_\pi^*} + \epsilon \frac{d\sigma_{RTT}}{d\Omega_\pi^*} \sin^2\theta_\pi^* \cos 2\phi_\pi \right.$$

$$\left. + \sin\theta_\pi^* \cos\phi_\pi \sqrt{\frac{\epsilon(\epsilon+1)}{2}}\, \frac{d\sigma_{ROT}}{d\Omega_\pi^*} + P \frac{d\sigma_P}{d\Omega_\pi^*} \right]$$

$$\Gamma_T = \frac{\alpha}{4\pi^2} \frac{K}{q^2} \frac{E'}{E} \left[2 + \frac{\cot^2 \frac{\theta_e}{2}}{1+\tau} \right]$$

$$\epsilon = \cot^2 \frac{\theta_e}{2} \Big/ \left[2(1+\tau) + \cot^2 \frac{\theta_e}{2} \right]$$

$$\frac{d\sigma_T}{d\Omega_\pi^*} = \frac{|\vec{\pi}^*|\, W}{M\, K} \left[|\mathcal{F}_1|^2 + |\mathcal{F}_2|^2 - 2z\, \mathrm{Re}(\mathcal{F}_1 \mathcal{F}_2^*) \right] + \frac{d\sigma_{RTT}}{d\Omega_\pi^*} \sin^2\theta_\pi^*$$

$$\frac{d\sigma_0}{d\Omega_\pi^*} = \frac{|\vec{\pi}^*|\, W}{M\, K} \frac{q^2}{q_0^{*2}} \left[|\mathcal{F}_7|^2 + |\mathcal{F}_8|^2 + 2z\, \mathrm{Re}(\mathcal{F}_7 \mathcal{F}_8^*) \right]$$

$$\frac{d\sigma_{RTT}}{d\Omega_\pi^*} = \frac{|\vec{\pi}^*|\, W}{2M\, K} \left[|\mathcal{F}_3|^2 + |\mathcal{F}_4|^2 + 2\, \mathrm{Re}\left(\mathcal{F}_2 \mathcal{F}_3^* + \mathcal{F}_1 \mathcal{F}_4^* + \mathcal{F}_3 \mathcal{F}_4^* z \right) \right]$$

$$\frac{d\sigma_{ROT}}{d\Omega_\pi^*} = -\frac{2\, |\vec{\pi}^*|\, W}{M K} \left[\frac{q^2}{q_0^{*2}} \right]^{1/2} \mathrm{Re}\left[(\mathcal{F}_1 + \mathcal{F}_4 + \mathcal{F}_3 z)\mathcal{F}_7^* + (\mathcal{F}_2 + \mathcal{F}_3 + \mathcal{F}_4 z)\mathcal{F}_8^* \right]$$

$$\frac{d\sigma_P}{d\Omega_\pi^*} = \left\{ \frac{d\sigma_{IU}}{d\Omega_\pi^*} + \epsilon \frac{d\sigma_{IP}}{d\Omega_\pi^*} + \epsilon \frac{d\sigma_{I00}}{d\Omega_\pi^*} \right\} \sin\theta_\pi^* \cos\phi_\pi + \frac{d\sigma_{IOT}}{d\Omega_\pi^*}$$

Eqn's A.1 (con't.)

$$\frac{d\sigma_{IU}}{d\Omega_\pi^*} = -\frac{|\vec{\pi}^*|W}{2MK}\ \mathrm{Im}\left[\mathcal{F}_3\mathcal{F}_4^*\sin^2\theta_\pi^* + \mathcal{F}_1\left(\mathcal{F}_3^* + \mathcal{F}_4^* z\right) - \mathcal{F}_2\left(\mathcal{F}_3^* z + \mathcal{F}_4^*\right)\right]$$

$$\frac{d\sigma_{IP}}{d\Omega_\pi^*} = -\frac{|\vec{\pi}^*|W}{2MK}\ \mathrm{Im}\left[2\mathcal{F}_1\mathcal{F}_2^* + \mathcal{F}_1\left(\mathcal{F}_3^* + \mathcal{F}_4^* z\right) - \mathcal{F}_2\left(\mathcal{F}_3^* z + \mathcal{F}_4^*\right) - 2\sin^2\theta_\pi^*\cos^2\phi_\pi\,\mathcal{F}_3\mathcal{F}_4^*\right]$$

$$\frac{d\sigma_{I00}}{d\Omega_\pi^*} = \frac{|\vec{\pi}^*|W}{MK}\left[\frac{q^2}{q_0^{*2}}\right]\mathrm{Im}\left[\mathcal{F}_7\mathcal{F}_8^*\right]$$

$$\frac{d\sigma_{I0T}}{d\Omega_\pi^*} = \frac{|\vec{\pi}^*|W}{MK}\left[\frac{q^2}{q_0^{*2}}\right]^{1/2}\mathrm{Im}\left[\begin{aligned}&\left(\mathcal{F}_1 - \mathcal{F}_2 z + \mathcal{F}_4\sin^2\theta_\pi^*\cos^2\phi_\pi\right)\mathcal{F}_8^* \\ &-\left(\mathcal{F}_2 - \mathcal{F}_1 z + \mathcal{F}_3\sin^2\theta_\pi^*\cos^2\phi_\pi\right)\mathcal{F}_7^*\end{aligned}\right]$$

$$\left.\begin{aligned}
\mathcal{F}_1 &= \sum_\ell \left(\ell M_\ell^+ + E_\ell^+\right) P'_{\ell+1}(z) + \left[(\ell+1) M_\ell^- + E_\ell^-\right] P'_{\ell-1}(z) \\
\mathcal{F}_2 &= \sum_\ell \left[(\ell+1) M_\ell^+ + \ell M_\ell^-\right] P'_\ell(z) \\
\mathcal{F}_3 &= \sum_\ell \left(E_\ell^+ - M_\ell^+\right) P''_{\ell+1}(z) + \left(E_\ell^- + M_\ell^-\right) P''_{\ell-1}(z) \\
\mathcal{F}_4 &= \sum_\ell \left(M_\ell^+ - E_\ell^+ - M_\ell^- - E_\ell^-\right) P''_\ell(z) \\
\mathcal{F}_7 &= \sum_\ell \left(\ell S_\ell^- - S_\ell^+\right) P'_\ell(z) \\
\mathcal{F}_8 &= \sum_\ell S_\ell^+ P'_{\ell+1}(z) - S_\ell^- P'_{\ell-1}(z)
\end{aligned}\right\} \quad (A.2)$$

where $P'_\ell(z)$ is the first derivative with respect to $z \equiv \cos\theta_\pi^*$ of the Legendre Polynomial $P_\ell(z)$ and $P''_\ell(z)$ is the second derivative.

Including only s and p pion-nucleon partial waves yields

$$\left.\begin{aligned}
\mathcal{F}_1 &= E_0^+ + 3z\left(M_1^+ + E_1^+\right) \\
\mathcal{F}_2 &= 2M_1^+ + M_1^- \\
\mathcal{F}_3 &= 3\left(E_1^+ - M_1^+\right) \\
\mathcal{F}_4 &= 0 \\
\mathcal{F}_7 &= S_1^- - S_1^+ \\
\mathcal{F}_8 &= S_0^+ + 3z\, S_1^+ .
\end{aligned}\right\} \quad (A.3)$$

c) Previous Experimental Work.

Five laboratories have done coincidence experiments in single pion electroproduction; Orsay,[55] Tokyo,[56,57] DESY,[58] Cornell,[59,60] and CEA.[61,62,63] Each of these laboratories has made measurements of the triply-differential cross section (Eq. A.1). Only the last two groups obtained data on π^+ production as well as data on π^o production. The CEA group have done the only extensive work. on angular distributions and no work has been done on polarization effects. Thus, only those terms which remain in Equation A.1 when P is set equal to zero have been studied.

The π^o production data have been interpreted mainly in terms of non-coincidence parameters, the γ-N-N* vertex form factors. The need for coincidence data to study the form factors has been to isolate the $p\pi^o$ mode which is known to be dominated by the intermediate N*. This simple interpretation is not possible for π^+ production due to the pion pole contribution. The γ-N-N* form factor interpretation depends on the assumption of purely narrow-resonance production for the region studied. Furthermore, the interpretation of data from limited angular regions in terms of integrated cross sections has required the assumption of an angular distribution, taken to be that of the dominant M_1^+ multipole amplitude.

Although these approximations are compatible with the earliest experimental accuracy, further work will demand a more sophisticated treatment. There already exists some evidence that the above model for π^o production is inadequate. The data of Baba, et. al.[56] and Mistretta et. al.[61,62] show significant scalar contributions to the π^o cross sections at $q^2 = 3$ and $6\ F^{-2}$. Furthermore, there is a 5% ratio of the amplitudes E_1^+/M_1^+ apparent in π^o photoproduction.[64] Mistretta et. al.[61,62] have detected the continuation of this E_1^+ amplitude into electroproduction.[64] In addition, they interpret the magnetic γ-N-N* form factor, G_m^* to be due solely to the M_1^+ and, having isolated M_1^+ from E_1^+ and S_1^+, calculate G_m^* from the value of M_1^+ alone. Earlier values of G_m^* include whatever contributions these and other multipoles may have made to the cross section before integration over the assumed angular distribution.

The most interesting questions in π^o production at this point are about the smaller amplitudes. The Mistretta identification of the non-zero scalar amplitude as S_1^+ is not conclusive. And since the quark model predicts that both E_1^+ and S_1^+ should not contribute to the resonance,[65] further study of these amplitudes is warranted.

The major interest in the π^+ production data has been in determining the pion form factor, F_π. Earlier work on the form factor have given limits on the pion radius, r_π:

$$r_\pi^2 = -6 \left. \frac{dF_\pi(q^2)}{dq^2} \right|_{q^2=0} \qquad (A.4)$$

The results from π-α scattering[71] is r < 1 F and from π-e scattering,[70] r < 3 F. If one expresses the form factor as

$$F_\pi(q^2) = \frac{1}{1 + \frac{q^2 r_\pi^2}{6}} \qquad (A.5)$$

then the results of the Cornell and CEA data for π^+ electroproduction combine to give[63]

$$r_\pi = (0.86 \pm 0.14)\ F, \qquad (A.6)$$

Both the Cornell and CEA results are obtained essentially from their measurements of the purely scalar part of the cross section. The Cornell group depended on theory to estimate the transverse part of the cross section in the $\theta_\pi^* = 0$ direction. The CEA group used the theory with the pion form factor as a free parameter in a fit of the angular distribution. Although the effect of the pion form factor on the scalar-transverse interference is large, the term itself is small due to the relative phase between the scalar amplitude (nearly real) and the transverse amplitude (nearly pure imaginary at resonance).

Although interest in F_π is fundamental, an understanding of the phenomenon of pion electroproduction requires a knowledge of six complex amplitudes (such as those in Eq. A.2). These have not received much attention as of yet. Mistretta, et. al. did not obtain a fit to the angular distribution for π^+ production as they did for π^0 production. The contribution of the pion form factor was thought not to be amenable to the simplified distribution due to s and p partial waves alone. However, the contributions of the Born term to the partial waves higher than p get successively smaller and a good fit might well have been obtained with just s and p partial waves.

A.3 KINEMATIC AND ISOSPIN PROPERTIES OF SINGLE PION PRODUCTION

The two charge modes of single pion production from hydrogen

$$\text{(hardons)} \longrightarrow \begin{matrix} p\pi^{o} \\ n\pi^{+} \end{matrix}$$

are most easily distinguished experimentally via the detection of the charged particle. Due to the significantly different masses of the proton and pion, each hadron corresponds to a kinematic situation different from that of the other. Typically, the protons are limited to a forward cone (whose axis points along the direction of $\vec{q}$) while the pions can emerge in all directions.

The folding forward of the proton momenta leads to a Jacobian enhancement at the edge of the laboratory cone. Furthermore, it becomes conceivable to measure the full angular phase space of the protons. If one is studying some effect in the N^* production from hydrogen, it becomes possible to determine experimentally the isospin (I) character of the effect. The following considerations demonstrate the method.

Since the decay of the N^* is via strong interactions, the decay must conserve isospin. Any change in isospin must, therefore, come from the electromagnetic production of the N* which does not conserve isospin. In the usual notation, the isospin decomposition of the singly charged pion-nucleon modes are

$$|p\pi^o\rangle = \sqrt{\frac{2}{3}}\left|\frac{3}{2}, \frac{1}{2}\right\rangle - \sqrt{\frac{1}{3}}\left|\frac{1}{2}, \frac{1}{2}\right\rangle$$

and

$$|n\pi^+\rangle = \sqrt{\frac{1}{3}}\left|\frac{3}{2}, \frac{1}{2}\right\rangle + \sqrt{\frac{2}{3}}\left|\frac{1}{2}, \frac{1}{2}\right\rangle$$

If one photo- or electro-produces either of the above states from a proton, $\left|\frac{1}{2}, \frac{1}{2}\right\rangle$, a definite isospin overlap exists. Thus, for some total production effect, E, a pure $\Delta I = 0$ effect would lead to

1/3 of the effect in the $p\pi^o$ mode, E_o

and

2/3 of the effect in the $n\pi^+$ mode, E_+.

Thus, $$E = E_+ + E_o$$

with $$E_o = 1/3\ E \quad \text{and} \quad E_+ = 2/3\ E.$$

Similarly, for a pure $\Delta I = 1$ effect, we expect

$$E_o = 2/3\ E \quad \text{and} \quad E_+ = 1/3\ E.$$

Of course, a similar analysis is possible for electromagnetic pion production from neutrons. The result is expressed by the same formulae above except that $+ \longrightarrow -$.

Frequently, this additional handle is not necessary. When at the first pion-nucleon resonance, for example, the isospin character of the resonance is known and the non-resonant backgrounds are small. However, for the more complicated regions of the spectrum, one may obtain some sensitivity to which of competing sources is contributing to an effect. If two competing resonances have different isospin, the ratio of the proton mode effect to the total production effect will tell which resonance is contributing.

For $\Delta I = 1$ effects, it is a potentially nice feature that the Jacobian enhancement enters as an additional enlargement to the $\pi^o p$ enhancement.

A.4 METHOD OF DATA ACQUISITION

The original intention in the coincidence experiment attempts was to record coincidence arm data for every electron trigger. Later reanalysis would have been used to separate the coincidence events from the bulk of the data. In this way, no extra time would have been necessary for the coincidence work. The interesting coincidence events were expected to occur at about one in twenty electron triggers. Rather than waste the triggers without coincidences, these triggers were to be used to record delayed coincidences. These delayed coincidences were to be used to make random backgrounds corrections.

The logic circuitry was set up to determine if an interesting coincidence had occurred for each electron arm trigger. If not, the electronic circuitry was used to sample random coincidence event information. This was done by applying the series of gates to the coincidence arm logic modules early relative to the coincidence-time rather than at the coincidence-time. Using early gating rather than delayed gating minimized effects which were truly correlated with the electron arm, i.e., non-random backgrounds. If the gate to the coincidence arm had been given after the true coincidence time, various effects of non-triggering "garbage" might effect later pulse discrimination. A photon shower or aperture-edge effects might cause such interference. K. Hanson[66] has observed such a difference in randoms rates between systems with pre- and post- coincidence-time gates.

None of this system was ever tested except on a simulating pulser. The high rates discussed in the section on backgrounds precluded any in-use tests of the logic or other circuit behavior.

A.5 BACKGROUNDS: THE END OF THE ATTEMPT

The coincidence arm experiment was eventually dropped because of the extremely high rates in the coincidence counters. The attempt to do the experiment with poorly protected counters stemmed from two factors:

1) The product of target length, beam intensity, and solid angle for the coincidence arm was 1/6 of that used in the experiment of Mistretta, *et. al.*[50]
2) The field of the polarized target was expected to bend away low energy charged particles, usually the largest part of coincidence backgrounds. The target field will *contain* charged particles with momentum less than 85 MeV/c. This limit is more advantageous than that of the Broom (sweeping magnet) or 1/4 inch of lead, both of which were used in previous experiments by this group.

The inference from these considerations was that backgrounds would not be a problem.

This inference was incorrect. The imposition of a high magnetic field at the target was an essentially different experimental situation from those of previous efforts by our group. The source of backgrounds was equally different. The backgrounds were not due to particles emerging from the target in the direction of the counters, but rather to particles emerging in the forward beam direction. These forward particles were then bent into the counters by the large magnetic field which one had hoped would do the shielding job. A particle of momentum 120 MeV/c initially going forward will just be bent into the beam side of the acceptance. Lower momentum particles will bend farther away from the beam direction into the acceptance. The lower limit of accepted momenta was determined by the curling up of particles.

The extrapolation of a calculation by K. W. Robinson[67] was used to estimate the real particle rate in the momentum acceptance 85-120 MeV/c. Robinson calculated the number of electrons and positrons produced by a 6 GeV incident electron on various radiation lengths of material. No angular distributions were included since virtually all radiation is forward.

We make the following assumptions in using the results of Robinson;

1) The numbers of low energy enectrons and positrons is not a sensitive function of the incident energy. Most of the low energy particles are expected to be due to the low energy bremsstrahlung which will not change much in the range from 3 to 6 GeV incident energy.

2) The number of secondary particles per energy bin is not a sensitive function of energy. See Figure A.3.

Figure A.3

ELECTRON - POSITRON PRODUCTION PER INCIDENT ELECTRON

$E_0 = 6$ GeV

(0.1 Radiation Length Radiator)

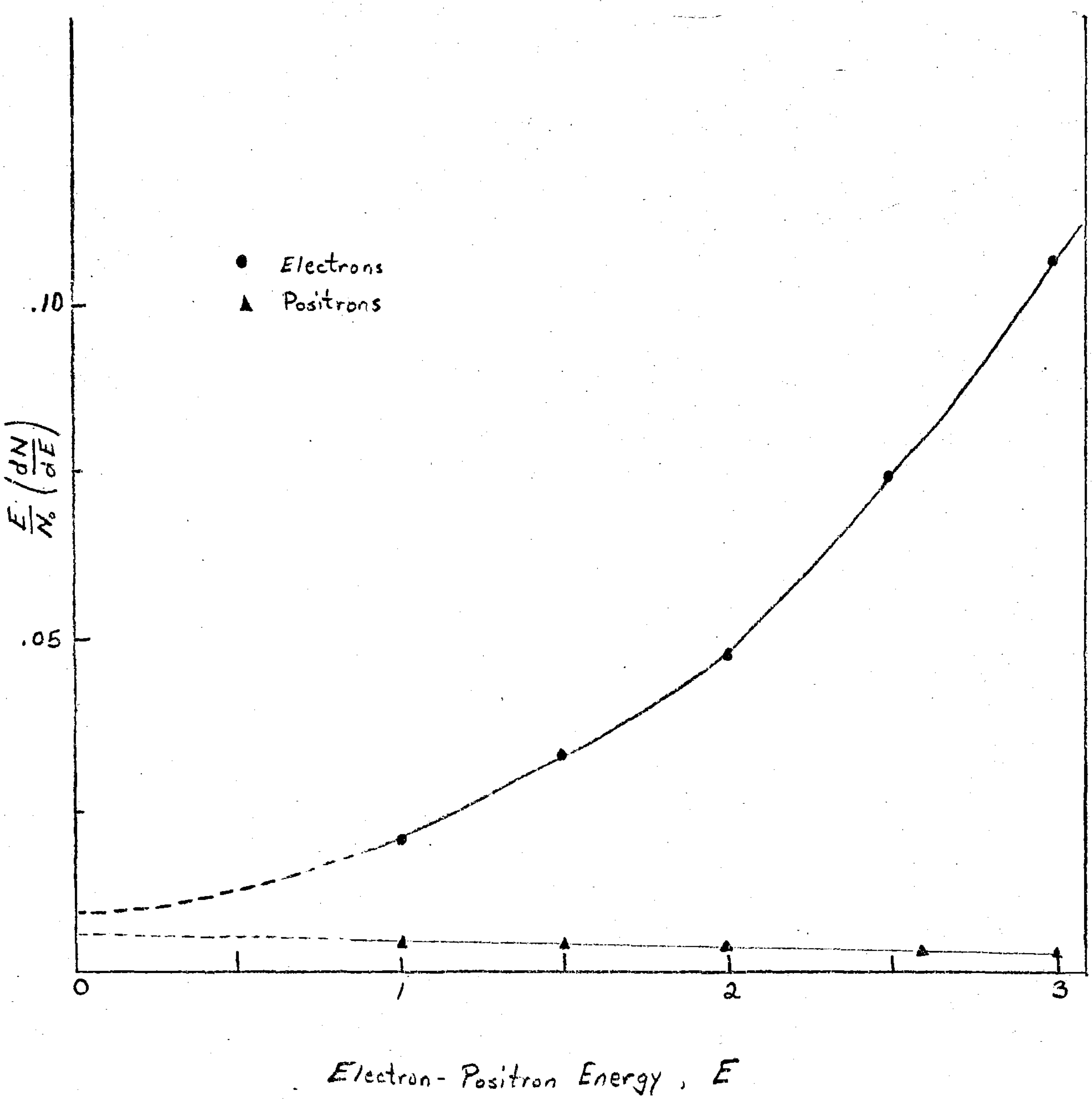

For a 3 nanoampere incident beam, 0.1 radiation length target, and a 35% energy bite centered at 100 MeV/c, one would expect a positron rate of 25 Mc/sec and an electron rate of 50 Mc/sec. For the polarity of target field used, we detected positrons. These particles were located at beam height in a plane perpendicular to the magnet field except for the small dispersion in the initial directions and the much larger dispersion caused by multiple scattering in the target. The multiple scattering alone causes an RMS scattering angle of 1.2°. This fills about 1/5 of the coincidence aperture. In an attempt to reduce this high flux of particles, a one inch high, two inch deep tungsten plug was placed at beam height 18 inches from the target ($\pm 1.6^{\circ}$ or 1/4 of the aperture). However, the 100 Mc Chronetics electronic discriminators could not handle the remaining singles rate. Later use of EG&G dc-coupled 200 Mc discriminators gave dc outputs during the spill. For pulses of 5 nsec. width, a dc output level implies an instantaneous rate in excess of 200 Mc. The difference between this lower limit and that calculated for the bending of forward particles might easily be explained by lower energy positrons and photons which shower in the (Al) wall of the inside edge of the aperture.

A.6 LIMITATIONS OF THE PRESENT TARGET

The limitations of the present target are threefold; (1) a limit on beam intensity due to local beam heating, (2) a limit on total charge per unit area due to radiation damage, and (3) a limit on solid angle due to the physical size of the coincidence aperture. The first two of these were particular concerns of J. Chen and are discussed in his thesis.[27] The last limitation was not a problem in the single arm experiment, but limits the usefulness of the present target for coincidence experiments.

The openings in the target walls were $\pm$ 6 2/3 degrees vertically. The horizontal apertures are incicated in Figure A.4. The horizontal apertures are not a serious problem for any of the electron-proton scattering experiments considered to date. However, the vertical aperture is restrictive. Two cases of this restriction are given in Section A.7. The use of a quadrupole magnet for the electron spectrometer necessarily tilts the electron scattering plane relative to the horizontal. For small angles, where rates are highest and the beam limitations are minimized, the tilt of the scattering plane is most severe. Typically, the coincident particles in the scattering plane cannot be detected. Figure A.5 gives an example of this problem.

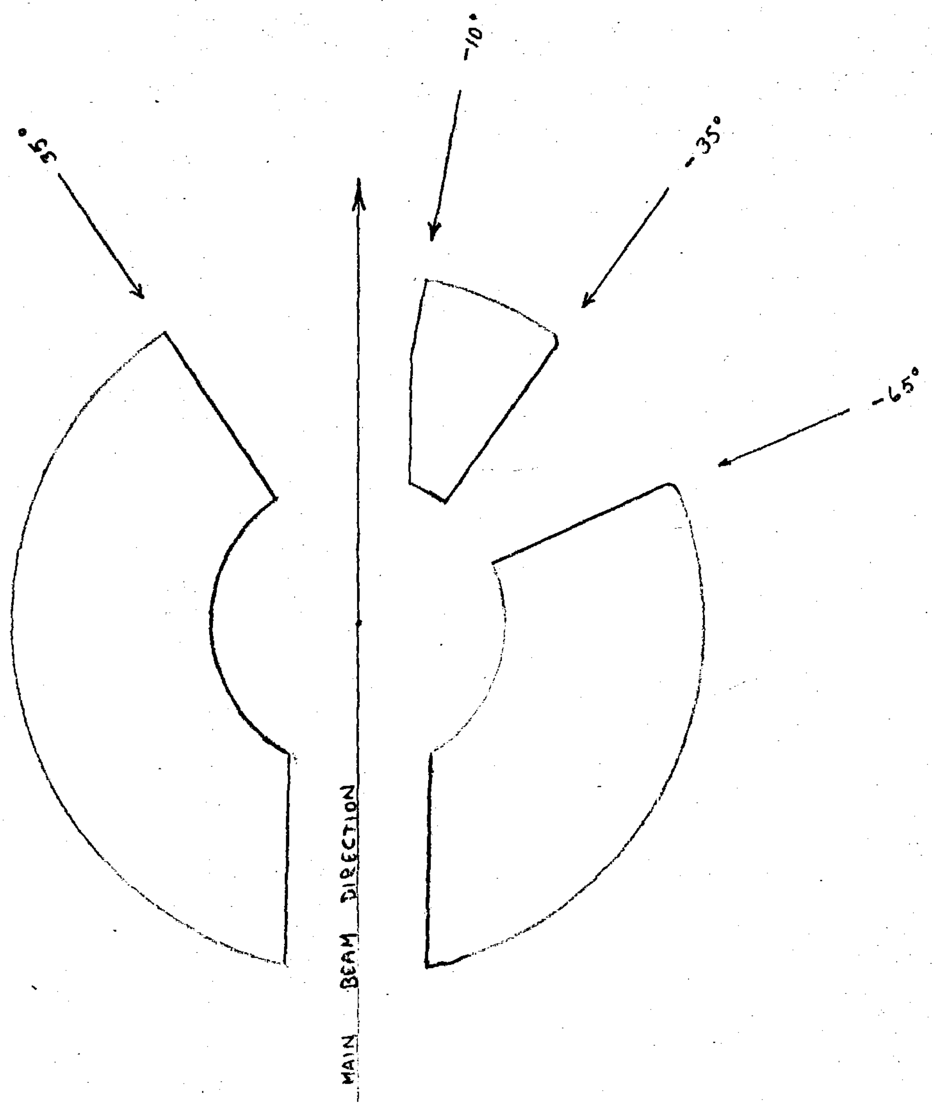

THE POLARIZED TARGET APERTURES

Figure A.4

Figure A.5

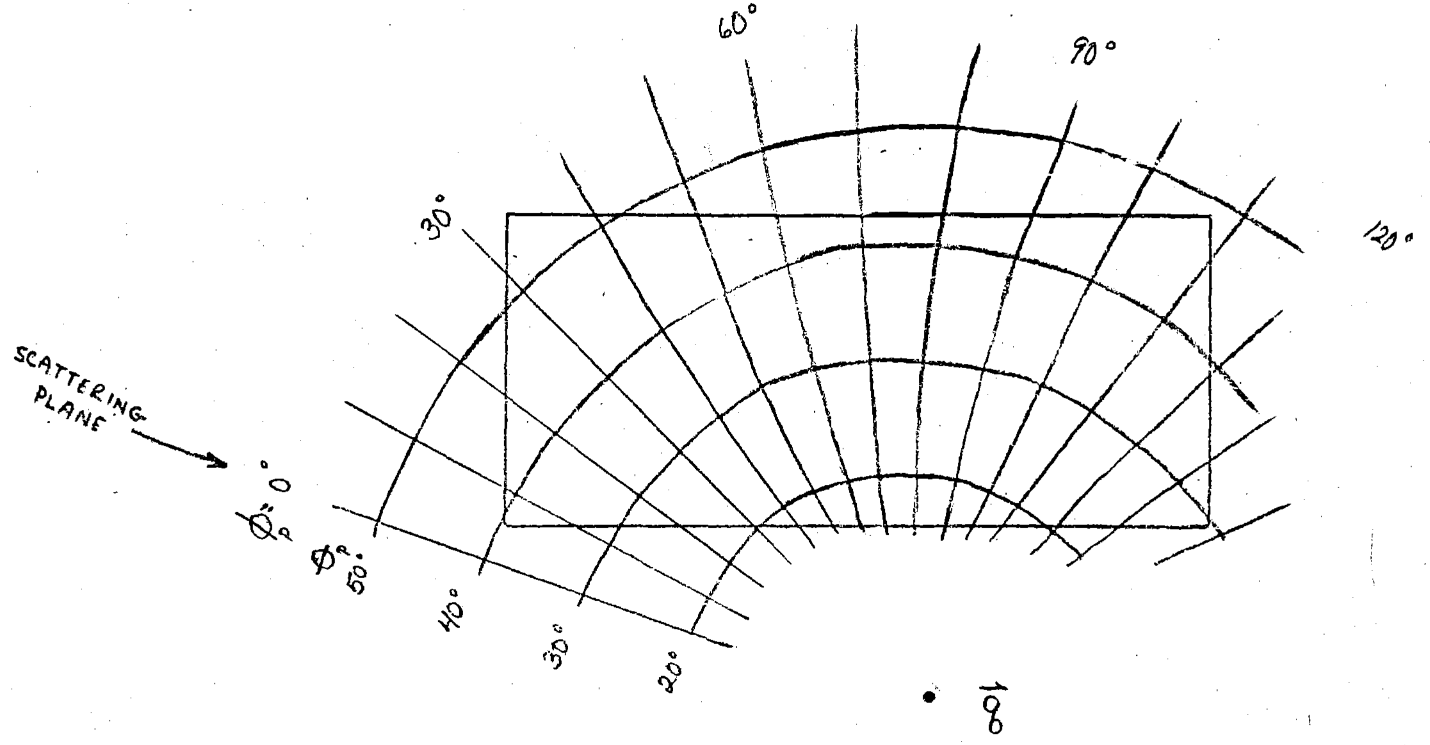

$E = 5.5$ GeV
$K = 320$ MeV
$\Theta_e = 5.8°$

MAPPING OF PROTON SOLID ANGLE GRID
THROUGH POL. TGT. FIELD
[WITH TARGET APERTURE SUPERIMPOSED]

Thus, when a scattering plane coincidence is desired, a dipole electron spectrometer will have a decided advantage for use with the present target. On the other hand, when the scattering away from the scattering plane is of interest, the quadrupole electron spectrometer may place the interesting solid angle in the proper direction for coincident particle detection. The region of the Jacobian enhancement perpendicular to the scattering plane is just such an interesting region. The important point here is that the present target apertures severely restrict the freedom of choice for coincidence solid angles available in a single experimental set-up.

A.7 CAN A USEFUL COINCIDENCE EXPERIMENT BE DONE?

a) Introduction.

Simplicity of operation and speed of implementation had the highest priority in the coincidence experiment attempts. Having noted that these attempts were dropped due to lack of time, it is appropriate to ask if a truly useful experiment could have been done given the necessary time and money.

We turn our attention in this final section of the appendix to two classes of experiments to see what might be accomplished. We consider first an experiment with elastic scattering of electrons from polarized protons, a search for two photon exchange effects. Then we look in some detail at the single pion production which has been the main focus of this appendix and which was the initial aim of the early coincidence attempts.

The discussion which follows should only be viewed as speculative. What insight it contains was gleaned from the rather hurried attempts to understand and implement a coincidence experiment.

b) Elastic Scattering Experiment.

As discussed in Section 1.4a, any polarization asymmetry in elastic scattering would be ascribed to an interference between the usual single photon exchange and a two photon exchange amplitude. One may, therefore, use a polarized target experiment as a test of possible two photon exchange diagrams in elastic electron-proton scattering.

Any two photon exchange effects are not likely to be greater than a few percent. Thus, any experiment, to be interesting, must produce sensitivity on this level. This requires even greater precision than that obtained for the Time Reversal Experiment. Two methods suggest themselves for increasing the statistical accuracy when the beam intensity is limited. (1) Select kinematic regions with a higher counting rate. (2) Remove as much as possible of the uninteresting scattering from counts entering the asymmetry measurement. We discuss the implications of each of these methods.

Highest rates are associated with the most forward electron scattering. But forward scattering leads to lower values of q^2. Since two photon exchange effects are not expected at low q^2, we start with $q^2 = 20\ F^{-2}$ as the lowest q^2 of interest. At 6 BeV incident energy, one obtains an electron scattering angle of 8.7^o. For the standard weekend of data taking (defined in Table A.2), one obtains 0.3×10^6 scatterings from free hydrogen. Total scattering from the hydrocarbon target would be about 2×10^6 counts. For a 20% average polarization, the uncertainty on the asymmetry would be

$$\pm\,\delta\alpha = \frac{1}{(1/7)(0.2)}\sqrt{\frac{1}{2.1\times10^6}} \sim 2.3\% \qquad (A.7)$$

The results of the similar calculation for $q^2 = 30\ F^{-2}$ are given in Table A.2.

In order to reduce the 2.3% uncertainty further, one may try to reduce the accepted scattering from the non-free protons in the target. The only method of doing this without a coincidence is to accept only the scattered electrons immediately in the region of the elastic peak as defined by the resolution of the system. In this experiment, it is not necessary to accept all scattering events in the radiative tail of the elastic peak. However, this technique will only reduce the non-free proton scattering by about 1/3, giving a new uncertainty of $\pm$ 1.9%. It should be remembered, however, that using a tight acceptance on a rapidly varying spectrum gives a very much greater sensitivity to small changes in incident energy and angle than was the case for the Time Reversal Experiment.

A more appropriate way of reducing the uninteresting scattering is via the coincidence technique. Essentially all scattering from neutrons can be eliminated by demanding a charged particle in coincidence with the electron.

TABLE A.2

q^2 (F^{-2})	θ ($^\circ$)	E (GeV)	VAMF	N ($\times 10^{+6}$)	$\delta\alpha$ (%)
20	8.7	6.0	5.8	2.39	2.3
30	10.9	6.0	4.3	.46	5.2
20	20	2.8	1.4	.39	5.6
	30	1.9	1.0	.15	9.0
30	20	3.4	1.4	.12	10.2
	30	2.4	1.0	.045	16.5

VAMF = vertical aperture mapping factor = $\left.\dfrac{\Delta\theta_{p,\pi}}{\Delta\theta_e}\right)_{\text{vertical}}$

N = number of counts obtained in a "standard weekend"

$d\Omega_e$ = 1.8 mstr.

Target = 1 inch ethanol

Running time = 30 hours of data acquisition

Beam intensity = 3 nanoamperes

$\delta\alpha$ = consequent asymmetry uncertainty ($\sqrt{\frac{1}{N}}$ x normalization factor due to polarization < 1 and non-free hydrogen scattering.)

No improvements ascribed to limited acceptances are included in N or $\delta\alpha$. (See text.)

Once one is going to use a coincidence counter, the needed sweeping magnetic field may as well be used to gain momentum resolution on the coincident charged particle. Making the coincidence counters only as large as necessary to be efficient for elastically scattered free protons, about 30% of the quasielastically scattered protons will not be detected. The resultant uncertainty would be $\pm$ 1.6%; better than the energy bite restriction because of the better discrimination against neutrons. Furthermore the spectrum of quasielastic proton angle and energy is much less rapidly varying than the electron energy spectrum.

The improvements due to reductions of electron energy acceptance and proton acceptance do not add directly since the rejection tends to be redundant. The redundancy is increased at forward angles.

The target used in the present experiment has a vertical aperture of $\pm$ 6 2/3°. The centers of our electron apertures are at vertical angles of $\pm$ 2.3° relative to the horizontal plane. The vertical aperture mapping factor (VAMF), the ratio of vertical components of the coincidence and electron apertures (listed in column 4 of Table A.2) shows that neither of the high energy elastic scattering points above could be done with the coincidence technique with the present target and apectrometer. Therefore, the results of a series of calculations is presented with VAMF's consistent with a coincidence measurement with the present apparatus. The larger electron scattering angle reduces the rate so that the statistical uncertainty detracts from interest in this technique.

It is clear from Table A.2 that the present apparatus is not sufficient to perform a useful experiment on the two photon exchange effect at the CEA. One could gain significantly by going to higher incident electron energies and, thereby, increase the rate further. The lead passes to SLAC. A polarized target with a larger aperture would still not be merited.

The major limitation is the beam ceiling imposed by target depolarization. If a new material is found which allows two orders of magnitude more beam, then a new era of polarized target experiments at electron accelerators will open. An increase in average polarization would also be most helpful. After all, a polarized target experiment is the ideal method of doing high q^2 asymmetry measurements. Although outgoing proton polarization is a measure of the same asymmetry as is measured in polarized target experiments, the outgoing proton momentum increases with q^2 causing a decrease in the analysing power of second scatterings.

For now, looking for second order effects like two photon exchange is not inviting. We now turn our attention to first order effects as they are found in inelastic electron scattering.

c) Single Pion Production Experiments.

1) The Asymmetry. In order to isolate a sifficiently simple term in the cross section so that a single experiment can make a useful measurement, we consider the asymmetry near cos ϕ = 0, i.e., $\phi = 90^\circ$ and 270°. This region corresponds to a strip of solid angle normal to the scattering plane in the $\vec{q}$ direction. For cos ϕ = 0, the cross section reduces to

$$\frac{d\sigma}{dE' d\Omega_e d\Omega_\pi^*} = \Gamma_T \left\{ \frac{d\sigma_T}{d\Omega_\pi^*} + \epsilon \frac{d\sigma_0}{d\Omega_\pi^*} - \epsilon \sin^2\theta_\pi^* \frac{d\sigma_{RTT}}{d\Omega_\pi^*} + P\sqrt{\frac{\epsilon(\epsilon+1)}{2}} \frac{d\sigma_{IOT}}{d\Omega_\pi^*} \right\} \quad (A.8)$$

which gives an asymmetry of the form

$$\alpha = P\left(\frac{q^2}{q_0^{*2}}\right)^{1/2} \sqrt{\frac{\epsilon(\epsilon+1)}{2}} \; \frac{\mathrm{Im}\left[(\mathcal{F}_1 - 3\mathcal{F}_2)\mathcal{F}_8^* - (3\mathcal{F}_1 - \mathcal{F}_2)\mathcal{F}_7^*\right]}{\frac{MK}{W|\vec{\pi}^*|}\left[\frac{d\sigma_T}{d\Omega_\pi^*} + \epsilon\left(\frac{d\sigma_0}{d\Omega_\pi^*} - \sin^2\theta_\pi^* \frac{d\sigma_{RTT}}{d\Omega_\pi^*}\right)\right]} \quad (A.9)$$

For ϵ near 1, the remaining terms are the same as those which contribute along the direction parallel to the $\vec{q}$ direction. This fact will be important when one considers π^+ production in an attempt to determine the pion form factor.

Keeping only the leading term in the transverse amplitude and using only s and p pion-nucleon partial waves, the numerator of the asymmetry contains

$$\frac{d\sigma_{IOT}}{d\Omega_\pi^*} = \frac{|\vec{\pi}^*|W}{MK}\left(\frac{q^2}{q_0^{*2}}\right)^{1/2} \mathrm{Im}\left\{M_1^+\left[z S_0^+ + (3z^2-2)S_1^- + 4S_1^+\right]^*\right\} \qquad (A.10)$$

Considering that the phase of the M_1^+ amplitude for the isospin 3/2 final state goes through 90° at resonance, one may expect a large interference with the nearly real non-resonant amplitudes. This is in direct contrast with the situation for the real part of the scalar-transverse interference. The real part of the interference was too small to be used to determine the pion form factor in the experiment of Mistretta, et. al.[50,63] In the asymmetry experiment, an additional advantage arises in that the contributions of the small amplitudes are reduced in importance since the amplitudes are mostly real. This is particularly important since these smaller amplitudes are so poorly known.

Another feature of the interference term is the distinctly different θ_π^*-dependence of the terms containing the three scalar amplitudes. If one can obtain a large enough range of angles θ_{π}^{*}, an unambiguous identification of a dominant scalar multipole may be possible in π^{o} production. The limitation in angle θ_{π}^{*} in the data of Mistretta, et. al. retarded a positive identification from that data.

2) Experimental Considerations. Angle and/or Momentum. The initial job of the apparatus is to distinguish events according to charge mode and kinematic properties. Given an electron of initial energy, E, scattered at an angle θ_e with energy E', one needs only one more variable to specify completely all the kinematic quantities of a single pion production event. The fourth variable may be either the momentum of the outgoing charged hadron or its center of mass angle, $\theta_{p,}^{*}$. A specification of the proton angle in the laboratory frame is not sufficient to uniquely determine the kinematic properties of a $p\pi^{o}$ event. The folding forward of the backward protons leads to a double valuedness in the angle-momentum relation. In past experiments, the lower energy backward protons simply did not get through the apparatus at the angles where data were analysed. Thus, the laboratory angle $\theta_{p,}$ was sufficient for complete identification.

If one selects the momentum as the fourth variable, thre is no need to use $\theta_{\vec{q}}$ directly in the definition of $\theta_{p,\pi}$. On the other hand, the two charge modes lead to entirely different momentum detection situations and one may not be able to take data on both modes simultaneously. For a given set of electron parameters, the π^+ momenta typically vary by only 15% across an aperture which includes the entire proton cone. The proton momenta change by a factor of two and are a very rapidly varying function of laboratory angle near the edge of the cone. See Figure A.6. For momentum definition of kinematics, the π^+ backgrounds can be small since the necessary momentum bite is so small. The proton backgrounds can only be reduced by combining laboratory angle with the momentum specification. Similarly, the π^+ momentum should suffice to identify the π^+ production mode. But angle-momentum correlation will probably be required to identify a $p\pi^0$ event. Of course, use of a lucite Cerenkov counter would be valuable, especially as an anti-counter in identifying protons.

A final point about momentum definition is that a coincidence experiment with the polarized target requires a large sweeping magnetic field just to set up a workable counter. Double purpose would be served if this field were also used for momentum definition.

If, instead of momentum, one selects the angle θ_p, to define kinematics, one can do both pion and proton detection at the same time. However, particle identification will need to be done separately. In this connection, one might use the required sweeping field to separate the pions and

Figure A.6

PION AND PROTON KINEMATICS

$E = 5.5$ GeV
$K = 320$ MeV
$q^2 = 12\ F^{-2}$

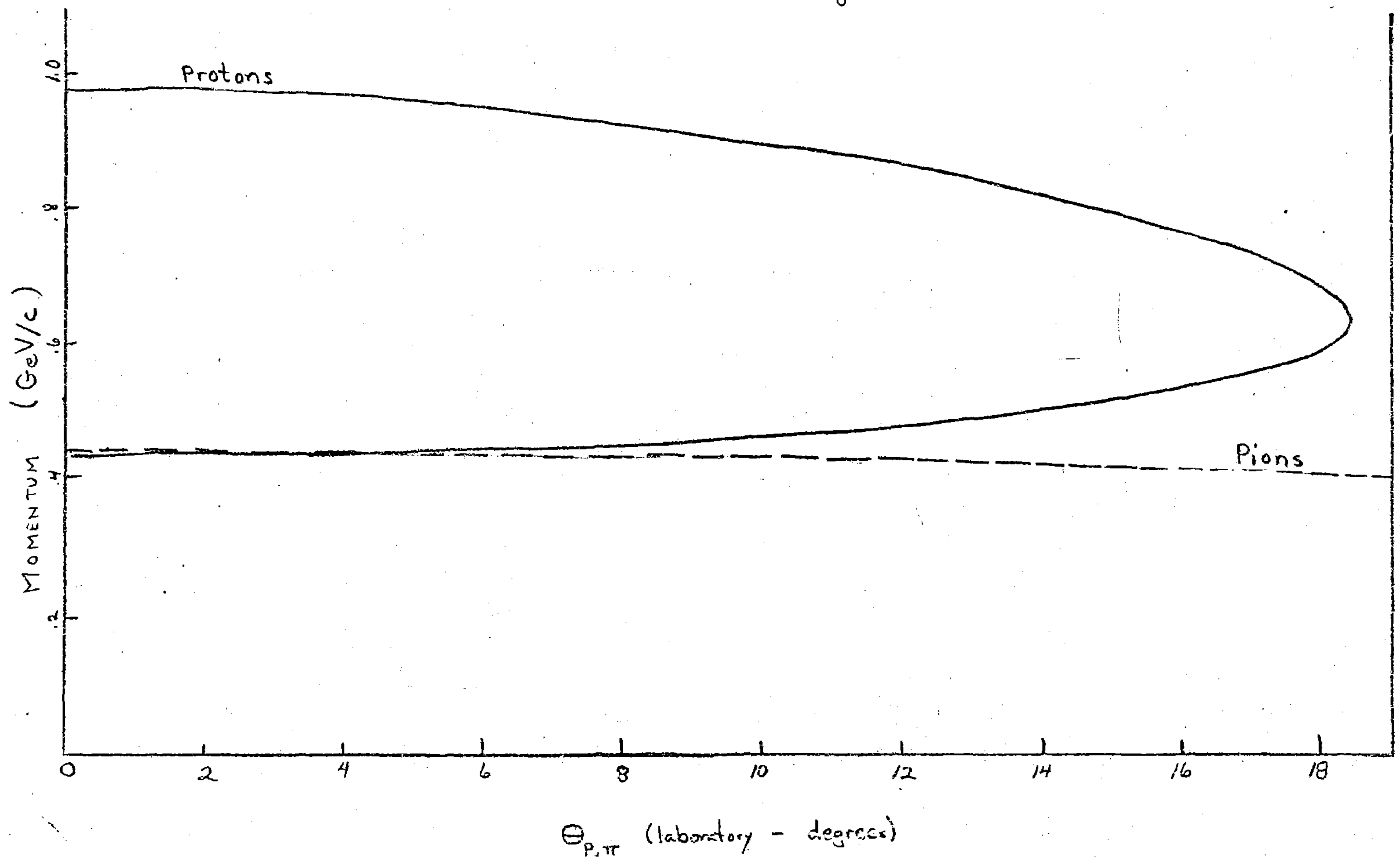

protons physically without doing as precise a measurement of momentum as might be required by proton momentum definition of kinematics. However, a single set of Cerenkov and dE/dx counters might be simpler for a sizable aperture. Furthermore, using these types of counters one may not be able to detect the backward protons as in the experiment of Mistretta, et. al.

Solid Angle (Rate) vs. Normalization Simplicity. When the target limits the beam before the rest of the system does, it is advisable to measure as large a solid angle as possible in order to increase the data rate. For π^+ production, there is little complication in taking a large laboratory solid angle. But for π^0 production, where a large laboratory solid angle corresponds to a large range of momenta, one may lose in simplicity what one gains in counting rate. In Section A.7c-1, it is suggested that interest should be centered on the band for which $\cos \phi = 0$. There is still the same range of proton momenta, but the initial position and direction of the proton are then specified and a simple hodoscope combined with a magnetic field should be sufficient to determine momenta. Of course, the limitation of solid angle to the region $\cos \phi = 0$ is not an easy experimental problem. One may, in fact, still have to determine directions far from the target rather than by apertures nearby.

As the detection system becomes more complicated by carefully limited acceptances, the evaluation of the ratio of free hydrogen to total scattering (k in Eq. 3.3) becomes more difficult. This directly affects the normalization of the asymmetry. Thus, the ratio should be known as well as any uncertainty in multipole amplitudes or theory in using the data to extract the pion form factor, for example.

If the final system becomes very restricted, it may well be advisable, if not mandatory, to do calibration runs on liquid hydrogen and carbon. No intensity limit on the beam would be implied by these target materials and, if one is set up for it, the calibration runs could be interspersed with the data runs. The calibration runs could serve to check alignment as well as to normalize the asymmetry.

As the determination of the ratio k becomes more complicated, the asymmetry measurement becomes more like an absolute measurement. In absolute measurements, the normalization cannot be overstressed. If on the other hand, the system remains simple, the normalization will not be a problem and one may use other measurements of the unpolarized angular distribution to extract absolute values of the amplitudes and of the pion form factor from the asymmetry measurement.

Of course, if the asymmetry turns out to be near zero, the importance of the normalization is reduced. A perfect example of this is the Time Reversal Experiment. However, in coincidence pion production experiments, one is looking for reasonably large asymmetries.

<u>Resolution Questions.</u> In order to take full advantage of the angle-momentum relationship, one must have

good resolution of angle and momentum. The angle in question, $\theta_{\pi,p}$, will be relative to the $\vec{q}$ direction, a direction which is itself determined from other physically measured quantities; the electron energies E, E' and scattering angle θ_e. A typical set of dependencies (taken from the kinematics of the first resonance run of the Time Reversal Experiment) are

$$\frac{\Delta\theta_q}{\Delta E/E} = -2.3^\circ/\%$$

$$\frac{\Delta\theta_q}{\Delta E/E'} = 2.3^\circ/\%$$

$$\frac{\Delta\theta_q}{\Delta\theta_e} = 3.4$$

Even with wire chambers to fix detected positions quite accurately, one must still include the effects of multiple scattering and the range of scattering locations as determined by the target length and beam width. In this regard, it must be remembered that the beam cannot be focused down to a narrow line since this would increase radiation damage and local heating problems in the polarized target. In the Time Reversal Experiment the beam width was 1 cm and the target length 2.5 cm. The target length alone contributed 1.6% (FWHM) to the resolution of the quadrupole spectrometer in the middle of its acceptance.

If one uses a more elaborate electron detection system, including ray tracing through the analysing fields in order to determine momenta, one can also obtain the scattering origin, but this requires a very powerful computing capability for the high statistics experiment implied by an asymmetry measurement. Without ray tracing for forward angle scattering (the electron), one is stuck with the target length effect. For wide angle scattering (the coincident hadrons), the beam width will be a limit.

For the coincidence arm, a vertical bend would assist in reducing sensitivity to the target length since the vertical coordinate will be defined well by the beam.

3) π^+ Production. The use of an asymmetry measurement to obtain the pion form factor, F_π, has been suggested by Goryachkin and Semikos[68] for low energy and $\theta^*_\pi = 0$. Asymmetries as large as 60% have been predicted at resonance using the theory of Fubini, Nambu, and Watagin[69] for $q^2 = 3\ F^{-2}$ and $r_\pi = 1$ F. An asymmetry at $\phi = 90,270^\circ$ at forward scattering angles has the same advantages as an experiment limited to $\theta^*_\pi = 0$. The same multipoles and,

therefore, the same projections of F_π enter the cross-section. This suggests one way of increasing the interesting solid angle beyond $\theta_\pi^* = 0$ for π^+ production.

Furthermore, an asymmetry is proportional to a term which may be represented schematically as

$$F_\pi / M_1^+$$

while the angular distribution contains a term of the schematic form

$$(\epsilon |F_\pi|^2 + |M_1^+|^2)$$

The former quantity is clearly more sensitive to F_π. And more important, the extraction of F_π from an asymmetry has a different dependance on the theory and is also less dependent on the exact values of the smaller multipole amplitudes than other electroproduction measurements.

The most advantageous system for π^+ production is one in which a large solid angle is detected with momentum definition of the kinematics. For the present target with its wide horizontal and narrow vertical aperture, a vertical bending magnet to remove the pions from the line of sight of the target is called for. This requires a bend on the order of 20^o for momenta around 500 MeV/c, that is, 225 kgauss-inch of magnetic field. A simple counter system is suggested schematically in Figure A.7. The two multiple counter arrays serve to determine the final pion direction and, thereby, momentum. For a given particle, one would expect a pair of counters to fire. A two dimensional array of the counters would give bands of coincidences for each momentum, the position along the band determined by the outgoing direction and the particular band by the momentum. Since the pion momentum is uniform (within about $\pm 5\%$) only for a given value of scattered energy, each scattered energy bin should have a different band and the bands should move monatonically across the 2-D array as one changes the scattered electron energy monatonically.

Although the above system should serve to select the charge mode as well as the kinematics for the lower q^2, an extra safeguard would consist of a plastic Cerenkov counter behind the last counter array. This counter would assist in background subtractions and insure that the lowest do not get confused with the pions of interest.

The decision to do a form factor asymmetry experiment will depend on the smallness of the attainable uncertainty. To get an idea of the rate, we report the results of a calculation for two cases below.

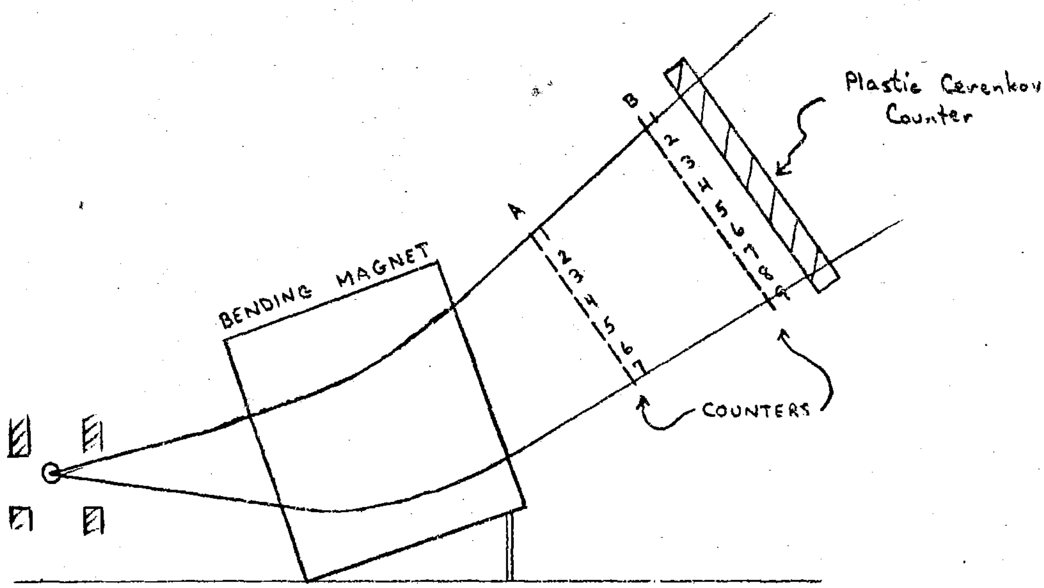

a) Schematic Side View of Apparatus

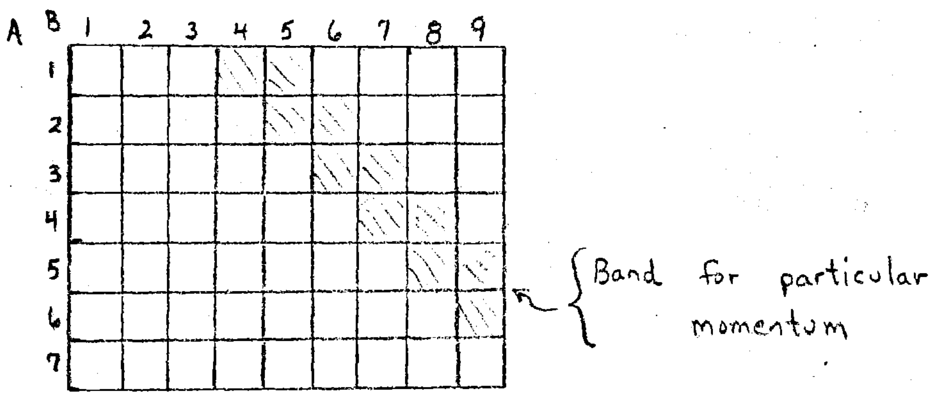

b) 2-D Display of Counter Coincidences

FIG. A.7 SIMPLE π^+ DETECTION APPARATUS

$q^2 (GeV/c)^2$	.05	.25
E(GeV)	2.0	4.0
K(GeV)	.320	.320
θ_e	6.8°	7.6°
Γ_T(/GeV-str)	9×10^{-2}	3×10^{-2}
$N_{free\ H}$ (std. weekend)$^{-1}$	1.2×10^4	3.5×10^3
$\delta\alpha$	$\pm 9\%$	$\pm 15\%$

The above rates for scattering from free hydrogen, $N_{free\ H}$, are for the standard weekend (Table A.2) of data taking, 50 mstr. pion solid angle in the pion-nucleon center of mass system, 200 MeV scattered electron energy bite, and 20 μb/str cross section for the virtual photon interaction. The values for the asymmetry uncertainties, $\delta\alpha$, are calculated with a ratio of free hydrogen scattering to a total scattering = 4 and an average polarization of 20%. None of these input parameters is difficult to obtain. In fact, one might easily do twice as well on the counting rate by working with broader acceptances which are still compatible with the present apparatus.

The above results should indicate the usefulness of a more specific design study and careful consideration of the running parameters. It seems quite reasonable to suppose that target improvements in the near future will make the asymmetry method an exciting possibility for pion form factor extraction from experiment.

4) π^o Production. The complications in laboratory kinematics for π^o production suggest limiting the aperture to the cos ϕ = 0 strip in order to select a more manageable laboratory momentum-solid-angle combination. Since there are typically 8 times as many protons as π^+'s in a given ϕ direction, the rates for π^+ production can be taken as lower limits for π^o production after limiting the aperture of the present apparatus. Furthermore, the kinematic region just suggested allows for the simplest interpretation.

The π^o production experiment would be most interesting with a target with a larger vertical aperture than that of the present target. However, careful selection of kinematic regions would allow a series of data points to be examined which contain a sizable range of θ_π^* and would, therefore, allow a determination of the dominant longitudinal multipole.

A π^o production asymmetry measurement contains both rate and the potential of measuring interesting amplitudes. What is required is a detection system capable of identifying the events of interest. A momentum measurement of protons would obviate the need for high resolution in electron detection, but is complicated by the broad range of proton momenta which would need to be measured. The design of such a system is beyond the scope of this work. It is, however, the point of this work to point out that a reasonable experiment is within the grasp of present apparatus and interpretable with present knowledge.

FOOTNOTES

1. J.H. Christenson, J.W. Cronin, V.L. Fitch and R. Turlay, Phys. Rev. Letters 13, 138 (1964).

2. J. Bernstein, G. Feinberg and T.D. Lee, Phys. Rev. 139B, 1650 (1965).

3. N. Barash-Schmidt, A. Barbaro-Galtieri, L.R. Price, M. Roos, A. H. Rosenfeld, P. Soding, C. G. Wohl, University of California Radiation Laboratory, Report No. UCRL-8030 (August, 1968).

4. L. Wolfenstein, Phys. Rev. Letters 13, 562 (1964).

5. N. Christ and T.D. Lee, Phys. Rev. 143B, 1310 (1966).

5a. Our notation is defined in the Appendix, Section 2b. The assumption of a vanishing lepton mass does not affect the polarization term and only affects the unpolarized term to order (M_e^2/EE'). See footnote 5. The assumption of single photon exchange is discussed in section 4a, of this chapter.

6. K.M. Watson, Phys. Rev. 95, 228 (1954). See also footnote 52.

7. J. Mar, B.C. Barish, J. Pine, D.H. Coward, H. DeStaebler, J. Litt, A. Minter, R.E. Taylor and M. Breidenbach, Phys. Rev. Letters 21, 482 (1968).

8. Footnote 7 and references therein.

9. F. Guérin and C. A. Pikketty, Il Nuovo Cimento XXXII, 971 (1964).

10. J.C. Bizot, J.M. Buon, J. Lefrançois, J. Perez-y-Jorba and P. Roy, Phys. Rev. 140, B1387 (1965).
G.V. DiGiorgio, E. Ganssauge, R. Gomez, G. Gorini, S. Penner, S. Serbassi, M.L. Vincelli, E. Amaldi and G. Stoppini, Il Nuovo Cimento XXXIX, 474 (1965) and references in DiGiorgio *et al.*

11. T.D. Lee, Phys. Rev. 140, B959 (1965).
T.D. Lee, Phys. Rev. 140, B967 (1967).

12. Footnotes 38 and 39. See also C. Bétourné, C. Feautrier, J. Peres-y-Jorba and D. Treille, Nuc. Phys. B5, 355 (1968).

FOOTNOTES (Cont.)

13. C. M. Mistretta, Thesis, Harvard University, 1968 (unpublished).

14. A. A. Cone, K. W. Chen, J. R. Dunning, Jr., G. Hartwig, Norman F. Ramsey, J. K. Walker and Richard Wilson, Phys. Rev. 156, 1490 (1967).

15. See Footnote 14, Eq. (22) and (23).

16. O. C. Kistner, Phys. Rev. Letters 19, 872 (1967).

17. M. Ataç, B. Chrisman, P. Debrunner and H. Frauenfelder, Phys. Rev. Letters 20, 691 (1968).

18. J. P. Hannon and G. T. Trammell, Phys. Rev. Letters 21, 726 (1968).

19. P. D. Miller, W. B. Dress, J. K. Baird, N. F. Ramsey, Phys. Rev. Letters 19, 381 (1967).

20. C. G. Shull and R. Nathans, Phys. Rev. Letters 19, 384 (1967).

21. N. Ramsey (private communication, November 1, 1968).

21a. G. Feinberg, Phys. Rev. 140B, 1402 (1965).

21b. G. Salzman and F. Salzmann, Phys. Letters 15, 91 (1965).

22. R. Prepost, R. M. Simonds and B. H. Wiik, Phys. Rev. Letters 21, 1271 (1968).

23. S. Barshay, Phys. Rev. Letters 17, 49 I1966).

24. M. Longo (private communication, November 8, 1968).

25. M. Goitein, Thesis, Harvard University, 1967 (unpublished).

28. R. J. Budnitz, Thesis, Harvard University, 1967 (unpublished), p. 4-18.

29. The "rear aperture" was used. Page 41 of Footnote 25.

FOOTNOTES

30. Number 20, pp. 262-276, Footnote 25.

31. F. Dell (private communication, 8/13/68). See also p. 202, Footnote 25.
F. Dell and M. Fotino, Cambridge Electron Accelerator Report No. CEAL-1043.

32. H. Winick, Cambridge Electron Accelerator Report No. CEAL-1015 (unpublished).

33. G. Lanza, Cambridge Electron Accelerator Report No. CEAL-25 (unpublished).

34. Page 34a, Footnote 13.

35. M. Goitein (private communication).

36. American Institute of Physics Handbook, Second Edition, D. E. Gray, ed. (McGraw-Hill, N.Y., 1963), p. 5-138.

36a. L. Hand, Proceedings of the 1967 International Symposium on Electron and Photon Interactions at High Energies, Stanford University, 1967.

37. J. L. Alberi, J. A. Appel, R. J. Budnitz, J. Chen, J. R. Dunning, Jr., M. Goitein, K. Hanson, D. C. Imrie, C. A. Mistretta, R. Wilson, Phys. Rev. (to be published);
K. C. Stanfield (private communication).

38. H. L. Lynch, J. V. Allaby, D. M. Ritson, Phys. Rev. **164**, 1635 (1967).

39. W. Bartel, B. Dudelzak, H. Krehbiel, J. McElroy, U. Meyer-Berkhout, W. Schmidt, V. Walther and G. Weber (private communication).

40. The result, quoted in Footnote 56, is also obtainable from Eq. A.1 using only M_1^+ and S_1^+ contributions to the $\mathcal{F}$'s of Eq. A.3.

41. From the data of Footnote 42, π^+ and π^0 production cross sections are about equal. From isospin considerations (Section A.3), the resonant part of π^+ production = 1/2 the resonant part of π^0 production (assumed purely resonant). Therefore, $(\sigma_{RES}/\sigma_{TOT}) = 0.75$.

FOOTNOTES (Cont.)

42. J. T. Beale, S. D. Ecklund and R. L. Walker, Cal. Tech. Report CTSL-42 (CALT-68-108).

43. Same as Footnote 14.

44. From the data of Footnote 42, there is little evidence of the resonance in forward and backward photoproduction. Only F_- can contribute to resonant single pion photoproduction in these directions (Appendix A of Footnote 5). The same result can be obtained from Eq. A.1 using only E_2^- and M_2^- contributions to the transverse $\mathcal{F}$'s with $E_2^- = 3\ M_2^-$.[46,47]

45. Argument at beginning of Footnote 44. See also C. A. Heusch, Lectures delivered at the International School of Physics "Ettore Majorana", Erice, Sicily, 1968 and Cal. Tech. Report CALT-68-171.

46. Y. C. Chau, R. G. Moorhouse, and N. Dombey, Rutherford Laboratory Preprint RPP/A16, revised (1967).

47. Equation (10) of S. D. Ecklund and R. L. Walker, Phys. Rev. 159, 1195 (1967).

48. And 49, not used.

50. Same as Footnote 13.

51. N. Zagury, Phys. Rev. 145, 112 (1966). See also Footnote 52.

52. F. A. Berends, A. Donnachie, and D. L. Weaver, Nuc. Phys. B4, 1 (1967).

53. For example, Footnotes 13 and 51.

54. Same as Footnote 6.

55. J. P. Perez-y-Jorba, P. Bounin, J. Chollet, Phys. Letters 11, 350 (1964).

56. K. Baba, N. Kajiura, S. Kaneko, K. Huke, R. Kikuchi, Y. Kobayashi and T. Yamakama, I.N.S. (Japan), Preprint (1968).